

SHOCK ANALYSIS OF AN ANTENNA STRUCTURE SUBJECTED TO
UNDERWATER EXPLOSIONS

A THESIS SUBMITTED TO
THE GRADUATE SCHOOL OF NATURAL AND APPLIED SCIENCES
OF
MIDDLE EAST TECHNICAL UNIVERSITY

BY

MEHMET EMRE DEMİR

IN PARTIAL FULFILLMENT OF THE REQUIREMENTS
FOR
THE DEGREE OF MASTER OF SCIENCE
IN
MECHANICAL ENGINEERING

SEPTEMBER 2015

Approval of the thesis:

**SHOCK ANALYSIS OF AN ANTENNA STRUCTURE SUBJECTED TO
UNDERWATER EXPLOSIONS**

submitted by **MEHMET EMRE DEMİR** in partial fulfillment of the requirements
for the degree of **Master of Science in Mechanical Engineering Department,**
Middle East Technical University by,

Prof. Dr. Gülbin Dural Ünver
Dean, Graduate School of **Natural and Applied Sciences** _____

Prof. Dr. Tuna Balkan
Head of Department, **Mechanical Engineering** _____

Prof. Dr. Mehmet Çalışkan
Supervisor, **Mechanical Engineering Dept., METU** _____

Examining Committee Members:

Prof. Dr. R. Orhan Yıldırım
Mechanical Engineering Department, METU _____

Prof. Dr. Mehmet Çalışkan
Mechanical Engineering Department, METU _____

Assoc. Prof. Dr. Yiğit Yazıcıoğlu
Mechanical Engineering Department, METU _____

Asst. Prof. Dr. Gökhan O. Özgen
Mechanical Engineering Department, METU _____

Asst. Prof. Dr. Bülent İrfanoğlu
Mechatronics Engineering Department, Atılım University _____

Date: 08.09.2015

I hereby declare that all information in this document has been obtained and presented in accordance with academic rules and ethical conduct. I also declare that, as required by these rules and conduct, I have fully cited and referenced all material and results that are not original to this work.

Name, Last name: Mehmet Emre DEMİR

Signature:

ABSTRACT

SHOCK ANALYSIS OF AN ANTENNA STRUCTURE SUBJECTED TO UNDERWATER EXPLOSIONS

Demir, Mehmet Emre

M. S., Department of Mechanical Engineering

Supervisor: Prof. Dr. Mehmet Çalışkan

September 2015, 183 pages

Antenna structures constitute main parts of electronic warfare systems. Mechanical design is as crucial as electromagnetic design of antenna structures for proper functioning and meeting high system performance needs. Failure of mechanical and electronic structures operating under shock loading is a common occurrence in naval electronic warfare applications. A complete shock analysis of the dipole antenna structure subjected to underwater explosions is performed to foresee adverse effects of mechanical shock phenomena on the antenna structure.

Theoretical models of the antenna structure; namely mathematical model and finite element model, are built on multi-degree-of-freedom approach. Modal properties are derived from Classical Beam Theory and transient responses to input shock loading are obtained by Recursive Filtering Relationship (RFR) Method for the mathematical model. Input shock loading is synthesized from assessed shock specification to classical shock input. Transient responses exerted from RFR method are also approximated by simplified and SDOF models. Finite element analysis of the analytical model is performed on ANSYS® platform. Comparisons of analytical results are presented for interchangeable use of proposed models.

Numerical results are verified with both modal and transient results collected from experimental analysis. Experimental analysis is performed for exact dimensions of antenna structure subjected to synthesized shock input criteria.

Shock severity for antenna structure is presented for both electrical and mechanical components. Design roadmap is drawn within the limitations set for proper antenna functioning with desired performance. Design limitations are determined by the verified mathematical model. Shock isolation theory is also explained and applied to the antenna structure in order to obtain shock responses below limitations mentioned. Thus, the complete shock analysis of the antenna structure is performed for antenna design to withstand underwater shock explosions.

Keywords: Underwater Explosions (UNDEX), Shock Profile Synthesis, Transient Response Analysis, Experimental Shock Analysis, Shock Isolation.

ÖZ

SU ALTI PATLAMARINA MARUZ KALAN BİR ANTEN YAPISININ ŞOK ANALİZİ

Demir, Mehmet Emre

Yüksek Lisans, Makina Mühendisliği Bölümü

Tez Yöneticisi: Prof. Dr. Mehmet Çalışkan

Eylül 2015, 183 sayfa

Elektronik harp sistemlerinin en önemli parçası anten yapılarıdır. Yüksek sistem performansı ve sürekli çalışabilen bir anten yapısı elde edebilmek için elektromanyetik tasarım kadar mekanik tasarım da kritik öneme sahiptir. Deniz platformunda çalışan elektronik harp sistemleri yüksek şok yüklemeleri altında çalıştığından, mekanik ve elektronik yapılarda sıklıkla arızalar veya deformasyonlar gözlenmektedir. Bu etkileri tahmin edilir hale getirebilmek, şoka dayanıklı tasarımlar ortaya koyabilmek ve tasarım aşamasında gerekli önlemleri alabilmek için bir dipol antenin şok analizi sunulmuştur.

Anten yapısı, matematiksel metotlar ve sonlu elemanlar metoduyla çok serbestlik dereceli olarak modellenmiştir. Antenin modal özellikleri Klasik Kiriş Teorisi ile, şok cevapları da Yinelemeli Filtreleme İlişkisi(YFİ) Metodu ile modellenmiştir. Antene etki eden şok tahriki, antenin dayanması gereken şok limitlerine göre sentezlenen klasik dalga profilleriyle verilmiştir. YFİ metoduyla elde edilen şok tepkilerine, basitleştirilmiş modellerle ve tek serbestlik dereceli modelle de yaklaşımlarda bulunulmuştur. Analitik modelin sonlu elemanlar analizi ANSYS® programı ile gerçekleştirilmiştir. Matematiksel model ve sonlu elemanlar analizi sonuçları kıyaslanarak gerektiğinde birbirlerinin yerine kullanımları

değerlendirilmiştir. Analitik sonuçlar deneysel modal analiz ve deneysel şok analizi ile doğrulanmıştır. Deneysel bir anten modellerine daha önce sentezlenen şok profilleri uygulanarak gerçekleştirilmiştir.

Antende yer alan elektriksel ve mekanik parçaların şoka karşı dayanımı sunulmuştur. Antenin çalışmasını ve istenen performansı sağlayabilmesi için belirlenen tasarım sınırları tasarım yol haritası içerisinde ortaya konmuş ve tasarım için incelenmesi gereken adımlar belirtilmiştir. Tasarım sınırları belirlenirken doğrulanmış olan matematiksel model kullanılmıştır. Antenin bu sınırlar içerisinde mekanik şoktan etkilenmeden çalışabilmesi için şok izolasyonu teorisi ve şok izolasyonu basamakları sunulmuştur. Çalışmada incelenen anten yapısının şok izolasyonu gerçekleştirilerek şoktan etkilenmeden çalışabilmesi sağlanmıştır.

Anahtar Kelimeler: Denizaltı Patlamaları, Mekanik Şok, Şok Profil Sentezi, Şok Tepki Analizi, Deneysel Şok Analizi, Şok İzolasyonu.

To My Family,

ACKNOWLEDGEMENTS

I would like to express my sincere gratitude to my advisor, Prof. Dr. Mehmet Çalışkan, for his guidance, support and technical suggestions throughout the study.

I am grateful to ASELSAN A.Ş. for the financial and technical opportunities provided for the completion of this thesis.

I would also like to express my sincere appreciation for Yunus Emre Özçelik, Rahmi Dündar, Emrah Gedikli, Murat Atacan Avgın, Yasin Özdoğan, Caner Asbaş, Durmuş Gebeşođlu, Ahmet Dindar, Ahmet Muaz Ateş, Özkan Sağlam and Merve Öztürk for their valuable friendship, motivation and help.

I would like to thank to Yusuf Başıbüyük for his guidance, help and comments throughout the drop experiments.

For their understanding my spending lots of time on this work, I sincerely thank to my family.

TABLE OF CONTENTS

ABSTRACT	V
ÖZ.....	VII
ACKNOWLEDGEMENTS	X
TABLE OF CONTENTS	XI
LIST OF TABLES	XV
LIST OF FIGURES	XVII
LIST OF SYMBOLS.....	XXI
LIST OF ABBREVIATIONS	XXIII
CHAPTERS	
1 INTRODUCTION	1
1.1 Naval C-ESM/COMINT Antennas	4
1.2 Mechanical Shock	5
1.3 Ship Shock and Underwater Explosions (UNDEX)	12
1.4 Motivation	13
1.5 Scope, Objective and Contribution of Work.....	14
1.6 Outline of the Dissertation	16
2 LITERATURE SURVEY.....	19
2.1 Historical Background.....	19
2.2 Literature Survey.....	21
3 SHOCK PROFILE SYNTHESIS	29
3.1 Theory: Shock Response Spectrum.....	29
3.2 Shock Response Spectrum for Naval Applications.....	35
3.3 Determination of Assessment Criteria from Shock Response Spectrum	37
3.4 Shock Synthesis.....	40

3.4.1	Longitudinal (X) Axis Shock Synthesis	41
3.4.2	Transverse (Y) Axis Shock Synthesis	42
3.4.3	Vertical (Z) Axis Shock Synthesis	43
4	MATHEMATICAL MODELING OF THE ANTENNA STRUCTURE.....	45
	Problem Definition	45
4.1	Modal Transient Response of the Antenna Structure Subjected to Base Excitation.....	47
4.1.1	Normal Modes, Natural Frequencies and Mode Shapes of the Antenna Structure.....	48
4.1.2	Effective Modal Mass and Participation Factor for the Antenna Structure	53
4.1.3	Transient Response of the Antenna Structure to Base Excitation...	54
4.2	Solution Methods for Transient Response of the Antenna Structure Subjected to Base Excitation.....	59
4.2.1	Multi-Degree-of-Freedom (MDOF) Solution Methods	61
4.2.1.1	Ramp Invariant Recursive Filtering Relationship Method.....	61
4.2.1.2	Other Numerical Methods	62
4.2.2	Single-Degree-of-Freedom (SDOF) Solution Methods	63
4.2.2.1	Convolution Integral Method	63
4.2.2.2	Digital Recursive Filtering Relationship Method	64
4.2.2.3	Newmark-Beta Method	64
4.2.2.4	Runge-Kutta 4 th Order Method	65
4.2.3	Simplified Solution Models.....	65
4.2.3.1	Absolute Sum Method (ABSSUM).....	65
4.2.3.2	Square Root of the Sum of the Squares (SRSS).....	66
4.2.3.3	Naval Research Laboratories Method (NRLM)	66
5	TRANSIENT RESPONSE ANALYSIS OF ANTENNA STRUCTURE	69
5.1	Modal Analysis of Antenna Structure	70
5.2	MDOF Transient Response Analysis of Antenna Structure	72
5.2.1	Determination of Analysis Parameters.....	72
5.2.2	MDOF Transient Response Analysis Results	79

5.3	Transient Analysis Results of Antenna Structure by Simplified Methods.....	86
5.3.1	Transient Response Results of ABSSUM Method	87
5.3.2	Transient Response Results of SRSS Method.....	88
5.3.3	Transient Response Results of NRL Method.....	88
5.4	Transient Analysis Results of Antenna Structure Using SDOF Models	90
5.5	Comments of Chapter 5.....	95
6	TRANSIENT RESPONSE ANALYSIS OF ANTENNA STRUCTURE BY FINITE ELEMENT ANALYSIS	97
6.1	Modal Analysis of Antenna Structure	98
6.2	Transient Response Analysis of Antenna Structure	101
6.3	Discussion for Chapter 6	106
7	EXPERIMENTAL ANALYSIS OF ANTENNA STRUCTURE.....	109
7.1	Introduction	109
7.2	Modal Verification of Antenna by Impact Hammer Test	110
7.3	Drop Experiment of Antenna Structure	118
7.4	Comments on Verification Results	124
8	SHOCK SEVERITY FOR ANTENNA STRUCTURE.....	127
8.1	Shock Effects on Antenna Performance.....	127
8.2	Shock Severity Limits for Electrical Components on Antenna Structure	131
8.3	Shock Stress Severity on Antenna Structure.....	136
8.3.1	Shock Stress from Single Mode Modal Transient Analysis	136
8.3.2	Shock Stress from Single Mode Direct SRS.....	137
8.3.3	Shock Stress from Four Mode Transient Analysis.....	137
8.3.4	Allowable Stress for Naval Applications	138
8.4	Antenna Limitations Caused by Shock Severity.....	140
8.5	Shock Isolation of Antenna Structure	141
8.5.1	General View on Shock Isolation.....	142
8.5.2	Shock Isolator Selection.....	144

8.6	Isolator Verification by Drop Experiment.....	147
8.7	Discussion	149
9	SUMMARY AND CONCLUSIONS	151
9.1	Summary	151
9.2	Conclusions	153
9.3	Future Work	154
	REFERENCES	157
	APPENDICES	
A.	CALCULATIONS OF SRS VALUES FROM BV043 STANDARD	165
B.	EQUIPMENT USED THROUGHOUT TESTS	169
C.	VELOCITY LIMITS OF MATERIALS	173
D.	“C” CONSTANTS FOR DIFFERENT TYPES OF ELECTRICAL COMPONENTS	175
E.	ATC® HIGH POWER FLANGE MOUNT RESISTOR	179
F.	TAICA ALPHA-GEL® MN SERIES ISOLATOR.....	181
G.	MATLAB® SCRIPT FOR FREQUENCY DOMAIN DIFFERENTIATION	183

LIST OF TABLES

TABLES

Table 1. 1 Shock Effects of Various Shock Pulses [6].....	10
Table 3. 1 Values for Acceleration-Time Calculation for Submarine.....	39
Table 3. 2 Calculated Acceleration-Time Signals	39
Table 3. 3 BV043 Shock Requirements	44
Table 3. 4 Calculated and Synthesized Shock Profiles	44
Table 4. 1 Values of $\beta_n l$ for first Five Mode of Cantilever Beam [44].....	51
Table 5. 1 Geometrical Properties of Antenna Structure.....	70
Table 5. 2 Mechanical Properties of Antenna Structure.....	71
Table 5. 3 Natural Frequencies of Antenna Structure for First Four Bending Modes	71
Table 5. 4 Modal Properties of the Antenna Structure	76
Table 5. 5 Maximum Shock Responses at the Antenna Tip.....	86
Table 5. 6 Transient Response Estimations of the Antenna Using ABSSUM Method	87
Table 5. 7 Transient Response Estimations of the Antenna Using SRSS Method..	88
Table 5. 8 Transient Response Estimations of the Antenna Using NRL Method..	89
Table 5. 9 Transient Response Results for Simplified Methods Using Two Modes	90
Table 5. 10 Transient Response Results for Simplified Methods Using Three Modes.....	90
Table 5. 11 SDOF Shock Responses at the Antenna Tip	91
Table 5. 12 Mathematical Model Responses at the Antenna Tip.....	95

Table 6. 1 Natural Frequencies of the Antenna Structure	101
Table 6. 2 Comparisons of Maximum Transient Responses	106
Table 7. 1 Natural Frequencies of Antenna Structure	115
Table 7. 2 Natural Frequencies of Antenna Structure with Tip Mass	116
Table 7. 3 Modal Damping Ratios of Antenna Structure	118
Table 7. 4 Maximum Absolute Acceleration Results of All Analyses.....	124
Table 8. 1 Relative Position Factors for Component on Circuit Board.....	134
Table 8. 2 Grade A Allowable Stress Criteria and Applicable Design Levels [6]	139
Table 8. 3 Shock Severity Limitations	141
Table C. 1 Severe Velocities, Fundamental Limits to Modal Velocities in Structures [59].....	173
Table C. 2 Severe Velocity Values from Sloan, 1985 [68].....	174
Table C. 3 Values from Roark, 1965, p 416 [69].....	173
Table D. 1 Constant for Different Types of Electronic Components [66]	175

LIST OF FIGURES

FIGURES

Figure 1. 1 Electronic Warfare Applications.....	1
Figure 1. 2 Subdivisions of Electronic Warfare: (I)Very/Ultra High Frequency COMINT,(II)Transportable V/UHF DF(Direction Finding),(III)Portable Jamming-Electronic Attack,(IV)High Frequency-Electronic Attack,(V)Electronic Support-ELINT,(VI)Submarine Electronic Surveillance Measurement,(VII) Air Defense Search and Fire Control Radars	3
Figure 1. 3 Nomenclature of Shock Duration [5].....	6
Figure 1. 4 Spring-mass System.....	7
Figure 1. 5 El Centro, California, Earthquake of May 18, 1940; North-South Component [6].....	8
Figure 1. 6 Athwartship Velocity Time History measured on a Floating Shock Platform nearby underwater explosion [6].....	8
Figure 1. 7 Examples of shock pulses	9
Figure 1. 8 Accelerated drop-table [8]	11
Figure 1. 9 USS OSPREY-MHC 51(left) [9] and CG 53(right-Courtesy of U.S Navy) Ships Full-Scale Shock Trials	12
Figure 1. 10 Underwater Antenna Platform	13
Figure 3. 1 Shock Response Spectrum Concept [38]	30
Figure 3. 2 Shock Response Spectrum Model [23].....	31
Figure 3. 3 Free-body Diagram of SDOF System [23]	31
Figure 3. 4 Time History of 40g 11ms Half-Sine Input Signal.....	34
Figure 3. 5 Acceleration Shock Response Spectrum for 40g 11ms Half-Sine Signal	34
Figure 3. 6 Shock Response Spectrum in four-way log paper [39]	35
Figure 3. 7 Shock Response Spectrum Regions [39]	36

Figure 3. 8	General Form of Double Half-Sine Shock Acceleration-Time Signal	38
Figure 3. 9	Axis Definitions for Submarine	40
Figure 3. 10	Defined by BV043 (blue) and Synthesized (red) Shock Profile Shock Response Spectrum for X Axis	41
Figure 3. 11	Defined by BV043 (blue) and Synthesized (red) Shock Profile Shock Response Spectrum for Y Axis	42
Figure 3. 12	Defined by BV043 (blue) and Synthesized (red) Shock Profile Shock Response Spectrum for Z Axis.....	43
Figure 4. 1	Antenna Structure Attached to the Platform	46
Figure 4. 2	Electrical Components Placed on Antenna Tip	46
Figure 4. 3	Antenna Model as a Cantilever Beam.....	48
Figure 4. 4	Antenna Model Subjected to Transient Base Excitation	54
Figure 4. 5	Solution Methodology of MATLAB® Script Built for RFR Method .	62
Figure 5. 1	Three-Dimensional Model of Antenna Structure.....	70
Figure 5. 2	First Four Bending Mode Shapes of Antenna Structure	72
Figure 5. 3	Shock Inputs Applied to the Antenna Platform	73
Figure 5. 4	Acceleration SRS for both Transverse Shock Inputs.....	74
Figure 5. 5	Relative Displacement SRS for both Transverse Shock Inputs.....	75
Figure 5. 6	Comparison of transient acceleration responses of antenna structure with respect to the number of modes included in the analysis.....	77
Figure 5. 7	Comparison of transient acceleration responses of antenna structure with respect to the number of modes included in the analysis (Zoomed View)	77
Figure 5. 8	Comparison of relative displacement responses of antenna structure with respect to the number of modes included in the analysis.....	78
Figure 5. 9	Comparison of relative displacement responses of antenna structure with respect to the number of modes included in the analysis (Zoomed View)	78
Figure 5. 10	Time History of 200g 8ms Half-Sine Acceleration Input.....	80
Figure 5. 11	MDOF Absolute Acceleration Response of the Antenna Tip.....	81
Figure 5. 12	MDOF Relative Displacement Response of the Antenna Tip	82

Figure 5. 13	MDOF Relative Velocity Response of the Antenna Tip	83
Figure 5. 14	MDOF Phase Portrait of the Antenna Tip	84
Figure 5. 15	Histogram Plot for MDOF Absolute Acceleration Response.....	85
Figure 5. 16	Histogram Plot for MDOF Relative Displacement Response	85
Figure 5. 17	SDOF Absolute Acceleration Response of the Antenna Tip.....	92
Figure 5. 18	Comparison of Absolute Acceleration Responses of the Antenna Tip	92
Figure 5. 19	SDOF Relative Displacement Response of the Antenna Tip	93
Figure 5. 20	Comparison of Relative Displacement Responses of the Antenna Tip	93
Figure 5. 21	Comparison of Phase Portraits of the Antenna Tip	94
Figure 6. 1	First Mode Shape of the Antenna Structure (FEA Result)	99
Figure 6. 2	Second Mode Shape of the Antenna Structure (FEA Result).....	99
Figure 6. 3	Third Mode Shape of the Antenna Structure (FEA Result).....	100
Figure 6. 4	Fourth Mode Shape of the Antenna Structure (FEA Result).....	100
Figure 6. 5	200g 8ms Half-sine Acceleration Input Defined to ANSYS®	103
Figure 6. 6	ANSYS® Absolute Acceleration Response of the Antenna Tip.....	104
Figure 6. 7	ANSYS® Relative Displacement Response of the Antenna Tip	105
Figure 6. 8	ANSYS® Relative Velocity Response of the Antenna Tip.....	105
Figure 7. 1	PCB PIEZOTRONICS® 086E80 Miniature Impact Hammer	111
Figure 7. 2	IOTECH® Data Acquisition System.....	111
Figure 7. 3	Antenna Attachment to the Experimental Set-up	112
Figure 7. 4	Hammer Test of Antenna Structure	113
Figure 7. 5	eZ-Analyst Screen During Experiment.....	114
Figure 7. 6	Measured FRF of Antenna Structure	114
Figure 7. 7	Modal Analysis by ANSYS®® with tip mass.....	116
Figure 7. 8	Response Curve Showing Half-Power Points and Bandwidth [44]...	117
Figure 7. 9	Drop Test Experiment.....	120
Figure 7. 10	Shock Input Measurement Taken From Drop Table	121

Figure 7. 11 Mathematical Model and Experiment Comparison	122
Figure 7. 12 FEA Model and Experiment Comparison.....	123
Figure 7. 13 Frequency Content of Measured Data	124
Figure 8. 1 Relative Displacement of the Antenna Tip	129
Figure 8. 2 Electromagnetic Analysis of Dipole Antenna by HFSS®	130
Figure 8. 3 Radiation Pattern HFSS® Analysis of Antenna with Maximum Allowable Deformed Position	130
Figure 8. 4 Relative Velocity Response of the Antenna from Updated Models ..	132
Figure 8. 5 Morse Chart for Mild Steel Beams [62].....	133
Figure 8. 6 Component Bending on the Antenna Structure [63].....	134
Figure 8. 7 Shock Damping by means of Isolators on, a) Acceleration-time plot, b) Force-displacement plot [63]	143
Figure 8. 8 Shock Velocity Formulation for Different Types of Shock [65].....	145
Figure 8. 9 Drop Experiment of Antenna with Isolator.....	147
Figure 8. 10 Acceleration Response for the Antenna with Isolator	148
Figure 8. 11 Relative Velocity Response of the Antenna with Isolator	149
Figure B. 1 General Specifications of IOTECH® WaveBook Data Acquisition System	169
Figure B. 2 General Specifications of PIEZOTRONICS® 356A01 Accelerometer	170
Figure B. 3 General Specifications of PIEZOTRONICS® 086E80 Impact Hammer	171
Figure B. 4 General Specifications of LANSMONT® PDT 80 Drop Table	172
Figure E. 1 General Specifications of ATC® High Power Flange Mount Resistor	179
Figure F. 1 General Specifications of Taico ALPHA-GEL® MN Series Isolator	181

LIST OF SYMBOLS

A	threshold pulse amplitude
a_0	maximum acceleration
c_c	critical damping constant
C_i	modal damping coefficient
D	threshold pulse duration
d_0	maximum relative displacement
E	modulus of elasticity
e_{res}	coefficient of restitution
ξ_n	modal damping ratio
f_{n_i}	natural frequency (in Hz)
g	gravitational acceleration
h	no rebound drop height
h_r	drop height with rebound.
I	area of moment of inertia
k_{beam}	beam stiffness
K_i	modal stiffness
L	antenna length
m	mass of the antenna

m_{eff}	effective modal mass
M_i	modal mass
Q	quality (amplification factor)
\hat{q}_{nj}	eigenvalue
T_e	effective shock duration
T_E	total shock duration
T_n	modal time variable
Δt	time step
Γ	participation factor
V	pseudo velocity
V_0	maximum pseudo-velocity
V_1	pseudo-velocity at shock event
v_1	velocity before impact
v_2	velocity after impact
$w(t)$	base displacement function
ω_n	natural frequency (in rad/s)
\ddot{X}_i	modal acceleration response
$Y_n(x)$	mode shape function
\ddot{Y}	acceleration base input
$(Z_i)_{max}$	maximum modal relative displacement

LIST OF ABBREVIATIONS

ABSSUM	Absolute Sum Method
ASME	American Society of Mechanical Engineers
COMINT	Communications Intelligence
DDAM	Direct Dynamic Analysis Method
DOFs	Degree of Freedoms
EA	Electronic Attack
EB	Euler Bernoulli
ELINT	Electronics Intelligence
EMP	Electromagnetic Pulse
EP	Electronic Protection
ES	Electronic Support
ESM	Electronic Surveillance Measurement
EW	Electronic Warfare
FEA	Finite Element Analysis
FEM	Finite Element Model
FFT	Fast Fourier Transform
IEEE	The Institute of Electrical Electronics Engineers
IFF	Identification Friend and Foe

MDOF	Multi Degree of Freedom
NRLM	Naval Research Laboratories Method
PCB	Printed Circuit Board
RFR	Recursive Filtering Relationship
RMS	Root-mean-square
RWR	Radar Warning Receivers
SDOF	Single Degree of Freedom
SIGINT	Signals Intelligence
SRS	Shock Response Spectrum
SRSS	Square Root of the Sum of the Squares
UNDEX	Underwater Explosions

CHAPTER 1

INTRODUCTION

General: Electronic Warfare

Electronic warfare (EW) can be defined as any possible action that is possible with the use of the electromagnetic spectrum or directed energy to control the spectrum, attack an opponent, or obstruct enemy assaults via the spectrum [1]. The main purpose of electronic warfare is to deny opponent attacks and ensure friendly unrestrained access to the electromagnetic spectrum. Electronic warfare applications can be seen in air, sea, land, and space applications for both manned and unmanned systems as illustrated in Figure 1.1. Targets of the applications can be humans, communications, radar, or other assets. In military applications, electronic warfare is used to support military operations by means of detection, denial, deception, disruption, degradation, protection, and destruction [2].



Figure 1. 1 Electronic Warfare Applications

Electronic warfare can be divided into three main subdivisions, namely, electronic attack, electronic protection and electronic support. Electronic attack (EA) applications are performed by active and passive ways. Active ways are jamming, deception and active cancellation; passive ways are chaff, towed decoys, radar reflectors and stealth. Electronic protection (EP) is also applied in active and passive ways. As technical modification to radio equipment is an active way; education of operators, enforcing strict discipline and modified battlefield tactics or operations are passive ways of electronic protection. Electronic support (ES) can be defined as an action of searching, interception, identification, and detection the location of radiated electromagnetic energy sources for the purpose of immediate threat recognition. Signals Intelligence (SIGINT), Communications Intelligence (COMINT) and Electronics Intelligence (ELINT) are three subgroups of electronic support applications.

- Purpose of SIGINT is to collect and analyze of information from radar and radio signals.
- Purpose of COMINT is to listen into, analyze and decode the military radio-traffic, teletype and fax signals.
- Purpose of ELINT is to collect and analyze the radar, Identification Friend and Foe (IFF), datalink, and missile firing signals. Radar Warning Receivers (RWR) is one of the examples of these types of applications.

Apart from these classifications, radar technologies are another subgroup of electronic warfare. The use of radar technologies is basically air-defense systems, antimissile systems; marine radars to locate enemy ship, ocean surveillance systems, outer space surveillance and rendezvous systems, guided missile target locating systems so on.



(I)



(II)



(III)



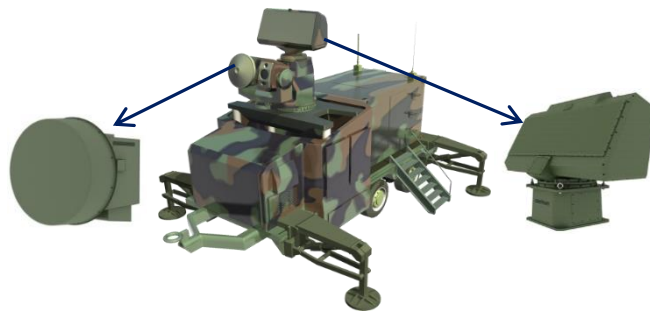
(IV)



(V)



(VI)



(VII)

Figure 1. 2 Subdivisions of Electronic Warfare: (I)Very/Ultra High Frequency COMINT,(II)Transportable V/UHF DF(Direction Finding),(III)Portable Jamming-Electronic Attack,(IV)High Frequency-Electronic Attack,(V)Electronic Support-ELINT,(VI)Submarine Electronic Surveillance Measurement,(VII) Air Defense Search and Fire Control Radars

For all these electronic warfare applications; antennas, receivers, transmitters, power unit, data collection and processing units, user interfaces and other residual components are gathered up for the complete operation quality and performance.

1.1 Naval C-ESM/COMINT Antennas

The Institute of Electrical and Electronics Engineers (IEEE) defines the antenna as; *“An antenna is a device that provides a means for radiating and receiving radio waves. In other words, it provides a transition from a guided wave or a transmission line to a free space wave or vice versa”* [3].

Antennas are the main components of electronic warfare applications mentioned in previous section. Therefore, for different applications, different type of antennas is possible to use. Naval ESM systems are the electronic warfare solutions in which ELINT and COMINT solutions are tailored together. COMINT part of the system consists of direction finding antennas and jamming antennas working in communication frequencies. Direction finding antennas are built on strong support masts and consist of dipole elements attached to the mast. These antennas are responsible for the electronic support by means of detecting the position of threat signal with minimum possible errors. Jamming antennas, on the other hand, consist of long thin structures and printed circuit boards and the electronic components like resistances, capacitances, baluns etc. attached. Jamming antennas use the reliable information gathered by direction finding antennas and creates jamming signals to those threats. Therefore, their main purpose is to create a disturbance signal when the signal which is possibly a threat is detected. Jamming dipole antennas are one type of antenna which can be used as Electronic Attack (EA) COMINT antenna. The reason for the use of those antennas is to achieve required frequency band with the certain amplitude and phase requirements. Jamming dipole antenna is a very simple structure which is composed of long and thin metal electronic circuit boards (or printed circuit boards). It is very vulnerable to vibration and shock especially

naval shock. Those types of antennas are used in field and on vehicle application with competence without any extra precautions for shock. However in naval applications; because of the shock levels reached in underwater explosions (explained in following section), shock analysis and design for naval shock is a must. In the scope of this thesis, the dipole jamming antenna subjected to underwater shock explosion is investigated.

1.2 Mechanical Shock

Mechanical shock is defined as a non-periodic excitation of a mechanical system. It is characterized by severity and suddenness that disrupts the equilibrium of the system usually causing significant relative displacements [4]. These non-periodic excitations can be caused by suddenly applied forces or by sudden changes in magnitude or direction of velocity. Mechanical shock is usually expressed as a single input pulse like half sine, saw-tooth, versed sine, triangular, rectangular and other possible forms with peak amplitude(in acceleration or velocity) and duration of the pulse. The duration of a shock pulse is the time required for the acceleration of the pulse to rise from some stated fraction of the maximum amplitude and to decay to this value. T_E is the “shock duration” which can be defined as the minimum length of time containing all time history magnitudes more than absolute value which is one-third of the shock peak magnitude absolute value, A_p . On the other hand, T_e is the “effective shock duration” which can be defined as the minimum length of continuous time that contains the root-mean-square (RMS) time history amplitudes more than the value which is one tenth of the peak RMS amplitude related to the shock event and the averaging time for the unweighted RMS computation is assumed to be between one tenth and one fifth of T_e [5].

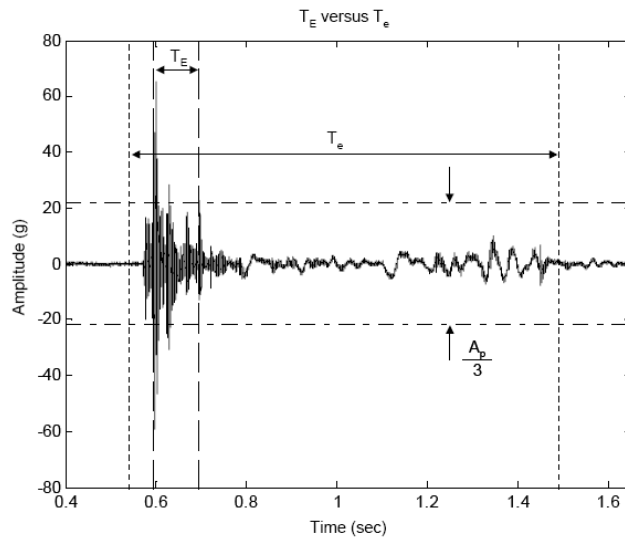


Figure 1. 3 Nomenclature of Shock Duration [5]

Sources of input pulses can be various. The well-known examples are drop, underwater explosion impact, ballistic impact, collision impact, gunfire, transportation, aircraft or missile maneuvers etc. The effects of mechanical shock created by these sources can be so severe that the system stores the high value of energy within a short period of time and releases it over a longer period of time with comparably lower peak value. If the peak value is held below limits with the extension of release time, the shock effect consequences may not be that harsh and harmful for the system. For analyzing the equipment such as antenna subjected to shock or vibration, it is convenient to represent the antenna as a spring mass system shown in Figure 1.4. In this case, transient force $f(t)$ is applied to a foundation which supports the antenna. It is mounted on to a base with a spring of stiffness k and a damper with damping c . The response characteristics of the antenna to such a loading have a relationship between the frequency of the applied transient force and the natural frequency of the system.

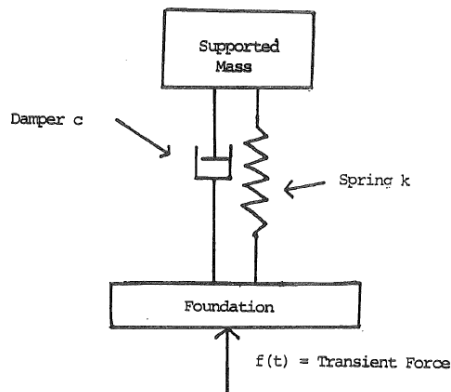


Figure 1. 4 Spring-mass System

If the spring is very stiff and the damping is small, the response of the antenna will be almost the same as the motion of base. If natural frequency of the system and the frequency of the transient force is nearly the same, the response of the equipment is much greater than the motion of base. If spring is very soft, the response of equipment has lower amplitude and longer duration motion than the base. As seen from these cases, the determining factor with respect to the shock response is the frequency relationship between the input and the system. Measured shock environments in the real world are usually presented in motion-time histories as illustrated in Figures 1.5 and 1.6.

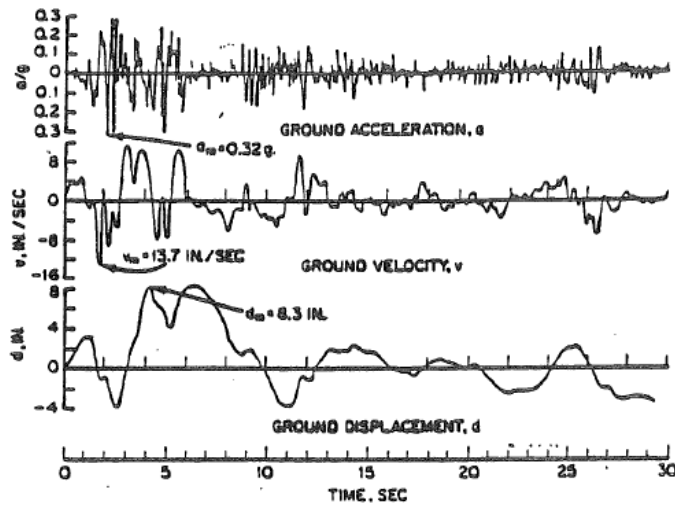


Figure 1. 5 El Centro, California, Earthquake of May 18, 1940; North-South Component [6]

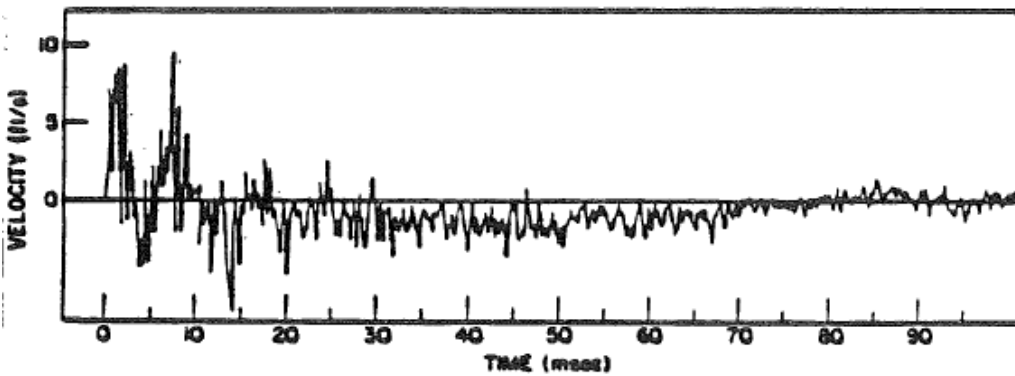


Figure 1. 6 Athwartship Velocity Time History measured on a Floating Shock Platform nearby underwater explosion [6]

These measurements produce very complex curves that are very difficult to describe with mathematical terms. They cannot easily be created in laboratory testing conditions. In order to achieve test requirements to simulate real life conditions, shock pulse is a desirable and convenient way to describe shock. Several ideal shock pulse shapes are displayed in Figure 1.7. These shock pulses are described by representations of acceleration as a function of time. They can be easily

reproduced in one laboratory to another. Furthermore, there are mathematical equations for describing these pulses in terms of any motion parameters.

Types of classical shock pulses are namely; square, half-sine, haversine, triangle, quarter-sine, sawtooth and parabolic cusp. Classical shock inputs are accepted and used for shock profile synthesis in MIL-STD-810G testing standard [5]. Another way of describing shock pulses are shock response spectra. Shock response spectrum concept will be discussed in following chapters. There are also types of shock inputs like pyroshock, which is short duration, high acceleration shock pulse and seismic shock which is low acceleration, long time, and high displacement shock input [7].

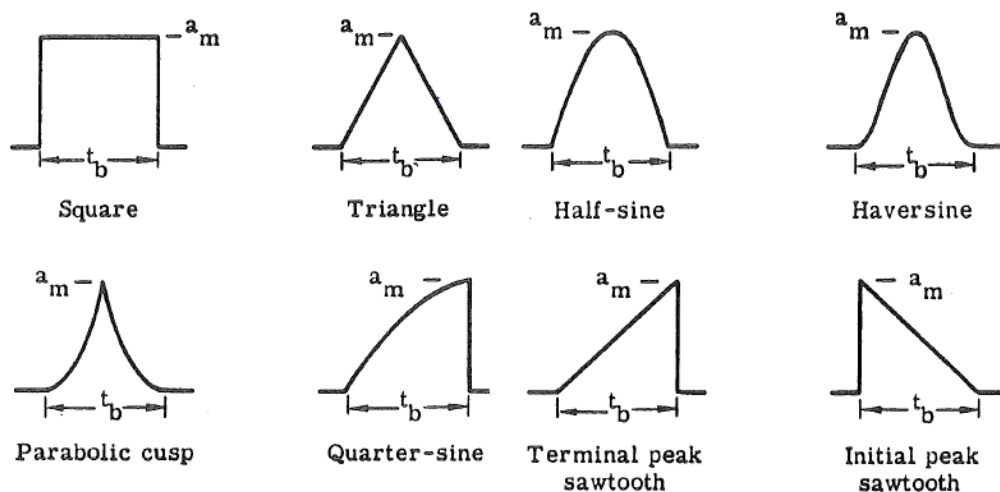


Figure 1. 7 Examples of shock pulses

Shock phenomenon is described as dynamic occurrence whose duration is short relative to the natural frequency of the system excited. Such effects can be caused by several sources. Handling, transportation and shipment are the most common sources of shock. Shock created during coupling of rail cars or cargo handling procedures can be the examples of these types of shock sources. Drop shock is

another special case of shock sources. During manufacturing processes machines or other heavy equipment may produce shock loading that may damage nearby equipment. Ballistic impact, collision impact and explosive shock are the sources that can usually be encountered in military applications. Blast impacts, landing of aero-vehicles, pyrotechnic excitation and earthquakes are among other type of sources. In particular for this thesis, the most important source is underwater explosions near ships and submarines producing a very serious shock environment. Considering the magnitudes and durations of the shock sources mentioned above, they show variety of shock effects from one application to another.

Table 1. 1 Shock Effects of Various Shock Pulses [6]

Type of Operation	Acceleration (g)	Duration (sec)
Elevators:		
Average in "fast service"	0.1-0.2	1-5
Comfort limit	0.3	1-5
Emergency deceleration	2.5	1-5
Public transit:		
Normal acceleration and deceleration	0.1-0.2	5
Emergency stop braking from 120 kph	0.4	2.5
Automobiles:		
Comfortable stop	0.25	3-5
Very undersirable	0.45	3-5
Maximum obtainable	0.7	3
Crash (potentially survivable)	20-100	0.1
Aircraft:		
Ordinary take-off	0.5	10-40
Catapult take-off	2.5-6	1.5
Crash landing(potentially survivable)	20-100	0.25
Seat ejection	10-15	0.25
Man:		
Parachute opening-40000 ft	33	0.2-0.5
6000 ft	8.5	0.5
Parachute landing	3-4	0.1-0.2
Fall into fireman's net	20	0.1
Approximate survival limit with well distributed forces (fall into deep snow bank)	200	0.015-0.03
Head:		
Adult head falling from 6ft onto hard surface	250	0.007
Voluntarily tolerated impact with protective headgear	18-23	0.02
Earthquake:		
Richter Scale Magnitude 6.5	0.5	20-30
Maximum possible shock	1.0	20-30
Underwater Shock:	40-2000	0.001-0.1
Pyrotechnic Shock (Stage Operation):	100-15000	0.0001-0.001

Shock testing is very important to simulate the shock environment in laboratory conditions in proper and reliable manner. For different shock environment,

different test methods should be selected. Determining factors of these methods are shock amplitude, shock duration and the dimensions of to-be-tested part. Shock testing methods can be classified as following [8].

- Simple Shock Pulse Machines
 - Drop Tables
 - Air Guns
 - Vibration Machines
- Complex Shock Pulse Machines
 - High-Impact Shock Machines
 - Lightweight Machines
 - Medium-Weight Machines
 - Heavy-Weight Machines
 - Hopkinson Bar
- Multiple Impact Shock Machines
- Rotary Accelerator

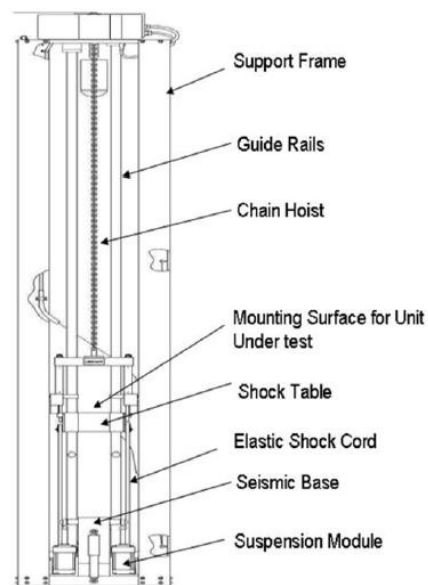


Figure 1. 8 Accelerated drop-table [8]

1.3 Ship Shock and Underwater Explosions (UNDEX)

The earliest naval mines were designed to breach the hull of a ship below the waterline and cause flooding. Over years, underwater warfare became more complicated and turned to water delivered and air delivered torpedoes, air delivered bombs, contact and influence mines and anti-ship missiles etc. Following years, especially after the World War II, navies studied on to understand the phenomena of underwater explosion and develop design methodologies to reinforce ships against the threat. Because, the effects of such explosions may collapse the whole structure of ships and submarines, or may cause severe damages to electronic equipment, warfare technologies or structural parts. Machinery and equipment for naval application must be designed to operate under these severe conditions. The shock conditions for naval applications are more severe than most of the other military operations like tanks and airplanes. Therefore, shock competitive ship/submarine design, component survival precautions and shipboard design improvements have become primary issues for underwater explosion survival.



Figure 1. 9 USS OSPREY-MHC 51(left) [9] and CG 53(right-Courtesy of U.S Navy) Ships Full-Scale Shock Trials

1.4 Motivation

COMINT high gain dipole antenna designed for electronic warfare is used on a submarine platform as a part of a C-ESM/COMINT system. Therefore, the complete system is to be operating with underwater platform requirements. In order to meet these requirements, the design considerations, analysis, tests and qualifications should be performed.

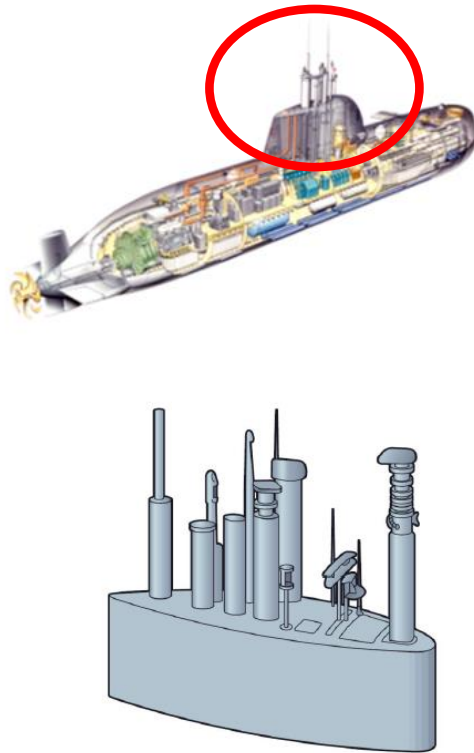


Figure 1. 10 Underwater Antenna Platform

Underwater shock disturbances may cause some malfunctions to antenna structure. In electromagnetic point of view, shock may cause changes in material dielectric strength, variations in magnetic and electrostatic field strength; material electronic circuit card(or board) malfunction, damage or electronic connection failure and

material failure as a result of increased or decreased friction. In mechanical point of view, shock may cause permanent mechanical deformation as a result of overstress of material, collapse of mechanical elements as a result of ultimate stress of the material being exceeded, accelerated fatigue of materials and material failure as a result of cracks, delamination or fracture of radome (radar-dome; composite, high strength mechanically protection material which allows electromagnetic waves to pass).

Because of these impending harmful consequences of shock disturbances on antenna structures mentioned above, customers require antenna structure (as the whole ELINT system) to endure operations without any failure, therefore, to pass certain quality assurance tests compatible with pre-specified military standards. In order to design a structure that can withstand to shock pulses or qualify the antennas designed before, and if necessary take shock isolation precautions for the system, complete shock analysis is essential.

1.5 Scope, Objective and Contribution of Work

In the scope of this thesis, shock analysis of the antenna structure subjected to underwater explosions is performed. Complete shock analysis consists of determination of underwater shock characteristics, analytical solution of shock phenomenon, finite element model solutions of shock phenomenon, shock testing and shock isolation of the antenna structure with the platform.

Design specifications of naval electronic warfare applications for foreign customers contain harsh naval shock survival criterion. Therefore, mechanical structures of those systems should withstand and pass laboratory test for naval shock. Preliminary design considerations should be taken and further actions should be carried with those shock analysis and tests beforehand. Thus, underwater explosion shock (UNDEX) should be analyzed analytically and should be qualified with

finite element models and experiments. Most of the customers of those C-ESM systems are foreign and since defense test method standards like MIL-STD-810F/G used in military applications do not contain underwater shock inputs and testing methods, other standards such as BV043 or STANAG are taken as reference. Therefore, shock inputs and testing methods are determined by shock profile synthesis of those standards into possible frequently used signals and methods. Mathematical model of antenna structure is built both SDOF and MDOF point of view. For these models, solution techniques and faster solution algorithms are provided. Pre-defined and synthesized shock pulses are used as input signals to solve those equations. Finite element model that describes the phenomenon is created for the problems analytically solved before. These finite element model verifications can be the guide for complex geometries that are very hard to build complete analytical model. Further, those analytical and mathematical models are validated with experiments. As shock loadings are very harmful for electronic components, isolation of the structure is needed. Therefore, shock isolation techniques are investigated and isolation alternatives are compared. Since commercial products do not meet the electrical requirements of antenna, a shock isolator for the antenna structure is designed. Analytical solution, finite element analysis and experiments are performed for this isolation case, afterwards.

Analytical and finite element model can be used instead of experimentally difficult verifications, as experiments of shock cases with high impact short time duration for big and bulk mechanical parts are very hard. Similarly, experimental analysis can be used instead of analytical or FE models when the system consists of elements that are hard to model like composite structures, isolator or other non-linear elements. Therefore, this study contains all possible ways for underwater shock analysis and design that can serve guidance for designers from preliminary designs to post-failure isolation problems.

1.6 Outline of the Dissertation

In chapter 2, background and literature surveys on topics relevant to the study are presented.

In chapter 3, shock profile synthesis is performed and shock inputs are determined with respect to the project requirements. Shock profiles are synthesized from BV043 standard into classical shock inputs which are capable to be performed in laboratory conditions.

In chapter 4, mathematical modeling of an antenna structure as a cantilever beam will be performed. Modal analysis using Euler-Bernoulli Beam Theory is used for continuous modeling of antenna structure. Then, transient response of the antenna to shock impulse is examined and integrated to mathematical model.

In chapter 5, results of mathematical built for antenna structure is presented. Multi-degree-of-freedom transient shock analysis using mathematical model is examined in detail and solutions of simplified models are presented. Finally, success of MDOF model is discussed and comparisons between alternative solution methods with MDOF are observed.

In chapter 6, transient finite element analysis of antenna structure is performed by means of ANSYS®. Modal analysis results and transient responses of antenna is presented and compared with mathematical model solutions.

In chapter 7, experimental analysis of antenna structure is performed. Mathematical model results and finite element analysis results are compared with experimental analysis results in order to observe accuracies for validation of these models.

In chapter 8, antenna performance criteria are discussed from both electromagnetic and mechanical point-of-views. Shock isolation theory is explained and shock isolation of antenna structure is performed. Finally, validations of isolation elements are performed by experimental analysis.

In chapter 9, results are summarized and evaluated together, while conclusion is drawn including the recommendations for future work.

CHAPTER 2

LITERATURE SURVEY

2.1 Historical Background

Theoretical and experimental studies dealing with shock are totally related to the basic laws of dynamics and fundamentals of vibration. Therefore, it is vital to mention about few developments about dynamics in general and particularly vibration. It is believed that the serious study on vibration has begun with Galileo. In his, “Discourse Concerning Two New Sciences” [10] published in 1638, fundamental law of oscillating pendulum is illustrated and the new phenomenon “resonance” is introduced. In the same years, Christian Huygens worked on compound pendulum with the analysis of restricted motion along a circular path and the theory of wave propagation.

Hooke’s search on stress and strain and Descartes’ development on the Cartesian coordinate system were important contributions on vibration analysis. However, Isaac Newton suggested the milestone law, namely the second law of motion, which is the basis of almost all vibration related equations of motions. Following Newton’s teachings about calculus use on vibratory problems, several mathematical techniques that advanced vibration analysis are introduced. Among them, Taylor Series is useful in response calculations, D’Alambert principle is applied to forced vibration problems and Lagrange equations are used to express equations of motion in terms of energy principle.

Principle of superposition was published by Daniel Bernoulli in 1755. Fourier, on the other hand, extended the principle and applied it to the theory of oscillations.

Fourier also proved the theorem, Fourier Transform, which states that any periodic function can be represented as a sum of sines and cosines.

Lord Rayleigh integrated all available information about sound and vibration and published the first complete, formal and useful presentation on sound and vibration. Up to and including the Rayleigh era, sound and other vibration phenomena were treated together. Beginning in the 20th century, specialization of vibration began and some of the sub-specialty categories like vibration engineering, flutter engineering, acoustical engineering are introduced. The first modern dissertation about mechanical vibration was written by Timoshenko including the topics as understanding of vibration, vibration isolation, vibration influence on fatigue life, vibration monitoring and so forth.

Although it is not certain, mechanical shock term was used to refer the need of specific areas compatible with the development of technology. With those developments in technology, military equipment is likely to withstand harsh effects of environments produced during warfare. For example, During World War I, shock testing machine for testing shipboard equipment to survive shock produced by the blast from ship guns was developed. With the necessity of detailed considerations of shock related phenomenon, some organizations like Shock and Vibration Information Center, Shock and Vibration Information Analysis Center were founded; several technical papers on shock problems are published in the proceedings of professional societies like ASME, IES and etc. , shock and vibration symposia and other specialized societies. Important textbooks in the field like The Shock and Vibration Digest, Harris' Shock and Vibration Handbook and Shock and Vibration Bulletins are published.

2.2 Literature Survey

In the study, numerous sources in literature were reviewed. Reviews were focused on shock concept, shock response spectrum theory, calculation of shock response spectrum, single degree of freedom and multi degrees of freedom mathematical modeling of shock, underwater shock phenomena, cantilever beam theories, numerical solutions of multi degrees of freedom shock, continuous modeling of cantilever beams, finite element modeling using commercial software like ANSYS®, shock testing methods, shock isolation and other topics relevant to the study. Only limited part of those sources are included to literature survey part for brevity.

The concept of shock spectra was first introduced in a printed manner by Maurice Biot [11-13]. He focused on the damage potential of earthquake motions. He defined earthquake spectrum (or response spectrum) as the maximum response motion from the series of single degree of freedom oscillatory systems in the frequency range of interest. In his PhD. Thesis [14], Biot showed the effective number of modes to be interested for design concerns. He focused on earthquake motions and he used the assumption that dynamic motion of the building does not affect ground's motion; however, studies demonstrated that this assumption is very conservative.

Mindlin [15] suggested that this response spectrum approach can be used for general types of shock motions. He suggested that damage potential of different shock motions can be compared with this method. Later, Housner [16] developed the first seismic spectra that can be attained by averaging of eight ground motion records. These records were obtained two each from following earthquakes, El Centro(1934), El Centro(1940), Olympia(1949) and Tekiachapi(1952).

Newmark [17], on the other hand, used the amplification factors applied to maxima values of ground motions respectively and used them to create earthquake design spectrum. In this spectrum, for different probabilities of occurrence and a range of

damping of the structure, amplification is listed. He also presented the relation for development of spectrum from ground motion maxima. Shock spectrum level becomes maximum ground acceleration level at relatively high frequencies which is the aforesaid feature seen in El Centro earthquake. Newmark [18] also proposed the series of single step integration methods to solve structural dynamic problems especially for blast and seismic loading. However, Newmark's methods have been applied to various dynamic analysis problems. Moreover, these methods have been improved and modified by researchers working in similar areas of structural dynamics applications.

Alexander [19] published a paper as a basic overview of a shock response spectrum containing the definition and history of shock response spectrum. He also summed up the events characterized by shock response spectrum and added milestone examples of those events. He also discussed the shock response spectrum analysis of linear multi-degree-of-freedom structures. He presented the formulation that used mode superposition in conjunction with shock response spectrum and estimated the maximum dynamic response of a linear system without solving the transient multi-degree-of-freedom equations of motions. Alexander also presented the history and development on naval shock design spectra specifically.

Tuma and Koci [20] proposed the new method of shock response spectrum calculation related to an acceleration signal which excites the resonance vibration of substructures. The maximum or minimum of the substructure acceleration response is determined by shock response spectrum as a function of the natural frequencies by means of a set of the single degree of freedom systems modeling for those substructures mentioned. The shock was recorded as acceleration signal in digital form and IIR digital filter was used to approximate the single degree of freedom systems. Then filter response corresponding to the sampled acceleration signal was straightforwardly calculated. Thus, the excitement partition of individual component of the impulse signal to the mechanical structure to resonate can be easily monitored by means of shock response spectrum.

Smallwood [21] simulated the improved recursive formula for calculating shock response spectra. The aim of this study is to enhance the recursive formulas that are based on impulse invariant digital simulation of a single degree of freedom system since the results of such simulations contain significant errors when the natural frequencies are greater than one sixth of the sample rate. To do this, one more filter was added to recursive filter and good results were obtained over a broad frequency range even for the frequencies exceeded the sample rate.

Kelly and Richman [22] shed light on some physical descriptions and mathematical representation of the shock response spectrum. This article has been taken as a reference and guidance in numerous books on the similar subjects and research studies. The main idea of this study was to correct several typographical errors in the Biot's presentation of a recursive algorithm for shock response spectrum calculations. Another purpose of this study was to present a MATLAB® implementation of the corrected algorithm.

Irvine [23] presented a complete study on shock response spectrum. In the study, he defined shock response spectrum and illustrated its physical meaning with real case examples. Irvine modeled the shock response spectrum and showed half sine and pyrotechnic impulse examples which are converted from time history to response spectrum. In this study, Irvine also derived the time response of the single degree of freedom system subjected to shock input. Calculating time response of the system, Z-transform method [24] was introduced for both acceleration and force shock cases. For calculating frequency domain solutions, Fourier spectra method is introduced. Irvine also gave significant information about the error sources of data collection of shock events, shock response spectrum slope and component qualification test methods in this study. In another study of Irvine [25], shock response of multi-degree-of-freedom systems are investigated. In this study, approximation methods that can simulate multi-degree-of-freedom system as the summation response of a series of single-degree-of-freedom systems are presented namely Absolute Sum, Square Root of the Sum of the Squares, Naval Research

Laboratories method. Results of these methods are compared to the mode superposition method on a simple example.

Parlak [26] performed an experimental analysis of the shock produced by repetitive recoil shocks due to machine gun firing. Integrated circuit piezoelectric accelerometers were located at four predetermined points in order to test the shock and vibration on the system. In order to define minimum shock profile that the electronic components can survive, shock response spectrum analysis was performed. The aim of the study was to use those equivalent shock profiles for shock qualification testing of similar equipment located on military low level air defense system.

Burgess [27] performed a study as a PhD. thesis on the use of experimental modal analysis techniques with Fourier transform methods in order to apply on the transient response analysis of structures. Primarily, linear structures were taken into consideration to examine the limits and validity of the approach. At the same time, errors related to the time aliasing within the inverse Fourier transform were derived. Several experimental procedures for modal analysis were applied to demonstrate the method on a beam structure. Further, the applicability of the same analysis and prediction techniques was explored. Prediction methods included using specific linear models and developing non-linear models that describe transient response. Linear multi degree of freedom systems were also examined in the scope of the study and structural nonlinearity was added to the models as concentrated single component.

Bhat et. al, [28] applied shock response spectrum analysis approach to obtain optimum design parameters for electronic devices. Bhat performed the analysis using commercial software ANSYS® and obtained the results of dynamic analysis of printed circuit board (PCB) in order to use for designing compliant suspension and cushions.

Wang et. al [29] created the mathematical modeling and mechanism analysis of a novel heavy-weight shock test machine simulating underwater explosive shock environment. They also performed numerical solutions to evaluate the limitations of shock test machine under various shock velocity inputs. The proposed test machine can produce nearly the same pulse forms as noted in standards as BV043/85 OR MIL-S-901D. The proposed system and mathematical model provided theoretical basis and design techniques.

Campos [30] showed the great correlation between analytical and experimental results using Euler-Bernoulli theory and finite element analysis to solve shock impulse acting on cantilever beam. Based on these correlations, Campos modeled the blade of an impeller as a cantilever beam and found out the mode shapes and natural frequencies to use this information for preliminary bladed impeller design. He also analyzed the mixed flow fan under ballistic shock impact by means of finite element analysis and classical theory in order to illustrate real system responses to shock loading with help of Full Method and Mode Superposition Method. Campos also investigated the effects of variation pulse width in the acceleration input while he was analyzing the shock loading under simple continuous structures using finite element analysis.

Haukaas [31] derived the fundamental governing differential equations for Euler-Bernoulli type beams namely equilibrium and section integration, material law and kinematics. He extended the study bending analysis, specifically, shear stress in bending and bi-axial bending for different type of structures with different cross-sections. He also explained the shear centre concept for both open cross-sections and closed cross-sections.

Yang [32] provided an interactive handbook containing formulas, solutions and MATLAB® toolboxes for stress, strain and structural dynamics problems. Fundamental terms like beam types, boundary and initial conditions, response time, effective excitement time, damping, modal damping and output control were introduced. Static analysis of Euler-Bernoulli (EB) beam was explained in order to

give useful information that will be the background of dynamic analysis. In dynamic analysis part, mode shapes of EB beams, time response and state space response of beams and internal forces were presented along with the governing equations and analytical solutions.

Remala [33] presented an overview of numerical integration methods for the solution of linear equations. In the study, central difference method, Newmark time integration method and Newton-Raphson were included. A simple example to calculate the response of spring-mass system were calculated using both central difference and Newmark method in order to illustrate how the methods are implemented to any vibration problem. Remala also presented general information about Newton-Raphson method as an implicit numerical integration method to solve nonlinear structural problems.

DeBruin [34] discussed the potential error source created by shock-isolation systems and provided a guideline to make configuration planning to ensure system performance, installation and operation of an antenna system. He explained the potential source of error the shock-isolation systems such as wire rope isolators or encapsulated wire rope selected to make system survive from the shock requirements of tracked vehicles, vehicles supporting large-caliber cannons and armored vehicles subjected to ballistic shock.

Parlak [35] studied the shock and vibration isolation of machine gun firing where machine gun together with isolator is located on a military platform. First predefined isolator on the system was used for field test in order to determine shock levels on the system. Then, a mathematical model compatible with the experimental result was built. Making some changes in the parameters of the model, it was possible to improve the model to simulate real world situations. Moreover, the study investigated the calculation of shock levels to test the materials which are subjected to repetitive shock pulses. SRS analysis was done to define shock specifications of the some equipment on the military platform.

Klembczyk [36] provided a guideline on numerous methods and applications of implementing isolation, shock absorbing and damping to dynamic systems and structures. Shock, vibration and structural control problems can be solved essentially with successful integration of these tools. Therefore, with this study, Klembczyk aimed to equip the engineers with basic understanding of isolation system attributes that have been proven to be reliable and effective to solve great amount of the shock and vibration isolation applications.

From these literature survey process, useful information about SRS calculation methodology and formulation is used especially sources from Biot [11-13] and Alexander [19]. As a solution alternative, Digital Recursive Filtering Relationship method and its applications are learned along with case studies [20-24]. During the modeling process of antenna structure as cantilever beam with Euler-Bernoulli Theory, various sources are scanned and useful information are extracted from these as presented in following chapters in detail [30-34, 36]. For MDOF transient analysis procedure, modal transient related topics are scanned along with Ramp Invariant Digital Recursive Filtering Method [23-25, 28]. Shock isolation for components are another important issue which is researched much. Useful information about shock isolation theory, methodology and case studies are found from literature [34-36]. Apart from these sources mentioned, some other sources are used for certain throughout the study in mathematical modeling chapter. The information exerted from these sources are presented in appropriate parts of the chapters while discussing the importance of those within the methodologies.

CHAPTER 3

SHOCK PROFILE SYNTHESIS

3.1 Theory: Shock Response Spectrum

In order to represent the input pulses or monitor the effect of shock motion on a structure, either the form of time history or commonly used form, namely, shock response spectrum (SRS) is used. While shock isolation, shock hazard monitoring; displacement, velocity and acceleration responses are represented generally in time domain, SRS can be used to verify a structure or a device can support transient disturbances encountered during its real life operational or environment conditions.

“A Shock Response Spectrum is a plot of the peak responses of an infinite number of single degree of freedom systems to an input transient” is the accepted definition of SRS [37]. The degree of freedom can be defined as the ability of an object to move along or around only one axis and these independent degree-of-freedom (DOFs) are selected as references to analyze transient phenomena. Instead of analyzing these DOFs in Fast Fourier Transform (FFT) process, the SRS is introduced as another mathematical tool inherently by this SDOF reference. Indeed, FFT algorithm is not well-matched to non-stationary signals of short duration. Due to the shortness of these oscillations, the severity can be characterized by their maximum effects on the SDOF set.

Even though the selected SDOF reference does not represent the equipment to be tested, one can assume that if two different excitations have the same severity (SRS), they will induce equivalent effects on this equipment. The notion of equivalence is that using synthesized pulse can replace complex or hard-to-generate excitation whose severity is the same. Typical examples can be simulation of

gunfire, seismic shock, underwater explosions, aircraft taking off, and so. Shock response spectrum is a useful tool for estimating the damage potential of a shock pulse, as well as for test level specification. MIL-STD-810F/G requires this format for certain shock environments.

As stated above, the shock response spectrum assumes that the mathematical shock pulse is applied as a common base input to a group of independent single-degree-of freedom systems as shown on Figure 3.1. The peak responses of each system for corresponding natural frequencies are given on SRS curves. In earlier applications, unless otherwise specified, systems are taken as undamped. However, damping is generally fixed to a constant value, such as 5% which is equivalent to an amplification factor of 10 [23].

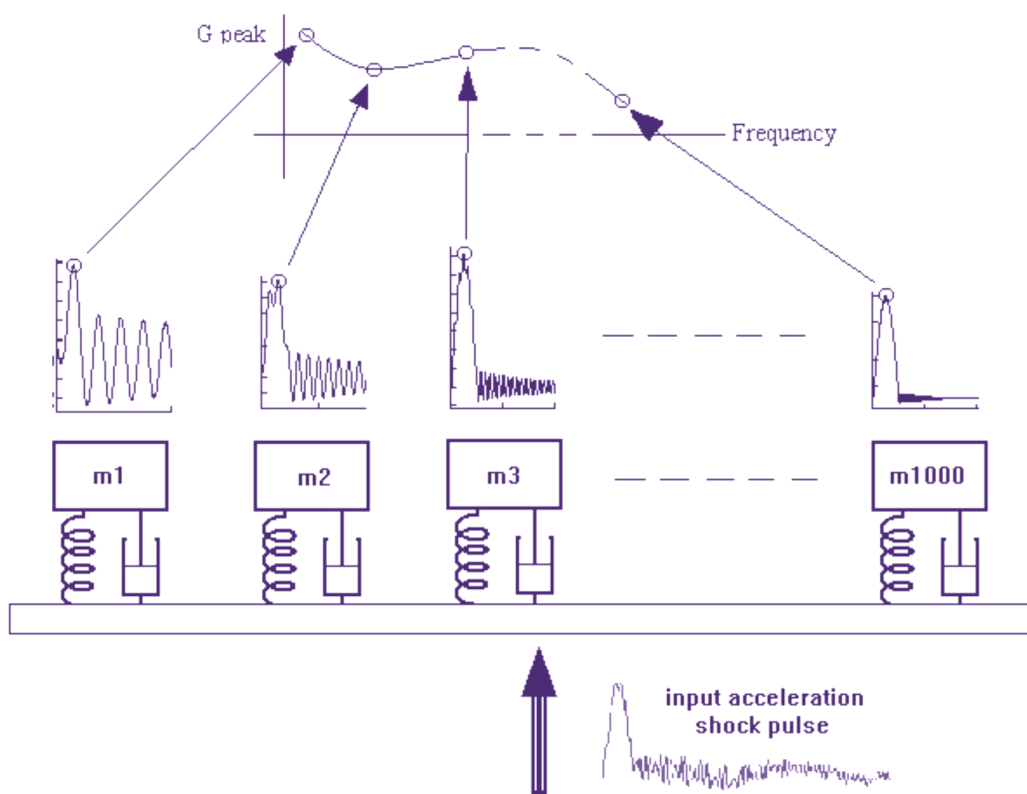


Figure 3. 1 Shock Response Spectrum Concept [38]

The shock response spectrum model can be drawn as following form given on Figure 3.2 as a complete series of single-degree-of freedom (SDOF) systems. For the system, \ddot{Y} is the common base input while \ddot{X}_i is the absolute response of the each system to the input mentioned. M_i represents mass, C_i represents damping coefficient, and K_i represents stiffness for each system, while f_{n_i} represents natural frequency.

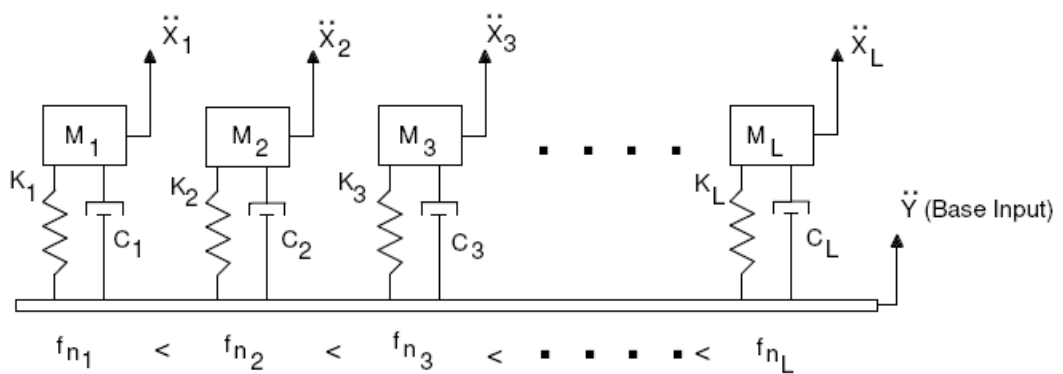


Figure 3. 2 Shock Response Spectrum Model [23]

Applying Newton's law of motion to a free body diagram of an individual system, following one-degree-of freedom is modeled.

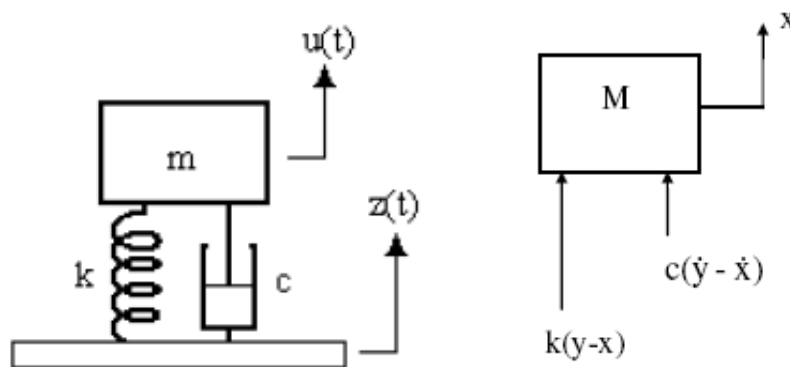


Figure 3. 3 Free-body Diagram of SDOF System [23]

According to the free-body diagram, following governing differential equation of motion can be written:

$$m\ddot{x} + c\dot{x} + kx = c\dot{y} + ky \quad (3.1)$$

Defining relative displacement as $z=x-y$ and substituting this into (1), following equation is obtained.

$$m\ddot{z} + c\dot{z} + kz = -m\ddot{y} \quad (3.2)$$

Natural frequency (ω_n), critical damping constant (c_c) and damping ratio (ξ) are,

$$\omega_n = \sqrt{\frac{k}{m}} \quad (3.3)$$

$$c_c = 2m\sqrt{\frac{k}{m}} = 2\sqrt{km} = 2m\omega_n \quad (3.4)$$

$$\xi = \frac{c}{c_c} \quad (3.5)$$

Furthermore, ζ is often represented by the amplification factor or quality Q, which is defined as $= 1/2\xi$.

Substituting these terms into (2), equation of motion becomes,

$$\ddot{z} + 2\xi\omega_n\dot{z} + \omega_n^2 z = -\ddot{y}(t) \quad (3.6)$$

Equation (3.6) does not have a closed form solution for the general case in which $\ddot{y}(t)$ is an arbitrary input function. Therefore the problem should be solved by convolution integral approach. After that, convolution integral is to be transformed into series for the case $\ddot{y}(t)$ is converted to a form of digitized data. Then, these digitized series of data is to be converted to a digital recursive filtering relationship to accelerate the calculation. The resulting formula for the absolute acceleration is given in Equation (3.7) as follows.

$$\ddot{x}_i = 2 \exp[-\xi \omega_n \Delta t] \cos[\omega_d \Delta t] \ddot{x}_{i-1} - \exp[-2\xi \omega_n \Delta t] \ddot{x}_{i-2} + 2\xi \omega_n \Delta t \ddot{y}_i + \dots$$

$$\omega_n \Delta t \exp[-\xi \omega_n \Delta t] \left\{ \left[\frac{\omega_n}{\omega_d} (1 - 2\xi^2) \right] \sin[\omega_d \Delta t] - 2\xi \cos[\omega_d \Delta t] \right\} \ddot{y}_{i-1} \quad (3.7)$$

where,

$$\omega_d = \omega_n \sqrt{1 - \xi^2} \quad (3.8)$$

Z-transform theory approach is described in many control systems or signal analysis textbooks. For this calculation Dorf, R. [24] is taken as reference. The derivation of the complete formulation is taken from Irvine's paper [23].

Equation (3.8) can be used to calculate the shock response spectrum. One should use this equation for each natural frequency to extract complete spectrum values. Equation (3.8) can be calculated via computer program such as MATLAB®, FORTRAN, and C/C++. In order to apply further synthesis calculations in this chapter, MATLAB® script is prepared. For the calculations damping ratio can be taken as constant for each degree-of-freedom as Q factor.

The alternate method, Fourier transform, can also solve the Equation (3.6); however frequency domain solution is not that useful for shock response spectrum applications. Therefore, digital recursive filtering approach is the best and fastest way to calculate the whole spectrum.

The example for an arbitrary half-sine input (Figure 3.4), Acceleration SRS is given in Figure 3.5. For this input (40g 11ms half-sine), frequency interval is scanned from 1 Hz to 10000Hz, with the modal damping factor value Q=10. Response is plotted on log-log scale in order to observe the wide range of response values together.

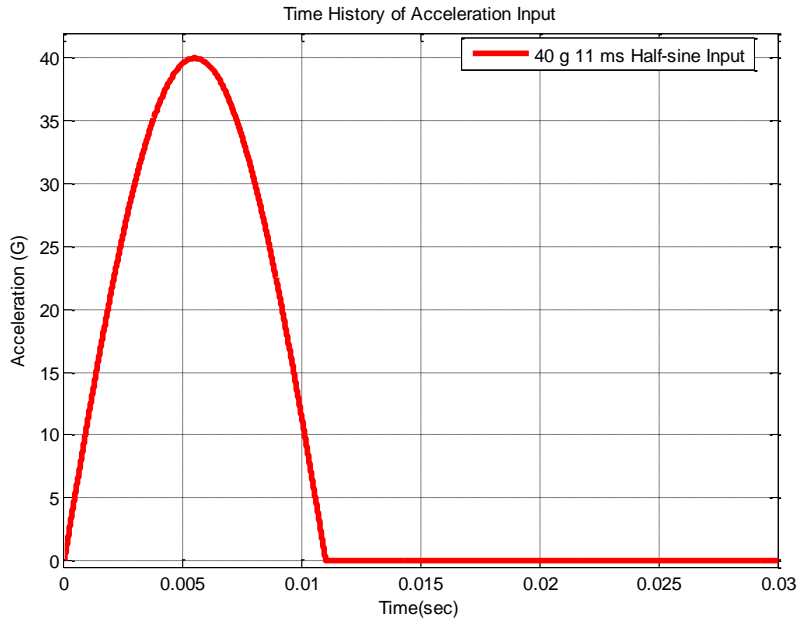


Figure 3. 4 Time History of 40g 11ms Half-Sine Input Signal

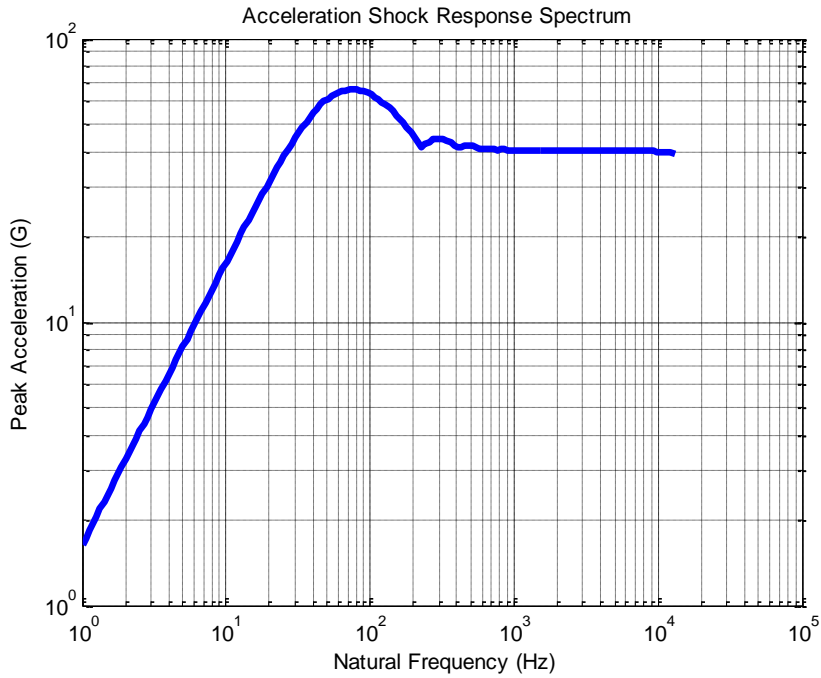


Figure 3. 5 Acceleration Shock Response Spectrum for 40g 11ms Half-Sine Signal

3.2 Shock Response Spectrum for Naval Applications

Shock response spectrum for naval applications is shown in logarithmic graph containing velocity, acceleration and relative displacement information together as shown in Figure 3.6.

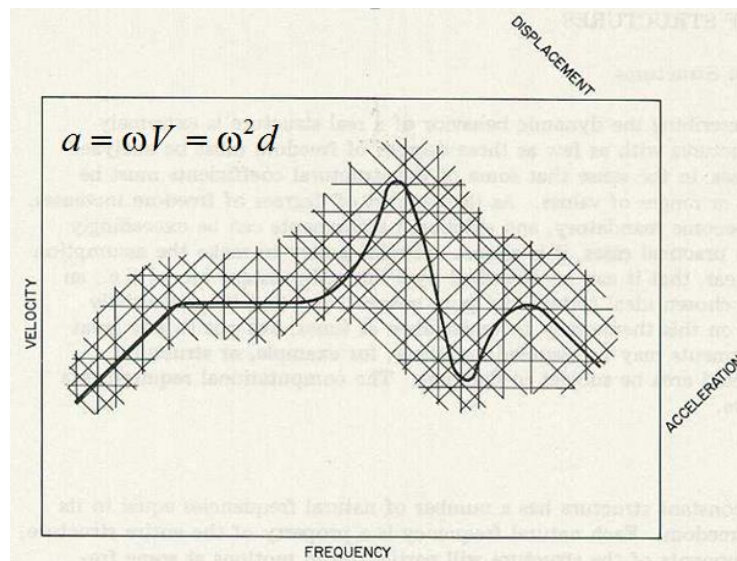


Figure 3. 6 Shock Response Spectrum in four-way log paper [39]

In Figure 3.6, d represents the maximum relative displacement of the single-degree-of-freedom system, a represents the maximum shock response acceleration obtained for shock input. The value of maximum acceleration in time history is half of the value of the acceleration value in spectrum. V is defined as pseudo velocity, because the relation (3.9) between velocity, acceleration and relative displacement is the approximate solution. The exact solution contains complex formula, this approach is preferred. Therefore, V is defined as pseudo velocity. In equations and the response spectrum, ω represents the corresponding natural frequency. The relation between velocity, acceleration and relative displacement is given below:

$$a = \omega V = \omega^2 d \quad (3.9)$$

Investigating the typical naval shock response spectrum (Figure 3.7), following properties of the spectrum is observed. The single-degree-of freedom system behaves highly resistive at high frequency region, namely REGION A. At this region spectrum has the maximum acceleration amplitude. At middle region of spectrum, the resonant region corresponding to shock input (REGION B). At lower frequencies, spectrum has almost constant velocity line. This frequency region (REGION V) is defined as velocity change region. The shock input related to this region can be defined as impulsive step velocity change. At the very left part of the spectrum (REGION D), relative displacement is dominant. Therefore, spectrum has maximum displacement value among the whole response spectra [39].

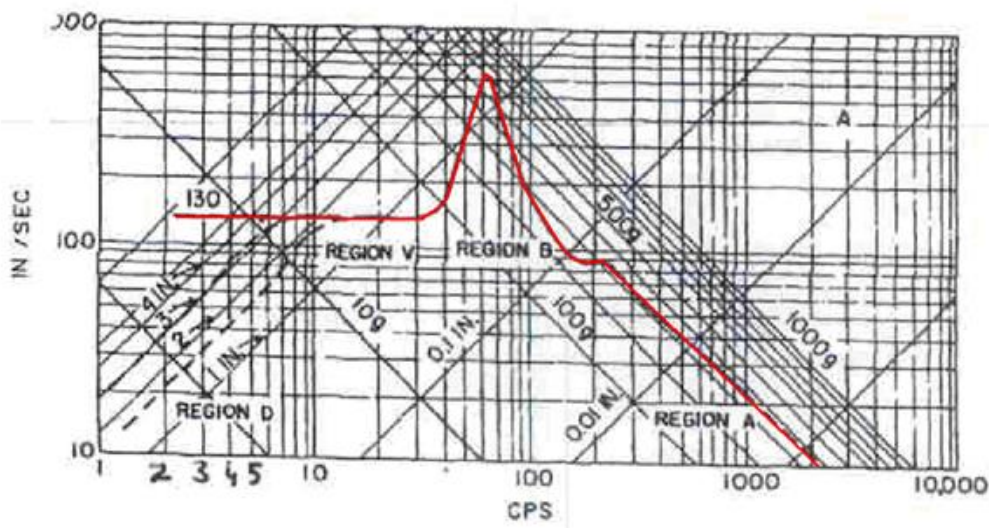


Figure 3. 7 Shock Response Spectrum Regions [39]

3.3 Determination of Assessment Criteria from Shock Response Spectrum

BV043 standard [39] is the building specification for ships of the German federal armed forces standard. MIL-S-901D [70] standard is a military specification for High Impact mechanical shock which applies to equipment attached on naval platforms. In this standard, shock qualification criteria of the structure is defined with shock testing procedures like full-scale ship/submarine tests and floating barge test. Since MIL-STD-810F/G does not cover any naval shock or underwater explosion testing standard, and in Turkey there is no facility to perform MIL-S-901D testing standard requirements, the equivalent, even harder to perform standard BV043 is typically taken as reference for naval projects, as a demand of customers. In BV043 standard, the shock loadings to act on the equipment attached on standard surface ship and submarine are defined briefly. It is possible to calculate standard time equivalence of the shock signal whose spectrum value is already known by means of BV043. In standards, generally, half-sine or saw-tooth shock forms are used because these types of forms are easy to be generated in laboratory conditions, as double half-sine form is used to in BV043 standard. In following part, double half-sine shock time shock signal determination process is presented. In order to define time input, a_2, a_4, t_1, t_2 and V_1 values should be calculated using tabulated a_0, V_0 and d_0 values from standard.

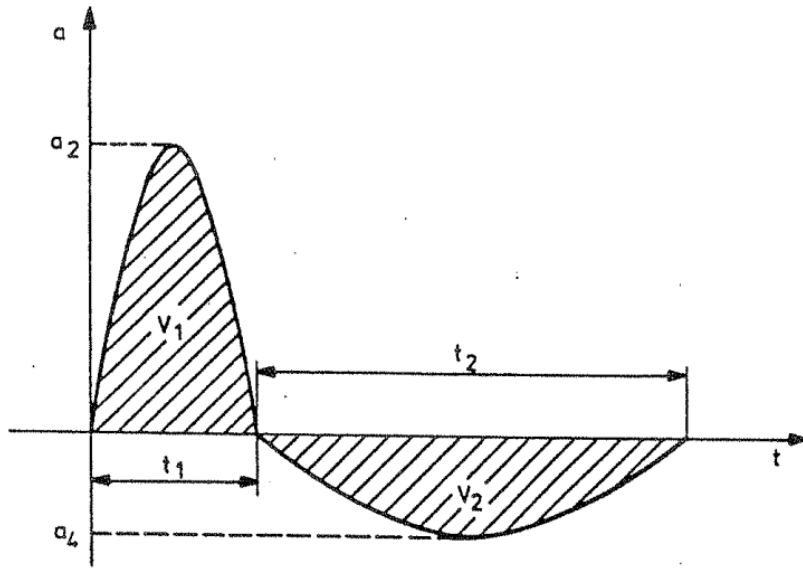


Figure 3. 8 General Form of Double Half-Sine Shock Acceleration-Time Signal

In standard following derivations are explained. The amplitude of the positive half-wave has to amount of half the maximum acceleration, a_0 . The surface below the each half wave has to be $2/3$ of the maximum pseudo-velocity, V_0 . The double integration of this acceleration course has to result a displacement of the foundation that is the maximum relative displacement, d_0 . Therefore, the following formulations can be written. Those formulae are directly used for acceleration-time calculation.

$$a_2 = 0.5a_0 \quad (3.10)$$

$$a_4 = \frac{-\pi V_1}{2t_2} \quad (3.11)$$

$$t_1 = \frac{\pi V_1}{2a_2} \quad (3.12)$$

$$V_1 = \frac{2}{3} V_0 = V_2 \quad (3.13)$$

$$t_2 = \frac{2d_0}{V_1} - t_1 \quad (3.14)$$

Table 3. 1 Values for Acceleration-Time Calculation for Submarine

SUBMARINE					
Diagram	Type of Submarine and direction of shock	Equipment installation location	d_o [mm]	V_o [m/s]	a_o [m/s ²]
7	<1000 t vertical	exterior structure	35	9	3,700
		interior structure	50	7	1,860
8	<1000 t transverse	exterior	35	8.5	3,250
		interior	35	4	1,100
8	<1000 longitudinal	exterior	17.5	4.25	1,626
		interior	17.5	2	550
9	>2000 t vertical	exterior	40	10	4,000
		interior	55	8	2,000
10	>2000 transverse	exterior	40	8.5	3,500
		interior	40	4.5	1,200
10	>2000 longitudinal	exterior	20	4.25	1,750
		interior	20	4.25	600

From Equations (3.10) to (3.14) and the tabulated values given in Table 3.1, acceleration-time signal for the equipment installed on submarine of class >2000t can be straightforwardly calculated. Found acceleration-time signals are tabulated below in Table 3.2. Sample calculation is given in Appendix A.

Table 3. 2 Calculated Acceleration-Time Signals

Double Sine Acceleration-Time Signals		
Shock Axis	Positive	Negative
Longitudinal (X)	90g 5.2ms	-53g 8.8ms
Transverse (Y)	179g 5.1ms	-101g 9.1ms
Vertical (Z)	205g 5.3ms	-158g 6.8ms

3.4 Shock Synthesis

In previous section, acceleration-time input signal is determined from shock response spectrum. However, double-sine shock input is hard to generate in laboratory conditions in Turkey. Therefore, double-sine signals extracted from BV043 standard should be synthesized to half-sine form. Performing this, testing procedure of the antenna will be so easy that half-sine form can be generated easily by means of drop table as an example.

In MIL-STD-810G Method 516.5, for shock profiles used in the form of shock response spectrum inside the 90% of 10-2000Hz frequency interval, -1.5/+3 dB tolerance is defined. Therefore, in this section half-sine shock profiles with minimum amplitude and time that contains the shock profiles (presented in Table 3.2) in -1.5dB tolerance (amplitude $\times 0.8414$) interval is derived. For shock response profile synthesis, previously written MATLAB® code in Section 3.1 is used. For SRS calculations, $Q=10$ is taken as preferred in MIL-STD-810G. For axis determination, following definition is used (Fig 3.9).

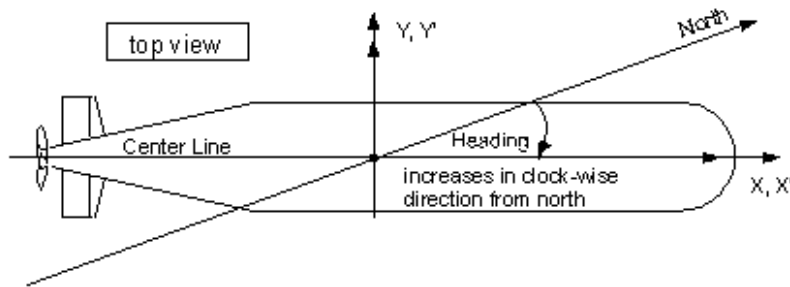


Figure 3. 9 Axis Definitions for Submarine

3.4.1 Longitudinal (X) Axis Shock Synthesis

In Part 3.3, longitudinal axis shock profile is calculated as 90g 5.2ms -53g 8.8ms double half-sine profile. In this part, half-sine shock profile that contains previously given double half-sine signal in -1.5dB tolerance with minimum amplitude and time. The calculated shock profile and profile found from BV043 standard is compared in shock response spectrum given in Figure 3.10.

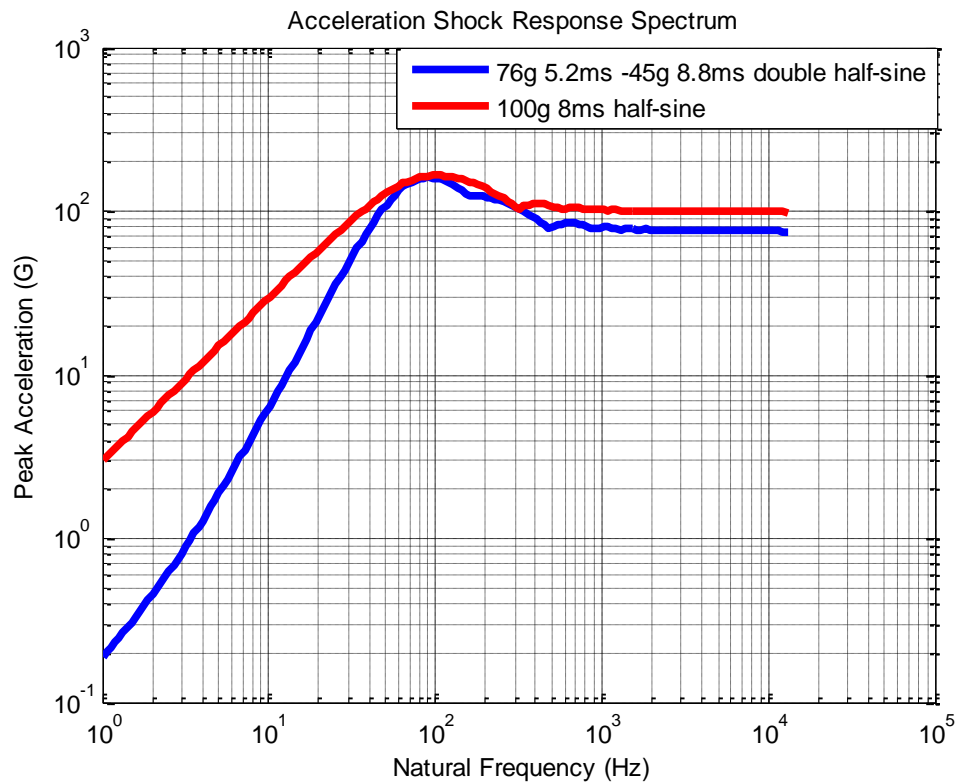


Figure 3. 10 Defined by BV043 (blue) and Synthesized (red) Shock Profile Shock Response Spectrum for X Axis

3.4.2 Transverse (Y) Axis Shock Synthesis

In Part 3.3, transverse axis shock profile is calculated as 179g 5.1ms -101g 9.1ms double half-sine profile. In this part, half-sine shock profile that contains previously given double half-sine signal in -1.5dB tolerance with minimum amplitude and time. Found shock profile and profile found from BV043 standard is compared in shock response spectrum given in Figure 3.11.

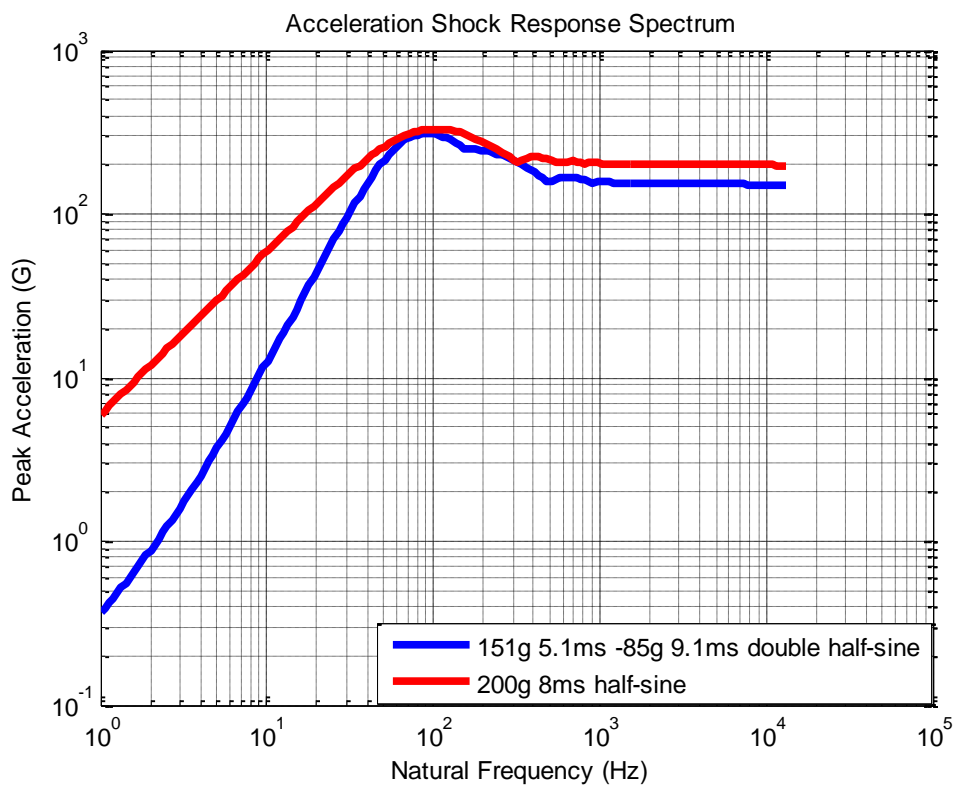


Figure 3. 11 Defined by BV043 (blue) and Synthesized (red) Shock Profile Shock Response Spectrum for Y Axis

3.4.3 Vertical (Z) Axis Shock Synthesis

In Part 3.3, vertical axis shock profile is calculated as 205g 5.3ms -158g 6.8ms double half-sine profile. In this part, half-sine shock profile that contains previously given double half-sine signal in -1.5dB tolerance with minimum amplitude and time. Found shock profile and profile found from BV043 standard is compared in shock response spectrum given in Figure 3.12.

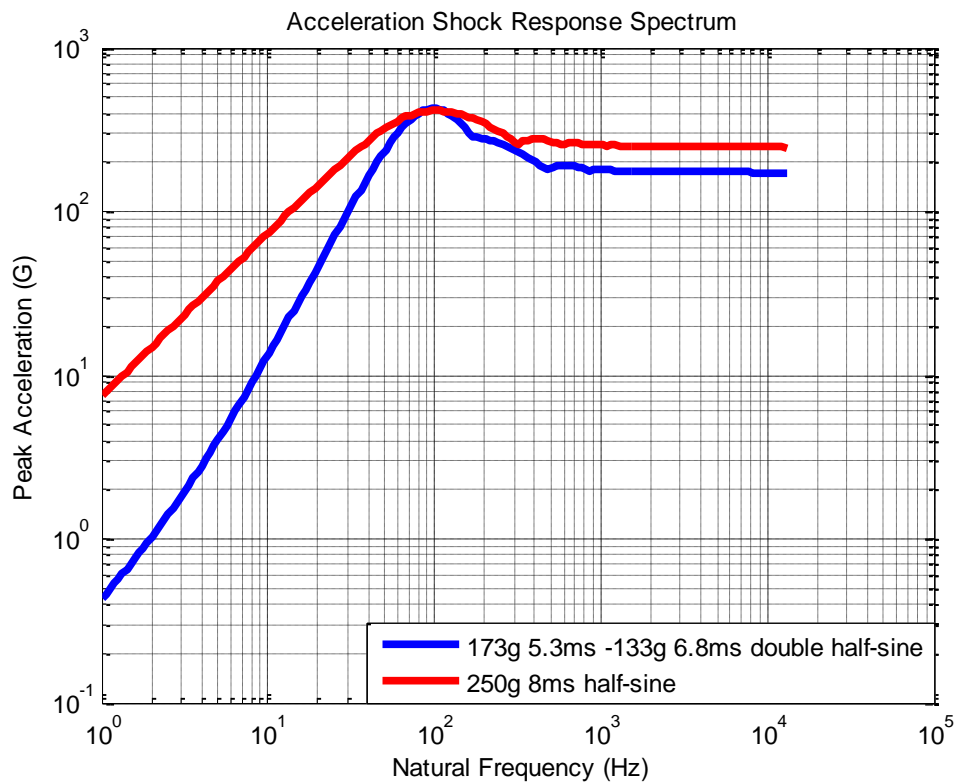


Figure 3. 12 Defined by BV043 (blue) and Synthesized (red) Shock Profile Shock Response Spectrum for Z Axis

For the complete shock analysis performed in this study, following shock profiles are used in order to satisfy corresponding BV043 shock criterion. As seen on plots, synthesized shock profiles fully cover the required profile.

Table 3. 3 BV043 Shock Requirements

BV043 SHOCK PROFILE REQUIREMENTS		
Shock Axis	BV043 Shock Requirement	Requirement After -1.5dB Tolerance
Longitudinal (X)	90g 5.2ms, -53g 8.8ms	76g 5.2ms, -45g 8.8 ms
Transverse (Y)	179g 5.1 ms, -101g 9.1ms	151g 5.1 ms, -85g 9.1 ms
Vertical (Z)	205g 5.3 ms, -158g 6.8ms	173g 5.3ms, -133g 6.8ms

Table 3. 4 Calculated and Synthesized Shock Profiles

Acceleration-Time Signals		
Shock Axis	BV043 SHOCK REQUIREMENT	SYTNYHESIS RESULTS
Longitudinal (X)	76g 5.2ms, -45g 8.8ms Double Half Sine	100g 8ms Half Sine
Transverse (Y)	151g 5.1 ms, -85g 9.1ms Double Half Sine	200g 8ms Half Sine
Vertical (Z)	173g 5.3 ms, -133g 6.8ms Double Half Sine	250g 8ms Half Sine

CHAPTER 4

MATHEMATICAL MODELING OF THE ANTENNA STRUCTURE

Problem Definition

C-ESM/COMINT antenna system is located on submarines and special type of navy ships. The location of the platform is just upper side of the periscope support. The dipole COMINT antenna mentioned in Chapter 1 is located vertically or horizontally in regards to the polarization needs. Attachment of antenna onto the platform can be basically described as fixing its base to the platform with bolted joints as illustrated in Figure 4.1. The other side of antenna is free. Therefore, for antenna structure, shock input can be categorized as “base acceleration” type input. Half-sine base acceleration shock input is determined for modeling as shock profiles under considerations are of half-sine. Moreover, dynamic response of antenna structure can be approximated by a cantilever beam since antenna structure shows similar boundary conditions and geometrical properties as cantilevered beams. For continuous modeling of antenna structure, Euler-Bernoulli beam model is used. Upon calculation of natural frequencies and mode shapes, these data is input into multi-degree-of-freedom transient analysis. Transient responses in terms of acceleration, relative velocity and relative displacement of the antenna structure are obtained exactly and numerically by different methods for MDOF models, and approximated; SDOF models. The major point of interest is the tip point response of the antenna, because electrical components are placed in the vicinity of the tip of the antenna. Typical electrical components are illustrated in Figure 4.2.

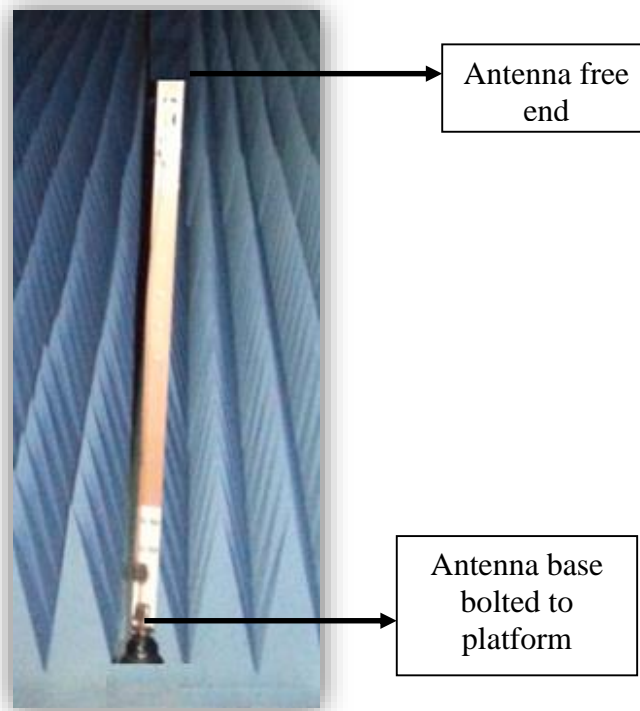


Figure 4. 1 Antenna Structure Attached to the Platform



Figure 4. 2 Electrical Components Placed on Antenna Tip

The beams for which the Euler-Bernoulli model is sufficient are called slender beams according to Majkut [40]. A beam is considered as a slender beam if beam length is at least ten times the thickness. The length of dipole antenna considered in this study is far more than ten times the beam thickness. Therefore, slender beam assumption is held. Apart from that criteria, following assumptions are made [30].

- Antenna material is homogeneous and isotropic.
- Antenna material obeys Hooke's Law.
- Antenna structure is straight and it has uniform cross section.
- Plane sections of antenna structure remain plane and perpendicular to the neutral axis [31].
- Deformations of antenna due to bending are much larger than those due to shear, therefore shear deformation effects are neglected [41].
- Area moment of inertia and cross sectional area of the antenna structure is constant [42].
- Plane sections of antenna structure perpendicular to the centroidal axis remain plane after deformation [43].
- The motion of antenna is solely translational in the vertical direction.
- Rotational inertia of antenna elements is considerably small comparing to translational inertia. Therefore, effect of rotational inertia can be overlooked.

4.1 Modal Transient Response of the Antenna Structure Subjected to Base Excitation

In this section, mathematical modeling of the antenna structure as a cantilever beam will be performed. Then, response of the antenna to shock impulse applied at its base is examined.

4.1.1 Normal Modes, Natural Frequencies and Mode Shapes of the Antenna Structure

The antenna structure can be modeled as in Figure 4.3.

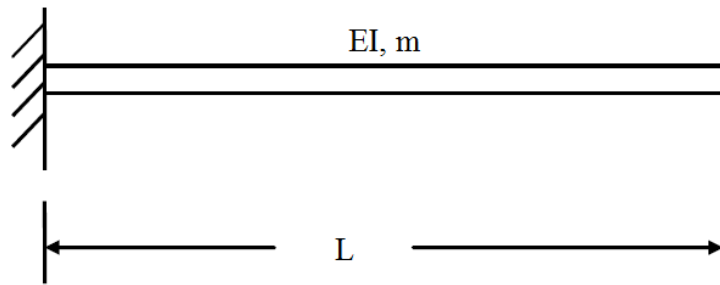


Figure 4. 3 Antenna Model as a Cantilever Beam

Governing differential equation of the beam for the transverse displacement $y(x,t)$ can be written as (4.1) according to classical beam theory [44].

$$-EI \frac{\partial^4 y}{\partial x^4} = m \frac{\partial^2 y}{\partial t^2} \quad (4.1)$$

where; E is the modulus of elasticity, I is the area of moment of inertia, L is the length and m is the mass of the antenna. In this equation shear deformation and rotary inertia is neglected according to Euler-Bernoulli theory.

In order to solve differential equation (Equation 4.1), the dependent variable (displacement) can be separated in Equation (4.2). By separation of variables;

$$y(x,t) = Y(x)T(t) \quad (4.2)$$

Letting a constant c to Equation (4.1) and separating both time and spatial variables, differential equation of mode shapes can be written as in Equation (4.3).

$$\frac{d^4}{dx^4}Y(x) - c^2 \left\{ \frac{m}{EI} \right\} Y(x) = 0 \quad (4.3)$$

The solution to Equation (4.3) is the general form of transverse mode shapes of the antenna structure.

General form of beam mode shapes can be presented as in (4.4)

$$Y(x) = a_1 \sinh(\beta x) + a_2 \cosh(\beta x) + a_3 \sin(\beta x) + a_4 \cos(\beta x) \quad (4.4)$$

Solving the differential Equation (4.3) with general form of $Y(x)$ yields the total displacement solution with respect to mode shapes.

$$\begin{aligned} & \beta^4 \{ a_1 \sinh(\beta x) + a_2 \cosh(\beta x) + a_3 \sin(\beta x) + a_4 \cos(\beta x) \} - \dots \\ & c^2 \left\{ \frac{m}{EI} \right\} \{ a_1 \sinh(\beta x) + a_2 \cosh(\beta x) + a_3 \sin(\beta x) + a_4 \cos(\beta x) \} = 0 \end{aligned} \quad (4.5)$$

There is only one solution of Equation (4.5), which is presented in Equation (4.6).

$$\beta^4 = c^2 \left\{ \frac{m}{EI} \right\} \quad (4.6)$$

In order to solve general differential equation of displacement solution presented in Equation (4.5), boundary conditions of antenna structure should be determined. From Equations (4.7) to (4.10) boundary conditions are presented.

The following boundary conditions can be specified for the antenna structure with fixed base ($x=0$).

$$Y(0) = 0 \text{ (zero displacement condition)} \quad (4.7)$$

$$\left. \frac{dY}{dx} \right|_{x=0} = 0 \text{ (zero slope condition)} \quad (4.8)$$

Following boundary conditions can be defined for antenna structure at the free end where $x=L$.

$$\left. \frac{d^2Y}{dx^2} \right|_{x=L} = 0 \text{ (zero bending moment condition)} \quad (4.9)$$

$$\left. \frac{d^3Y}{dx^3} \right|_{x=0} = 0 \text{ (zero shear force condition)} \quad (4.10)$$

These boundary condition can be applied to the general solution in Equation 4.5 and to its derivatives.

$$\begin{bmatrix} \sin(\beta L) + \sinh(\beta L) & \cos(\beta L) + \cosh(\beta L) \\ \cos(\beta L) + \cosh(\beta L) & -\sin(\beta L) + \sinh(\beta L) \end{bmatrix} \begin{bmatrix} a_1 \\ a_2 \end{bmatrix} = \begin{bmatrix} 0 \\ 0 \end{bmatrix} \quad (4.11)$$

a_1 and a_2 constants should be zero in order to satisfy Equation (4.11). Moreover, the determinant should also be set to find a nontrivial solution. Therefore, the solution is presented in Equation (4.12).

$$\cos(\beta_n L) + \cosh(\beta_n L) = -1 \quad (4.12)$$

Equation (4.12) can be defined as the frequency equation of cantilever beam [44]. It is a non-linear equation and the roots can be determined by means of a combination of graphical and numerical methods. There exist an infinite number of roots which represents the possible modes of vibration phenomena. Since the system taken into consideration is a continuous system, there are infinite numbers of natural frequencies. The roots of Equation (4.12) are displayed in Table 4.1 [44].

Table 4. 1 Values of $\beta_n l$ for first Five Mode of Cantilever Beam [44]

n (modes)	$\beta_n L$
1	1.87510
2	4.69409
3	7.85409
4	10.99554
5	$(2n-1)\pi/2$

Using modal β_n values, separated time equation can be written as follows [44].

$$T(t) = b_1 \sin \left[\left\{ \beta_n^2 \sqrt{\frac{EI}{m}} \right\} t \right] + b_2 \sin \left[\left\{ \beta_n^2 \sqrt{\frac{EI}{m}} \right\} t \right] = 0 \quad (4.13)$$

Therefore, the natural frequency of antenna structure ω_n can be defined as;

$$\omega_n = \beta_n^2 \sqrt{\frac{EI}{m}} \quad (4.14)$$

For individual modes, β_n values given in Table 4.1 are inserted into Equation (4.14) in order to find corresponding natural frequency.

Finding natural frequencies of antenna structure, next step is to find eigenvectors.

For eigenvectors, general solution expressed by Equation (4.4) is recalled.

$$Y(x) = a_1 \sinh(\beta x) + a_2 \cosh(\beta x) + a_3 \sin(\beta x) + a_4 \cos(\beta x) \quad (4.15)$$

Eigenvectors can be found with directly applying boundary conditions (Equations 4.7-4.10) to Equation (4.4) and its derivatives. Eigenvector equation presented in Equation (4.16) becomes as follows:

$$Y(x) = a_2 \left\{ \left[\cosh(\beta x) - \cos(\beta x) \right] - \frac{[\cosh(\beta L) + \cos(\beta L)]}{[\sinh(\beta L) + \sin(\beta L)]} \left[\sinh(\beta x) - \sin(\beta x) \right] \right\} \quad (4.16)$$

For generalized modal eigenvectors in arbitrary scale, Equation (4.17) can be written.

$$Y(x) = a_n \left\{ \left[\cosh(\beta_n x) - \cos(\beta_n x) \right] - \frac{[\cosh(\beta_n L) + \cos(\beta_n L)]}{[\sinh(\beta_n L) + \sin(\beta_n L)]} \left[\sinh(\beta_n x) - \sin(\beta_n x) \right] \right\} \quad (4.17)$$

These eigenvectors can be mass-normalized as in Equation (4.18).

$$\int_0^L m Y_n^2(x) dx = 1 \quad (4.18)$$

After mass-normalization, the leading coefficient of all modes becomes one. Thus, mass-normalized eigenvectors can be written using β_n values are taken from Table 4.1. In order to determine mode shapes of an antenna structure, mass and length information is enough for non-dimensional eigenvectors. Mode shapes are viewed basically the visual behavior of antenna structure at natural frequencies. Graphically, mode shapes can be displayed by plotting corresponding eigenvector equation with respect to antenna length.

4.1.2 Effective Modal Mass and Participation Factor for the Antenna Structure

The effective modal mass is an important method for judging whether the mode is significant or not. Modes with relatively high effective masses can be readily excited by base excitation. Considering an antenna structure modeled as a cantilever beam, there is infinite number of modes present. In order to perform transient analysis of the antenna structure, for brevity, only limited number of modes should be included through analysis.

“In order to determine how many modes should be included in the analysis, the number should be high enough so that the total effective modal mass of the model is at least 90% of the actual mass [45].”

The participation factor (Γ) for cantilever beam with constant mass density can be defined by Equation (4.19) [45]. It should be noted that $Y_n(x)$ is the corresponding mode shape. Therefore, participation factors are non-dimensional.

$$\Gamma_n = m \int_0^L Y_n(x) dx \quad (4.19)$$

Effective modal mass is, however, is a dimensional property. It is defined by the vector which represents the displacement of the mass. For cantilever beams, Equation (4.20) can be written for effective modal mass.

$$m_{eff,n} = \frac{\left[\int_0^L m(x) Y_n(x) dx \right]^2}{\int_0^L m(x) [Y_n(x)]^2 dx} \quad (4.20)$$

As given in Equation (4.18), eigenvectors, $Y_n(x)$ can be mass-normalized. In terms of mass-normalized eigenvectors, Equation (4.21) can be written for effective modal mass.

$$m_{eff,n} = [\Gamma_n]^2 = \left[\int_0^L m(x) Y_n(x) dx \right]^2 \quad (4.21)$$

4.1.3 Transient Response of the Antenna Structure to Base Excitation

Antenna model corresponding to the transient base excitation can be sketched as Figure 4.4.

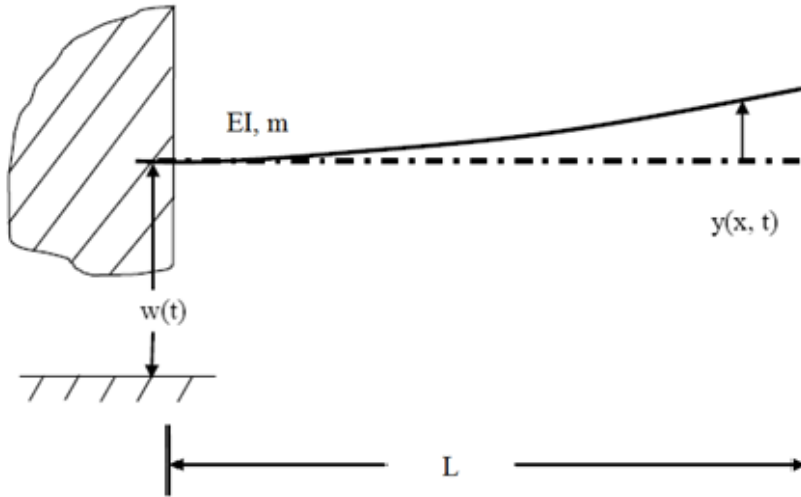


Figure 4. 4 Antenna Model Subjected to Transient Base Excitation

The forced transient response equation for a cantilever beam with beam excitation is given in Equation (4.22) [46].

$$EI \frac{d^4 y}{dx^4} + m \frac{\partial^2 y}{\partial t^2} = -m \frac{\partial^2 w}{\partial t^2} \quad (4.22)$$

In Equation (4.22), $y(x,t)$ is the relative displacement with respect to the base and $w(t)$ is the base displacement while the term on the right-hand-side is the inertial force.

For the dependent variable $y(x,t)$, Equation (4.23) is written.

$$y(x,t) = \sum_{n=1}^m Y_n(x) T_n(t) \quad (4.23)$$

With the expansion of $y(x,t)$, governing equation can be written in the form of Equation (4.24).

$$EI \frac{\partial^4}{\partial x^4} \left[\sum_{n=1}^r Y_n(x) T_n(t) \right] + m \frac{\partial^2}{\partial t^2} \left[\sum_{n=1}^r Y_n(x) T_n(t) \right] = -m \frac{\partial^2 w}{\partial t^2} \quad (4.24)$$

Equation (4.25) is obtained in terms of β_n values as:

$$EI \beta_n^4 \left[\sum_{n=1}^r Y_n(x) T_n(t) \right] + m \left[\sum_{n=1}^r Y_n(x) \frac{d^2}{dt^2} T_n(t) \right] = -m \frac{d^2 w}{dt^2} \quad (4.25)$$

Each term is multiplied by an arbitrary mode shape function $Y_p(x)$. Therefore Equation (4.26) is written as;

$$EI \beta_n^4 \left[\sum_{n=1}^r T_n(t) Y_n(x) Y_p(x) \right] + m \left[\sum_{n=1}^r Y_n(x) Y_p(x) \frac{d^2}{dt^2} T_n(t) \right] = -m \frac{d^2 w}{dt^2} Y_p(x) \quad (4.26)$$

In order to calculate the complete response of the antenna, integration is performed over the antenna length.

$$\begin{aligned} & \frac{EI\beta_n^4}{m} \sum_{n=1}^r \left\{ T_n(t) \int_0^L m Y_n(x) Y_p(x) dx \right\} + \sum_{n=1}^r \left\{ \frac{d^2}{dt^2} T_n(t) \int_0^L m Y_n(x) Y_p(x) dx \right\} = \dots \\ & - \frac{d^2 w}{dt^2} \int_0^L m Y_p(x) dx \end{aligned} \quad (4.27)$$

Orthogonality of the eigenvectors $Y_n(x)$ and $Y_p(x)$ is exploited for simplifications in Equation (4.27). Orthogonality conditions are presented in Equations (4.28) and (4.29).

$$\int_0^L m Y_n(x) Y_p(x) dx = 0 \text{ for } n \neq p \quad (4.28)$$

$$\int_0^L m Y_n(x) Y_p(x) dx = 1 \text{ for } n=p \quad (4.29)$$

Making use of Equations (4.18) and (4.24) and orthogonality properties, differential equation (4.27) becomes a complete form presented in Equation (4.30).

$$\frac{d^2}{dt^2} T_n(t) + \omega_n^2 T_n(t) = -\Gamma_n \frac{d^2 w}{dt^2} \quad (4.30)$$

Finally, damping term is included to the differential equation in the form of modal damping ratio ξ_n .

$$\frac{d^2}{dt^2} T_n(t) + 2\xi_n \omega_n \frac{d}{dt} T_n(t) + \omega_n^2 T_n(t) = -\Gamma_n \frac{d^2 w}{dt^2} \quad (4.31)$$

$$\ddot{T}_n(t) + 2\xi_n \omega_n \dot{T}_n(t) + \omega_n^2 T_n(t) = -\Gamma_n \ddot{w}(t) \quad (4.32)$$

Damped natural frequency can be defined by Equation (4.33), as

$$\omega_d = \omega_n \sqrt{1 - \xi^2} \quad (4.33)$$

The discrete form of Equation (4.32) is inefficient to solve even on a computer. Therefore, time variable T_n can be solved from a ramp invariant recursive filtering relationship [21, 46]. The term recursive refers to the fact that the response at any time depends in part on the responses at all previous times. The term filtering refers to the fact that the system itself behaves as a simple low-pass filter. In fact, the time integration process itself is a low pass filtering operation. The derivation of the filtering relationship may be performed by an extensive number of steps in the time domain. However, it is a very inefficient and time-consuming process. Therefore, derivation of the coefficient of time variable is performed by frequency domain transformation methods, particularly the series of Z-transform, Laplace Transform and Inverse Laplace Transform methods.

Time variable T_n is found via RFR method as presented in Equation (4.34), noting that Δt is the time step.

$$\begin{aligned}
T_{n,i} &= 2 \exp[-\xi\omega_n\Delta t] \cos[\omega_d\Delta t] \cos[\omega_d\Delta t] T_{n,i-1} - \exp[-2\xi\omega_n\Delta t] T_{n,i-2} + \dots \\
&\frac{1}{m\omega_n^3\Delta t} \left\{ \begin{aligned} &2\xi \left[\exp(-\xi\omega_n\Delta t) \cos(\omega_d\Delta t) - 1 \right] + \exp(-\xi\omega_n\Delta t) \dots \\ &\left[\frac{\omega_n}{\omega_d} \left[2\xi^2 - 1 \right] \sin(\omega_d\Delta t) \right] + \omega_n\Delta t \end{aligned} \right\} \left\{ -\Gamma_n \ddot{w}_i \right\} + \dots \\
&\frac{1}{m\omega_n^3\Delta t} \left\{ \begin{aligned} &-2\omega_n\Delta t \exp(-\xi\omega_n\Delta t) \cos(\omega_d\Delta t) + 2\xi \left[1 - \exp(-2\xi\omega_n\Delta t) \right] \dots \\ &-2 \frac{\omega_n}{\omega_d} \left[2\xi^2 - 1 \right] \exp(-\xi\omega_n\Delta t) \sin(\omega_d\Delta t) \end{aligned} \right\} \left\{ -\Gamma_n \ddot{w}_{i-1} \right\} + \dots \\
&\frac{1}{m\omega_n^3\Delta t} \left\{ \begin{aligned} &(2\xi + \omega_n\Delta t) \exp(-2\xi\omega_n\Delta t) + \exp(-\xi\omega_n\Delta t) \dots \\ &\left\{ \frac{\omega_n}{\omega_d} \left[2\xi^2 - 1 \right] \sin(\omega_d\Delta t) - 2\xi \cos(\omega_d\Delta t) \right\} \end{aligned} \right\} \left\{ -\Gamma_n \ddot{w}_{i-2} \right\}
\end{aligned} \tag{4.34}$$

Time variables T_n and eigenvectors Y_n are sufficient enough to solve for antenna relative displacement, relative velocity and relative acceleration.

Antenna relative displacement is given in Equation (4.35), where n is the mode number.

$$y(x, t) = \sum_{n=1}^r Y_n(x) T_n(t) \tag{4.35}$$

Antenna relative velocity is expressed in Equation (4.36).

$$\dot{y}(x, t) = \sum_{n=1}^r \dot{Y}_n(x) T_n(t) \tag{4.36}$$

Antenna relative acceleration is expressed in Equation (4.37) through time differentiation.

$$\ddot{y}(x, t) = \sum_{n=1}^r \ddot{Y}_n(x) T_n(t) \tag{4.37}$$

Antenna absolute acceleration $A(x,t)$ can be found by summation of base acceleration input and antenna relative acceleration as presented in Equation (4.38).

$$A(x,t) = \dot{w}(y) + \ddot{y}(x,t) \quad (4.38)$$

4.2 Solution Methods for Transient Response of the Antenna Structure Subjected to Base Excitation

In this section, solution methods for transient response of the antenna structure subjected to base excitation are presented. Solution methods are categorized, namely, as multi-degree-of-freedom solutions, single-degree-of-freedom solutions and approximate solutions.

The main purpose of this chapter is to derive the multi-degree-of-freedom transient solution of antenna structure and develop the solution algorithm of the model derived. Multi-degree-of-freedom solution methods of antenna structure are the solution to the mathematical model presented in Section 4.2. Therefore, solution methodology is focused specifically on recursive filtering relationship (RFR). Recursive algorithm for this methodology uses the modal analysis results of continuous modeling with classical theory presented in Sections 4.2.1 and 4.2.2. The solution algorithm calculates the modal analysis results of antenna structure and makes use of these results on transient response calculations. At the same time, ramp invariant recursive filtering relationship employed used to solve the series of equations presented in Section 4.2.3. Thus, a complete transient analysis of antenna structure based on continuous modal analysis is achieved. For multi-degree-of-freedom solution, exact transient solution of antenna structure subjected to the classical pulse input can be calculated. Exact solution is also calculated in order to compare algorithm solutions to the exact solution. RFR method can be applied to

various shock inputs, while the use of exact solution is limited only to the classical pulse input (e.g. half-sine input).

Solution methods employing single-degree-of-freedom model are also presented in this section. In this study, these methods are built before multi-degree-of-freedom methods in order to foresee the behavior of antenna structure with the assumption that the antenna structure possesses only one mode. Regard to the participation factor of modes of MDOF structure, SDOF assumption may yield very close estimation. For single-degree-of-freedom analysis, convolution integral solution, RFR method, Runge-Kutta fourth order method and Newmark-beta numerical integration methods are presented. Single-degree-of-freedom methods can be used to monitor general shock response behavior of antenna structure to transient impulse. For simple geometries, these methods can be used for shock analysis with certain amount of errors. The source of these errors is the lumped mass assumption. Lumped mass theory uses the natural frequency of the lumped mass of the system and equivalent stiffness. Therefore, lumped mass results do not include participations of all modes whose effective modal percentages are relatively high. Thus, single-degree-of-freedom modeling with lumped mass theory presents responses with certain amount of error. SDOF modeling results can also be used for approximate response calculations. With the use of corresponding response values for acceleration, displacement or velocity for each natural frequency, approximate solutions can be obtained by simplified methods.

In this section, simplified methods are also presented. Simplified modal combination methods are used to estimate the multi-degree-of-freedom response. Estimations require only eigenvalues, eigenvectors and the modal participation factors of the system. Therefore, modal analysis results are combined as the summation of single-degree-of-freedom results for multi-degree-of-freedom estimation. Due to their simplicity and speed, simplified methods can be used for the modal analysis for simple structures to determine the general shock response behavior of the system.

4.2.1 Multi-Degree-of-Freedom (MDOF) Solution Methods

4.2.1.1 Ramp Invariant Recursive Filtering Relationship Method

Transient response of antenna structure is obtained in Section 4.1, Recursive Filtering Relationship (RFR) uses the ramp invariant technique which models the slope between adjacent points of the input excitation. Modal analysis of the system should have been performed before using the RFR technique and the system is reduced to uncoupled mass, damping and stiffness matrices [47, 48]. The response in physical coordinated can be obtained from the modal responses after the transient analysis. Initial conditions are all kept at zero. Therefore, the response to initial conditions can be solved exactly by using Laplace transforms, if preferred.

In the analysis, the time step should be selected so that there are at least ten points per cycle corresponding to the highest natural frequency of interest. Therefore, sample rate should be a least ten times the highest frequency of interest. As Smallwood proposed in his paper [21], with the improved ramp invariant method, the analysis can be performed at a sampling rate two times the highest frequency. Still, to be safe side, at least ten times rule is recommended for the users. The number of modes which are included the analysis can be determined by participation factors of individual modes. As noted in Section 4.2.2, the number of modes included should be high enough so that the total effective modal mass of the model is at least 90% of the actual mass.

In order to obtain transient response of antenna structure, a MATLAB® code is developed including the modal analysis with classical approach presented in Sections 4.2.1 and 4.2.2. It also includes the solution algorithm with the solver of the equations presented in Section 4.2.3. Solution algorithm behind the written code is presented in Figure 4.5.

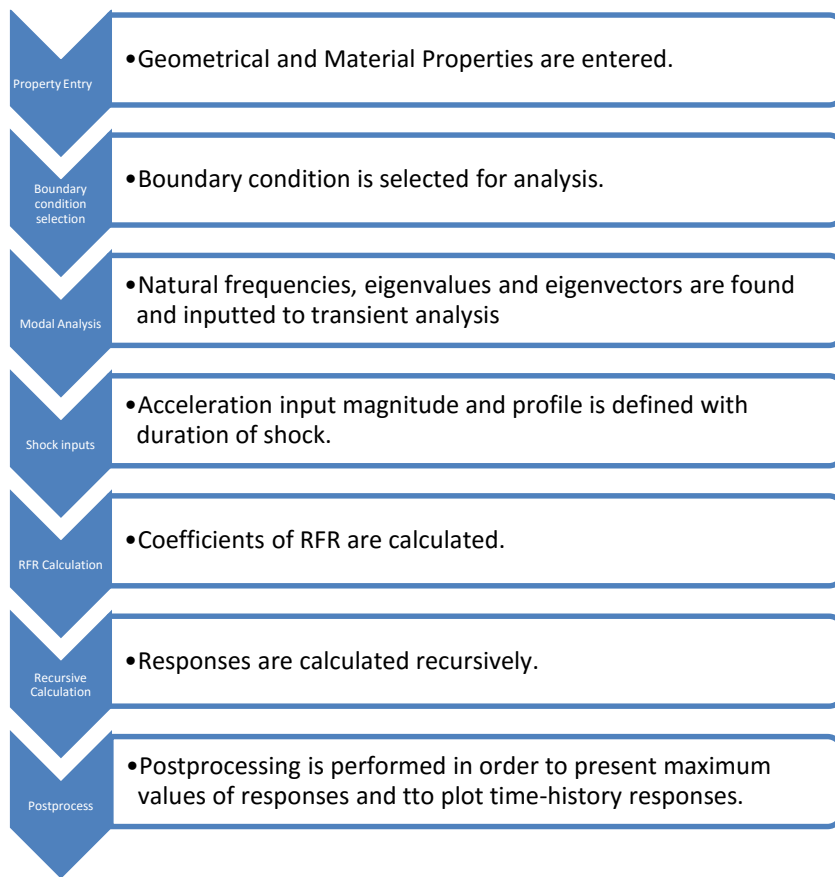


Figure 4. 5 Solution Methodology of MATLAB® Script Built for RFR Method

4.2.1.2 Other Numerical Methods

In order to solve antenna response model with numerical integration, there exist some other frequently used numerical methods. Among these numerical integration methods, Newmark-Beta time integration method, Backward-Euler method and central difference method are implemented in various commercial finite element programs for both linear and non-linear problems. Newton–Raphson method is also among those standard techniques which are specified with large deflection nonlinearities. The important parameters for these methods are selected time step, convergence criterion, modal analysis integration to the algorithm, solution accuracy and computational efficiency. Numerical methods are especially used for

nonlinear numerical integration which is very time consuming and computation efficiency dependent process. The solution algorithms are based on spatial discretization of the system with the governing equilibrium equation of structural dynamics [51, 52].

4.2.2 Single-Degree-of-Freedom (SDOF) Solution Methods

For SDOF modeling of antenna structure, antenna structure should be represented as a lumped mass model. Antenna stiffness can be calculated by Equation (4.39).

$$k_{beam} = \frac{3EI}{L^3} \quad (4.39)$$

Natural frequency of the beam with lumped mass assumption is presented in Equation (4.40).

$$f_n = \frac{1}{2\pi} \sqrt{\frac{3EI}{mL^3}} \quad (4.40)$$

Remaining part is the solution of the response equation of the SDOF system at its natural frequency.

4.2.2.1 Convolution Integral Method

The convolution integral method yields an exact solution for the response only if the system and the input pulse can be analyzed in analog form rather than digital form. Therefore, this is impractical. The nested series representation of the convolution integral is also not commonly used because it is numerically inefficient. However, digital recursive filtering relationship representation of the

convolution integrals with discrete time domain gives the numerically practical solution.

4.2.2.2 Digital Recursive Filtering Relationship Method

This method is previously introduced in Chapter 3 while shock response spectrum is obtained. In this method, convolution integral is represented as digital recursive filtering relationship. The derivation of the shock response equation is performed using Z-transform. The ramp invariant simulation is preferred in this method since better accuracy is achieved with the addition of a filtering term. As discussed in MDOF use of this method, constant time step is used. The result of acceleration shock response is already presented in Equation (3.7). Solutions of transient response analysis are calculated via previously built MATLAB® code in Chapter 3. The outcome of this analysis is that, the ramp invariant digital recursive filtering relationship found for this calculation is used as the starting point of the numerical engine of MDOF modal transient analysis presented in Sections 4.2.3 and 4.3.1 for respective response parameters.

4.2.2.3 Newmark-Beta Method

The Newmark-Beta method is performed for a variable time step for the input. It can be used for the direct integration of a system of uncoupled mass, damping, and stiffness matrices. It can be applied to an uncoupled system as well. This method is derived from the continuous time equation in a general form as presented in Equation (4.39) [50, 51]. In order to compare SDOF solution techniques, MATLAB® code for this method is prepared for the transient response analysis.

4.2.2.4 Runge-Kutta 4th Order Method

The Runge-Kutta method extends the Taylor series method by estimating higher order derivatives at points within the time step. Among the methods built on Runge-Kutta method, Runge-Kutta 4th Order Method is preferred for arbitrary input function. [46]. Again, in order to compare SDOF solutions exerted from different techniques, MATLAB® code is prepared for transient response analysis via Runge-Kutta 4th Order Method.

4.2.3 Simplified Solution Models

In some cases, MDOF solution of antenna structure may be too difficult to handle with complete model and SDOF solution may contain unacceptable amount of error. Simplified solution methods can offer the best solution for such cases. Simplified methods use the SDOF responses of each modal response separately of antenna structure and sum those modal responses by different methods. These methods cannot present the faithful responses as MDOF models but it presents far better approximates than the SDOF models in most cases.

4.2.3.1 Absolute Sum Method (ABSSUM)

The absolute sum presents a conservative approach since this method is based on the assumption that the maxima of all modes can be observed at the same instant of time, i.e. with no phase difference. Maximum relative displacement $(z_i)_{\max}$ can be calculated from modal coordinates. Equation (4.42) is used for the estimation for

this method. Noting that \hat{q}_{nj} is the corresponding eigenvalue. Absolute acceleration can also be found by the same formulation.

$$(z_n)_{\max} \leq \sum_{j=1}^r |\Gamma_j| |\hat{q}_{nj}| |z_{j,\max}| \quad (4.41)$$

4.2.3.2 Square Root of the Sum of the Squares (SRSS)

This method approximates the relative displacement of MDOF system with the square roots of the squares of the summation values for modal maximum relative displacements. The estimated relative displacement is presented in Equation (4.43). Absolute acceleration is also found by the same formulation.

$$(z_n)_{\max} \approx \sqrt{\sum_{j=1}^r [\Gamma_j \hat{q}_{nj} z_{j,\max}]^2} \quad (4.42)$$

4.2.3.3 Naval Research Laboratories Method (NRLM)

“NRL method is a statistical estimate of the maximum response created by taking the response for the mode that exhibits the largest response. [54]” The maximum relative displacement value is calculated from modal coordinates as presented in Equation (4.44). For absolute acceleration the same procedure is applied.

$$(z_n)_{\max} = |(\hat{q}_{nj})(\Gamma_n z_n)_{\max}| + \sum_{k=1, k \neq j}^r |(\hat{q}_{nk})(\Gamma_k z_k)_{\max}| \quad (4.43)$$

In this chapter, mathematical model of the antenna structure is presented, and solution alternatives of these models are proposed. In this study, distributed parameter modeling of the antenna with classical theory and MDOF modeling and transient response solution of the antenna structure by RFR method are applied to simulate shock response of antenna structure subjected to underwater explosions as close as possible. For completeness, SDOF models are also presented with different solution alternatives in order to foresee the response characteristics of antenna structure. In addition to that, simplified methods are also presented for shock analysis. With these methods, shock response of structures whose effective modal masses of leading modes are high can be approximated better than SDOF approximations.

CHAPTER 5

TRANSIENT RESPONSE ANALYSIS OF ANTENNA STRUCTURE

Mathematical model of the antenna structure is built on the basis of modal analysis by means of continuous modeling with classical approach (Euler-Bernoulli Beam Theory) and MDOF modal transient analysis with RFR method which is presented in Chapter 4. Apart from that model, SDOF transient model and simplified models are also presented for completeness. In this chapter, transient response analysis is performed by these models. Following the roadmap of analysis procedure, first, MDOF transient response analysis which is the main purpose of the study is performed by RFR method. Modal analysis outputs such as natural frequencies, mode shapes and participation factors are used as inputs for RFR transient analysis. Therefore, this analysis can also be called as Modal Transient Analysis because of the use of modal matrices built in continuous modeling. Shock profiles simulating underwater explosions obtained in Chapter 3 are also used as acceleration inputs. The output of analysis includes displacement, acceleration and velocity shock responses obtained at any point on the antenna structure. Critical displacement and acceleration response ranges are investigated with Phase Portrait plots. Histograms also present the reluctance of antenna structure to failure or electromagnetic malfunctions.

Secondly, simplified methods are presented involving three different methods presented in Chapter 4. Maximum absolute acceleration and relative displacements are estimated by means of these methods. A comparative evaluation of results is carried to understand the efficiency of these simplified models in predicting the antenna response to shock input as described. Finally SDOF transient analysis is presented. For SDOF transient analysis, three different methods are used. Results

of these methods are compared between each other and compared with MDOF results. Since SDOF transient analysis methods are based on very primitive and geometry-independent model, it is expected that responses are not very close to MDOF models naturally. For all analysis procedures, MATLAB® scripts are built and results are obtained by means of these scripts.

5.1 Modal Analysis of Antenna Structure

Antenna structure and base platform mentioned in Chapter 4 is sketched in Figure 5.1. Important geometric parameters are labeled on the figure. Numerical values of these parameters are presented in Table 5.1. These dimensions are determined by electromagnetic design of the antenna structure.

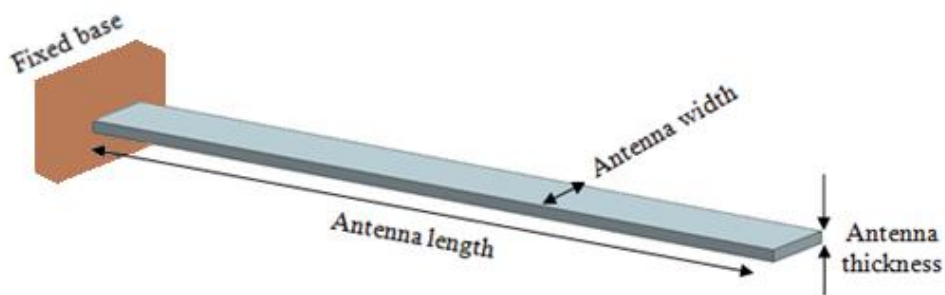


Figure 5. 1 Three-Dimensional Model of Antenna Structure

Table 5. 1 Geometrical Properties of Antenna Structure

Geometrical Properties	
Antenna length (mm)	370
Antenna width (mm)	20
Antenna thickness (mm)	2

Generally 5000 or 6000 series of aluminum alloys are used for antenna structures due to the strength, corrosion, weight, machining and electrical conductivity concerns. AA6061-T6 material is used for the dipole antenna considered in this thesis. Mechanical properties of AA6061-T6 are presented in Table 5.2.

Table 5. 2 Mechanical Properties of Antenna Structure

Mechanical Properties of AA6061-T6	
Young Modulus (GPa)	68.9
Density (kg/m ³)	2768
Poisson's Ratio	0.33

Modal Analysis of antenna structure is performed via MATLAB® code written. Geometric properties and material properties of antenna structure are introduced to the code as input parameters which are tabulated as in Table 5.1 and 5.2. Using Table 4.1, Equations (4.14) and (4.17); natural frequencies and mode shapes are calculated. Results are presented in Table 5.3 and Figure respectively. Noting that number of modes included into the transient analysis should be determined before the analysis. After certain amount of modal mass percentage of degree-of-freedom, transient response of the antenna does not change significantly. Procedure for the selection of number of modes to be included to the transient analysis is explained in Section 5.2 briefly.

Table 5. 3 Natural Frequencies of Antenna Structure for First Four Bending Modes

Natural Frequencies of Antenna Structure	
First Mode Natural Frequency (Hz)	11.78
Second Mode Natural Frequency (Hz)	73.79
Third Mode Natural Frequency (Hz)	206.62
Fourth Mode Natural Frequency (Hz)	404.90

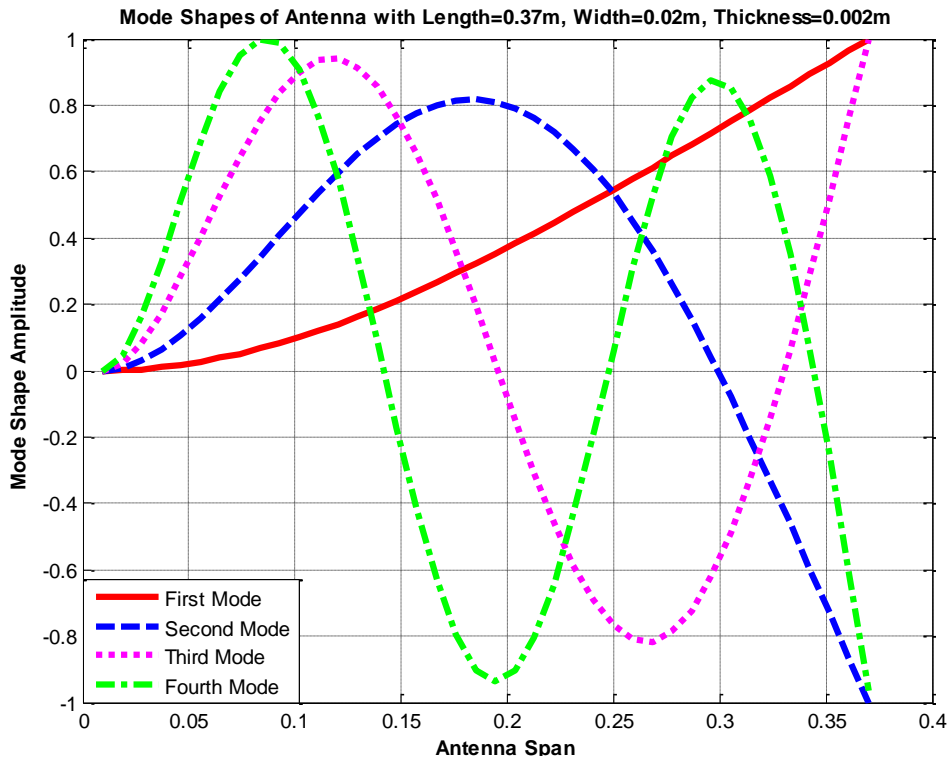


Figure 5. 2 First Four Bending Mode Shapes of Antenna Structure

5.2 MDOF Transient Response Analysis of Antenna Structure

5.2.1 Determination of Analysis Parameters

Electromagnetic point of view requires that the antenna structure should be maintained perpendicularly with respect to its base ground. In other words, the antenna structure should be avoided from excessive amount of bending and electronic components placed in vicinity of antenna tip should be in the same longitudinal direction with the antenna base where the power to the antenna is supplied. Antenna performance is directly proportional to the straightness of aluminum beam in longitudinal direction. This means transverse shock inputs to the antenna structure are very critical, because such lateral shock inputs subject the beam with bending. However, shock inputs in vertical direction which is acting on the antenna longitudinal axis, only create the longitudinal motion of antenna with

the base. Therefore longitudinal distance between antenna structure and the other antennas used in the system does not change and bending motion of antenna structure is not observed. This implies that there is no change in antenna performance individually and no change in system performance due to such loading. In addition to that, from stress standpoint, maximum stress values for these three inputs are investigated and maximum stress for transverse loading is observed as higher than maximum stress obtained from vertical loading due to buckling. Thus, maximum stress is observed at the face near to the antenna base due to the bending motion caused by transverse loading.

Considering the shock inputs synthesized and tabulated in Table 3.4, transverse and longitudinal shock inputs to the base can create bending motion to the antenna structure with regards to the placement of antenna. However, vertical shock input to the base does not create bending motion as illustrated in Figure 5.3.

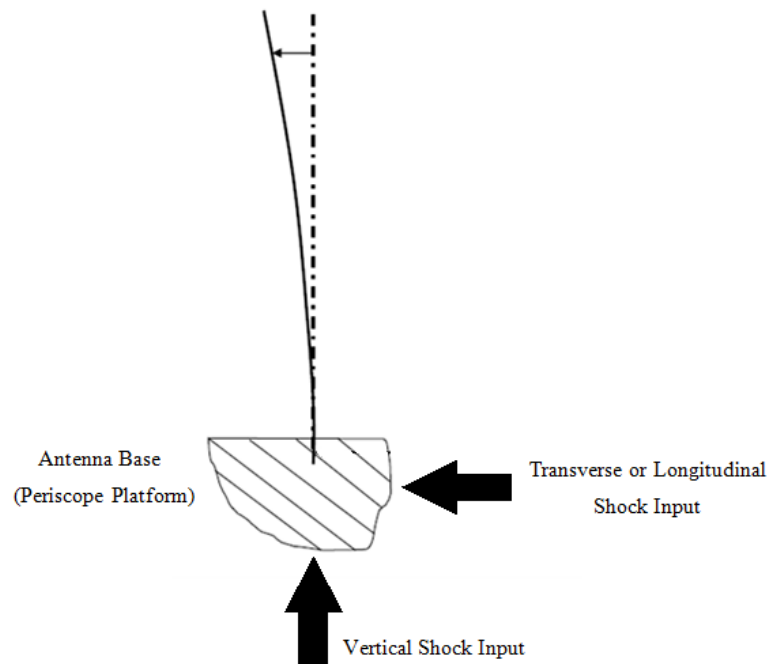


Figure 5. 3 Shock Inputs Applied to the Antenna Platform

As seen in Figure 5.3, transverse and longitudinal shock inputs should be considered for this study. Transverse and longitudinal inputs are considered together, because regarding to the antenna attachment to the platform, these two axes can be interchanged. Therefore, both inputs are the candidates of bending motion of antenna structure and may severe the electrical components or trigger antenna structure failure. In order to compare the effect of both transverse shock inputs SRS curves of the acceleration shock inputs (100g 8ms half-sine and 200g 8ms half-sine) are plotted together. As the acceleration response is important for component and material failure and the relative displacement response is important for antenna performance, both graphs are plotted and examined in Figure 5.4 and Figure 5.5.

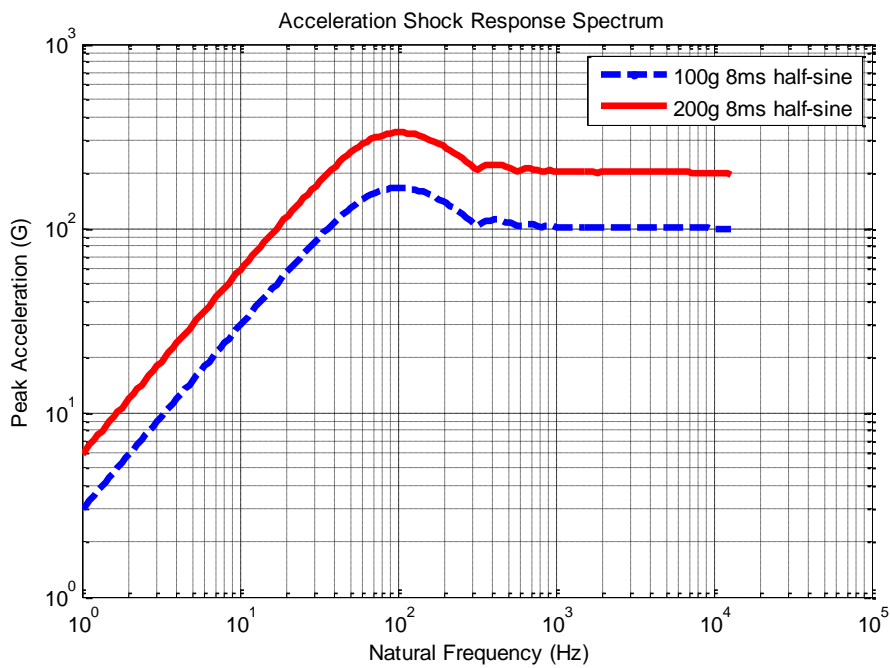


Figure 5. 4 Acceleration SRS for both Transverse Shock Inputs

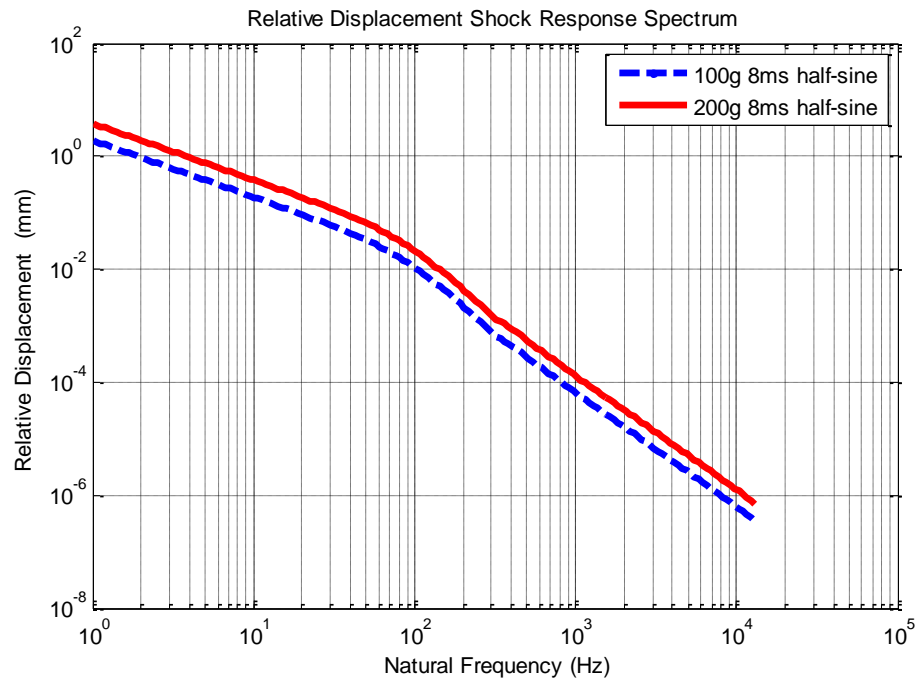


Figure 5.5 Relative Displacement SRS for both Transverse Shock Inputs

As shown in Figure 5.4 and 5.5, 200g 8ms half-sine shock input includes the response levels of 100g 8ms shock input. Therefore it is logical to perform the analysis with 200g 8ms half-sine shock input to be on the safe side.

After the shock input is determined, number of modes to be included in transient analysis is determined. *“In order to determine how many modes should be included in the analysis, the number should be high enough so that the total effective modal mass of the model is at least 90% of the actual mass [45].”* Therefore, effective modal masses of first 8 modes are calculated and tabulated in Table 5.4.

Table 5. 4 Modal Properties of the Antenna Structure

Mode	Natural Frequency (Hz)	Participation Factor	Effective Modal Mass (kg)	Modal Mass Percentage (%)
1	11.78	0.1585	0.0251	61.22
2	73.79	0.0878	0.0077	18.78
3	206.62	0.0515	0.0027	6.59
4	404.90	0.0368	0.0014	3.41
5	669.33	0.0286	0.0008	1.95
6	999.86	0.0234	0.0005	1.22
7	1396.50	0.0198	0.0004	0.98
8	1896.24	0.0172	0.0003	0.49

From results given in Table 5.4, first four modes are sufficient to include the analysis since the total effective modal mass percentage of first four modes is 90%. Comparison of transient responses of the antenna structure with respect to the number of modes included to the analysis is presented in Figures 5.6-5.9. As concluded from these graphs, after two modes results are changing in an interval of 0.04%. Therefore, it is concluded that 4-mode analysis suffices to obtain acceptably accurate results from MDOF transient analysis by RFR Method.

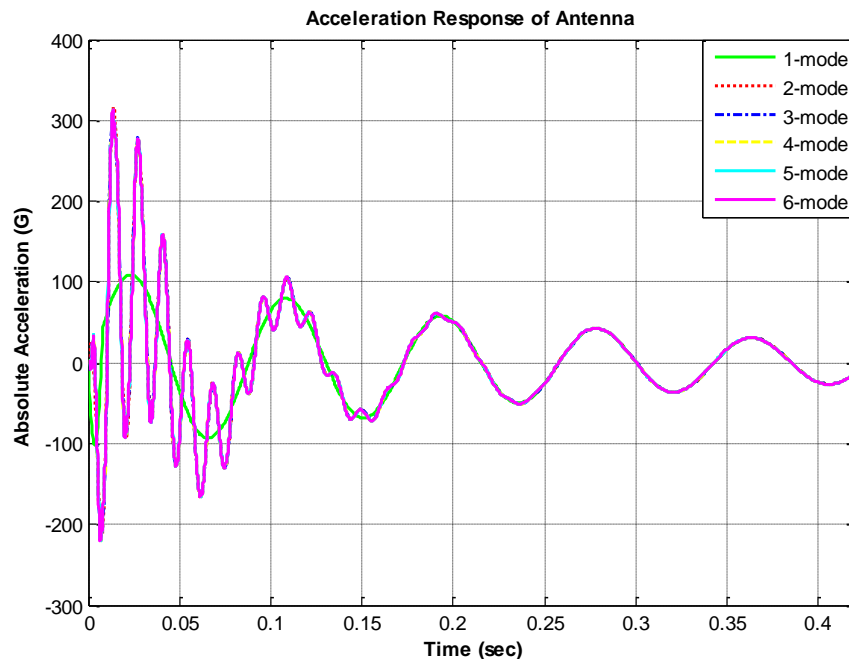


Figure 5. 6 Comparison of transient acceleration responses of antenna structure with respect to the number of modes included in the analysis

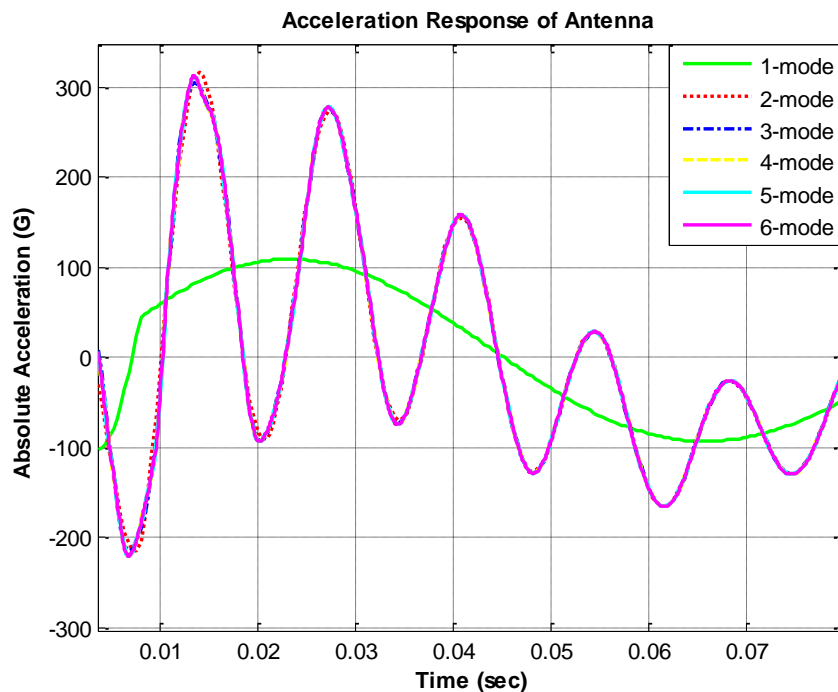


Figure 5. 7 Comparison of transient acceleration responses of antenna structure with respect to the number of modes included in the analysis (Zoomed View)

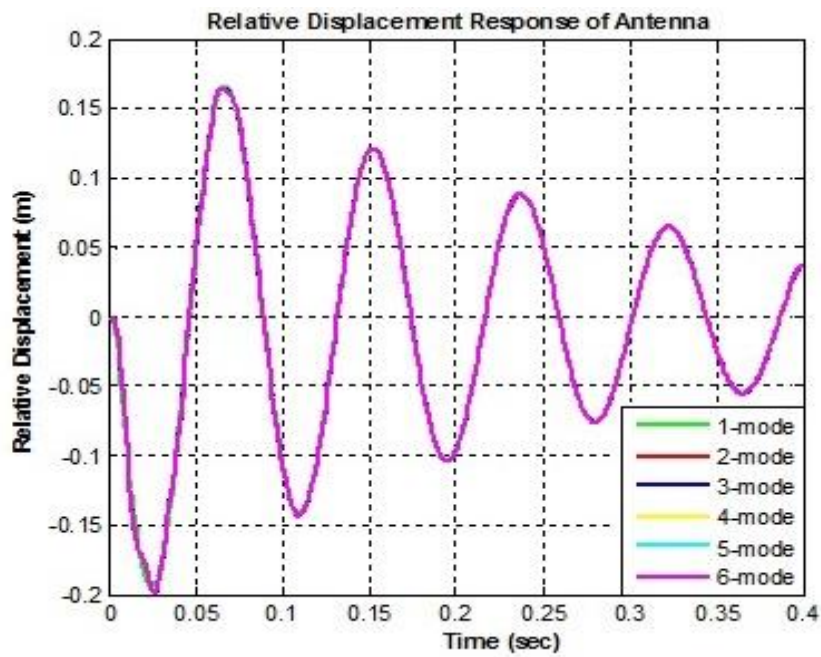


Figure 5. 8 Comparison of relative displacement responses of antenna structure with respect to the number of modes included in the analysis

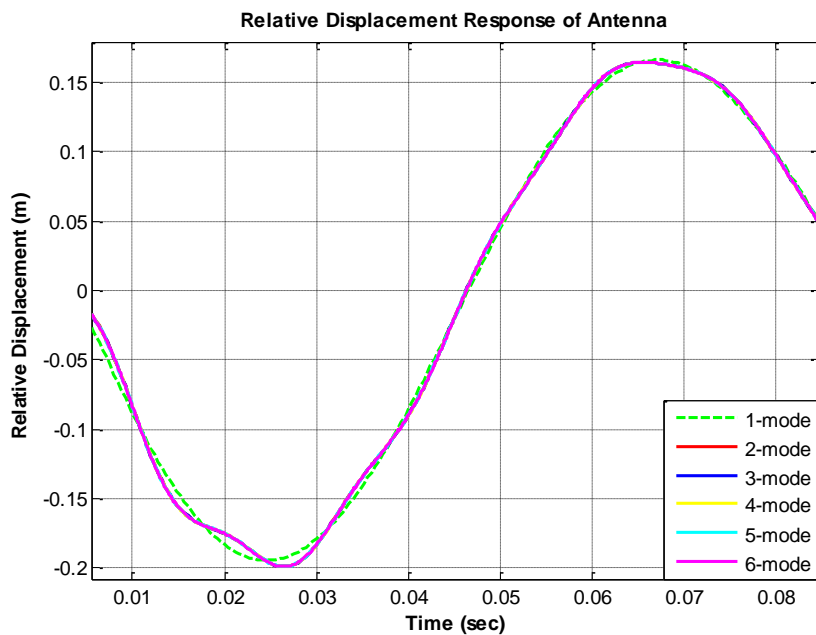


Figure 5. 9 Comparison of relative displacement responses of antenna structure with respect to the number of modes included in the analysis (Zoomed View)

5.2.2 MDOF Transient Response Analysis Results

MDOF transient response analysis of antenna structure is performed for 200g 8ms half-sine acceleration shock input to the antenna base, including 4 modes of antenna structure. Outputs are measured from the antenna tip where electrical components are placed and the antenna structure has maximum deformation nearby. As outputs, absolute acceleration is designated in order to monitor the effect of shock explosion to the antenna structure. Results are expressed in gravitational acceleration “g”. Acceleration output is the best determinate for damage potential and severity of underwater explosions on antenna structure. Endurance of electrical components and fatigue concerns are determined from acceleration output. As another output, relative displacement of the antenna tip is measured. Maximum deflection is monitored at the antenna tip, therefore the antenna performance is directly proportional to the deflection amplitude of the structure. Thus, relative displacement is another important output of the transient analysis. As an additional study, relative velocity of antenna tip is considered. From relative velocity response, stress value at antenna tip can be estimated. This is an estimation process because since shock pulses are applied to the structure for very small interval of time, stresses obtained from the analysis are called “pseudo stress”. Therefore, correction of those stresses will be performed and strength calculations of beam structure and electrical components will be calculated. Relative velocity outputs are presented in this section and stress calculation is performed and discussed in Chapter 8.

For the analysis procedure, formulations presented in Sections 4.1 and 4.2.1 are used and calculations are performed via MATLAB® script built for the complete MDOF transient response analysis using RFR Method. In MATLAB® script, procedure presented in Figure 4.5 is followed. Modal damping ratio is taken as 0.05 for all four modes [23].

A 200g 8ms half-sine acceleration shock input presented in Figure 5.10 is adopted as the input in the analysis.

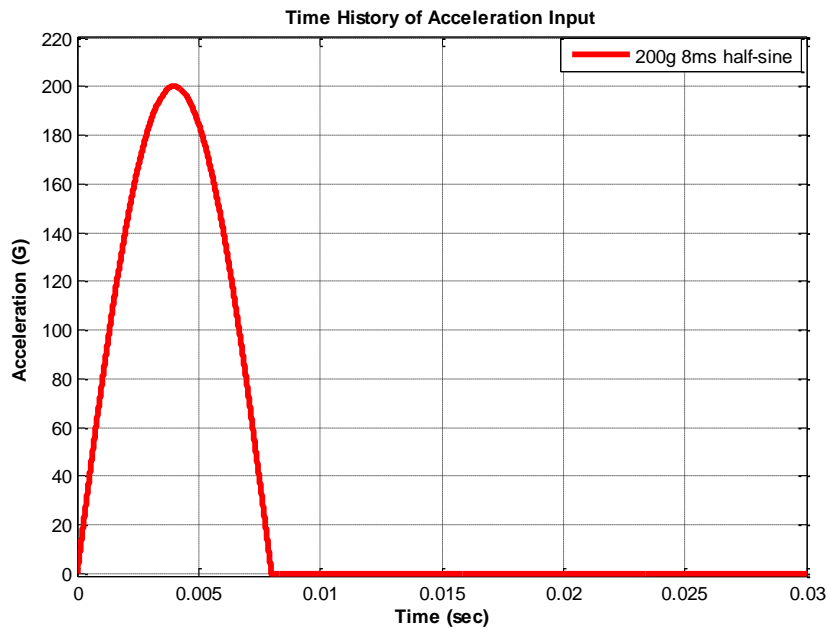


Figure 5. 10 Time History of 200g 8ms Half-Sine Acceleration Input

Absolute acceleration response of the antenna tip to the shock 200g 8ms shock input is illustrated in Figure 5.11. Peak value of response is measured as 310.6 g.

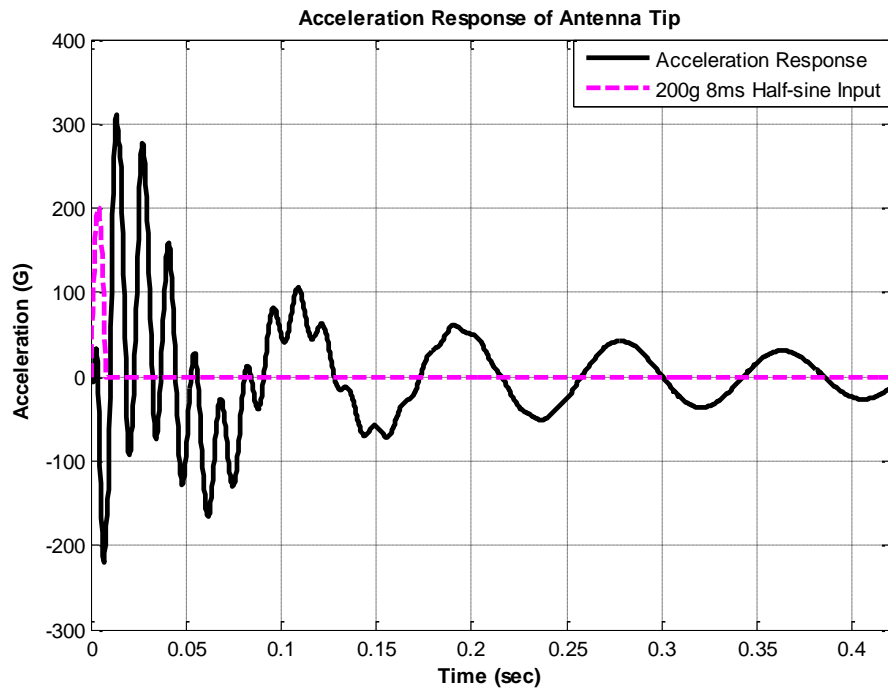


Figure 5. 11 MDOF Absolute Acceleration Response of the Antenna Tip

Relative displacement response of antenna structure is shown in Figure 5.12. For relative displacement, maximum value is measured as 0.199 mm.

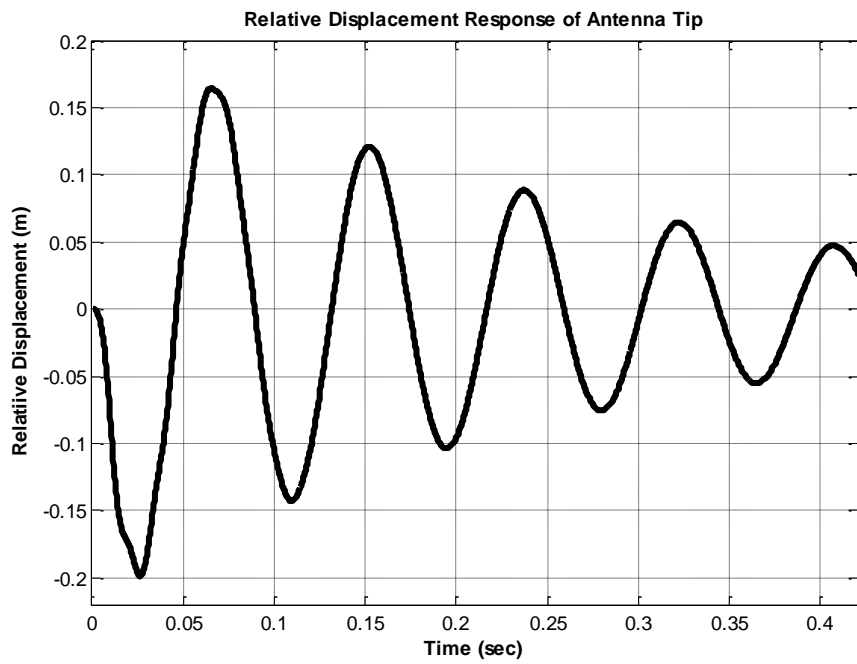


Figure 5. 12 MDOF Relative Displacement Response of the Antenna Tip

Relative velocity response of the antenna tip is displayed in Figure 5.13. Maximum velocity at the tip point is measured as 18.58 m/s.

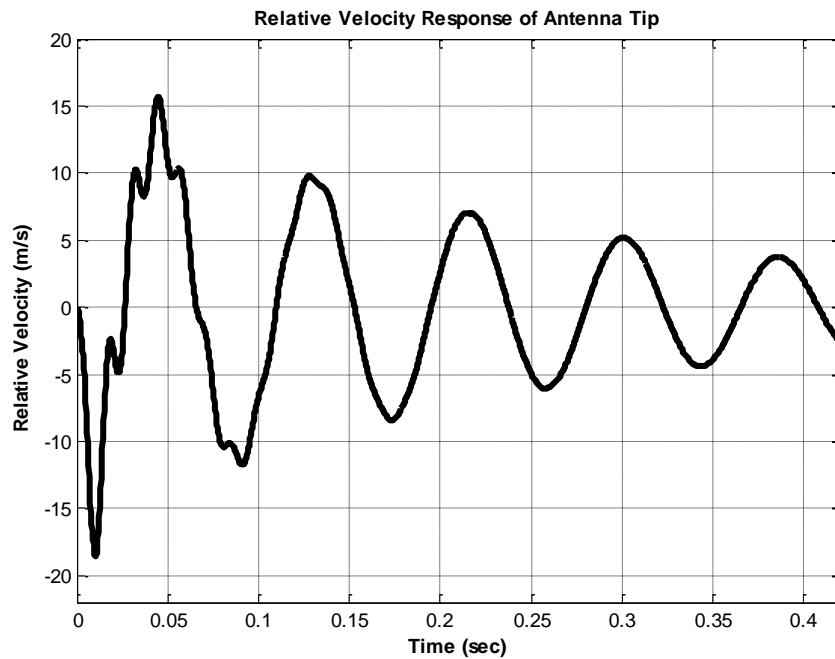


Figure 5. 13 MDOF Relative Velocity Response of the Antenna Tip

From design standpoint, phase portrait is a useful tool to determine the boundaries of the parameters to be designed. For the MDOF transient response analysis, relative displacement and absolute acceleration values are plotted in phase portrait diagram and the effect of shock can be investigated for both parameters. In addition to that, for shock isolation process phase portraits give designer an insight for the limits of design parameters that are to be isolated to the values inside of the design boundary curve. The phase portrait for the analysis is presented in Figure 5.14.

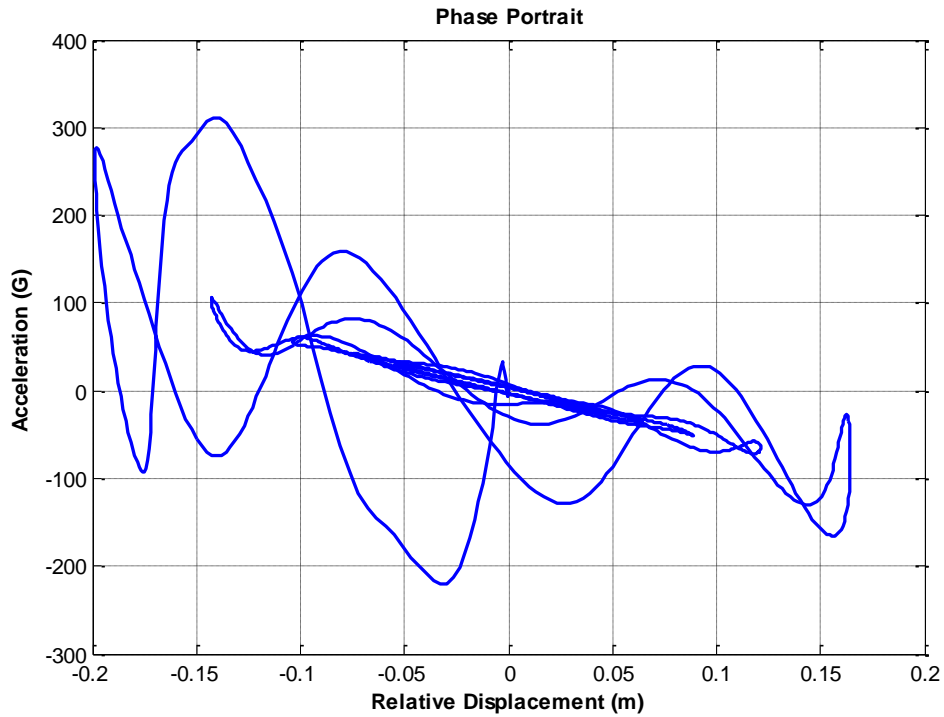


Figure 5. 14 MDOF Phase Portrait of the Antenna Tip

The distribution of absolute acceleration and relative displacement responses of the antenna tip can be monitored by means of histogram diagrams. In order to plot histogram diagrams for responses, 1719 total response points are taken. The distribution of responses is presented out of 1719 possible response points. Histogram plots are shown in Figures 5.15 and 5.16.

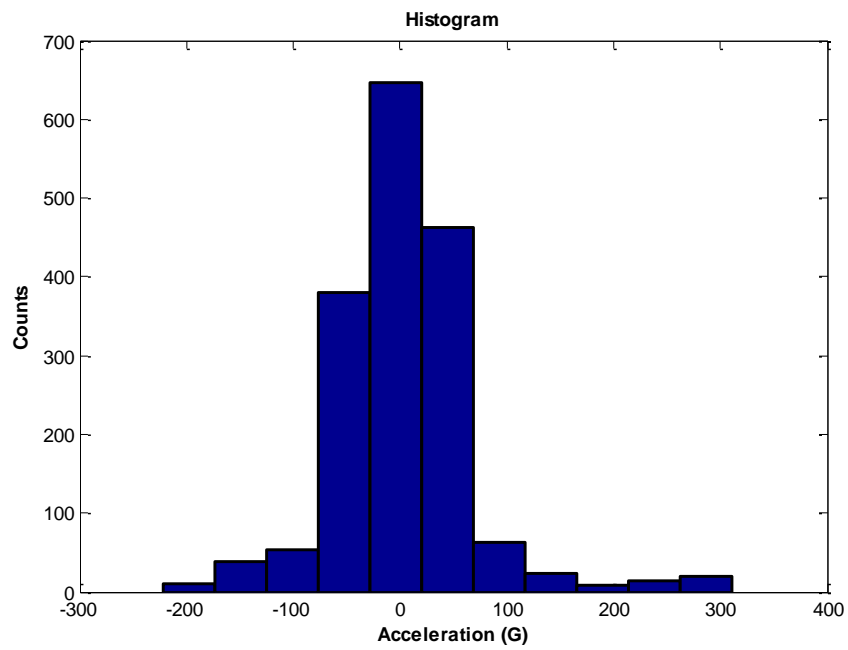


Figure 5. 15 Histogram Plot for MDOF Absolute Acceleration Response

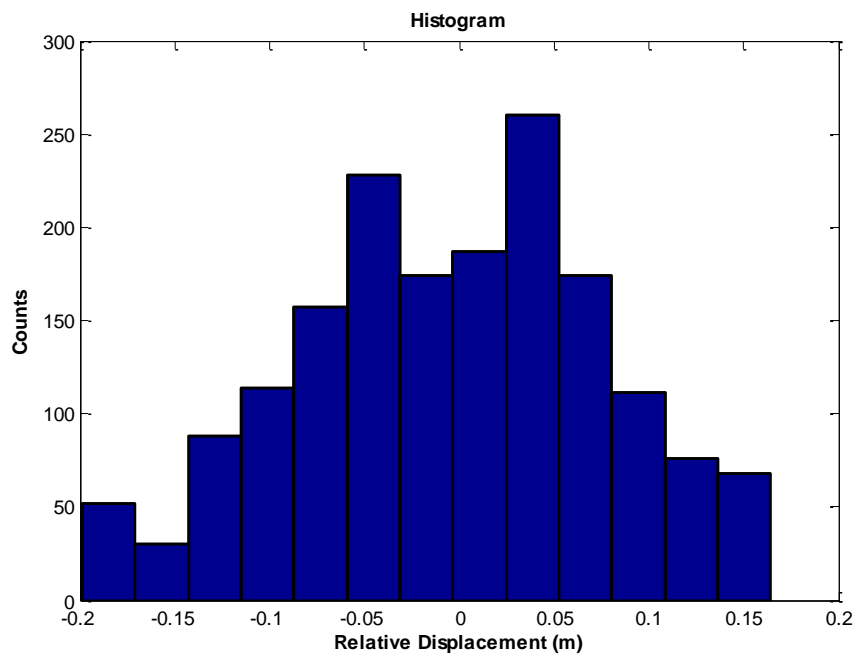


Figure 5. 16 Histogram Plot for MDOF Relative Displacement Response

MDOF transient response analysis of the antenna structure subjected to 200g 8ms half-sine shock input is performed by RFR Method. In order to conduct further studies like component endurance, shock isolation, stress analysis and component fatigue absolute acceleration, relative displacement and relative velocity time histories are concerned. Furthermore, phase portrait and histogram plots are also presented in order to find out the allowable region for shock design procedures. Maximum response values found by MDOF analysis through RFR Method is tabulated in Table 5.5.

Table 5. 5 Maximum Shock Responses at the Antenna Tip

MDOF Maximum Transient Responses	
Absolute Acceleration (G)	310.6
Relative Displacement (m)	0.199
Relative Velocity (m/s)	18.58

5.3 Transient Analysis Results of Antenna Structure by Simplified Methods

In this section, transient analysis results of the antenna structure are presented by three different methods mentioned in section 4.2.3. These simplified methods are proposed for estimating the MDOF response. For analysis, eigenvalues, eigenvectors and modal participation factors of the system or estimates of those are required along with SRS values of corresponding natural frequencies. Since simplified methods provide maximum values of responses, results obtained from these methods are compared to maximum values of MDOF modal transient analysis performed in Section 5.2.

5.3.1 Transient Response Results of ABSSUM Method

ABSSUM equation is again given in Equation (5.1).

$$(z_n)_{\max} \leq \sum_{j=1}^r |\Gamma_j| |\hat{q}_{nj}| |z_{j,\max}| \quad (5.1)$$

Equation (5.1) can be solved using, eigenvalues and participation factors taken from MDOF modal transient analysis in Section 5.2. Relative displacement and acceleration values are acquired from SRS analysis to 200g 8ms half-sine acceleration input. The procedure is performed by means of MATLAB® script. Results are tabulated in Table 5.6.

Table 5. 6 Transient Response Estimations of the Antenna Using ABSSUM Method

Response	Modal Transient Results (MDOF RFR Method)	ABSSUM Method
Absolute Acceleration (G)	310.6	380.7
Relative Displacement (m)	0.199	0.212

5.3.2 Transient Response Results of SRSS Method

SRSS equation is again given in Equation (5.2).

$$(z_n)_{\max} \approx \sqrt{\sum_{j=1}^r [\Gamma_j \hat{q}_{nj} z_{j,\max}]^2} \quad (5.2)$$

Equation (5.2) can also be solved with same inputs explained in Section 5.3.1. The procedure is performed by means of a MATLAB® code written. Results are tabulated in Table 5.7.

Table 5.7 Transient Response Estimations of the Antenna Using SRSS Method

Response	Modal Transient Results (MDOF RFR Method)	ABSSUM Method
Absolute Acceleration (G)	310.6	292.8
Relative Displacement (m)	0.199	0.199

5.3.3 Transient Response Results of NRL Method

NRL equation is again given in Equation (5.3).

$$(z_n)_{\max} = |(\hat{q}_{nj})(\Gamma_n z_n)_{\max}| + \sum_{k=1, k \neq j}^r |(\hat{q}_{nk})(\Gamma_k z_k)_{\max}| \quad (5.3)$$

Table 5. 8 Transient Response Estimations of the Antenna Using NRL Method

Response	Modal Transient Results (MDOF RFR Method)	ABSSUM Method
Absolute Acceleration (G)	376.6	292.8
Relative Displacement (m)	0.211	0.199

Simplified methods use the superposition of the mode shapes and SRS responses of corresponding natural frequencies with the weight of participation factor. For ABSSUM method, absolute response values of the number of selected modes are superposed together. Therefore, the response is expected to be the highest than the exact response or MDOF modal transient analysis response. Thus it can be concluded that ABSSUM method provides the maximum possible response value of the structure considered, and designs should be made assuming the exact response is lower than the response obtained from this method. Therefore, ABSSUM method can be used for determining the maximum response limit of antenna structure. Inherently, SRSS and NRL methods are expected to yield closer estimates of antenna structure. For NRL method, two-mode analysis produces the same result with the ABSSUM method because formulations become the same for this case. SRSS method is observed as the better estimate using considerably lower number of modes. Considering two-mode and three-mode analysis, SRSS results are the best estimated. Response values are tabulated for those three methods using two and three modes in Table 5.9 and 5.10. Comparing both cases, two-mode analysis is to be selected for future analysis since estimates are closer for this case as proposed in literature [53].

Table 5. 9 Transient Response Results for Simplified Methods Using Two Modes

Response	ABSSUM Method	SRSS Method	NRL Method
Absolute Acceleration (G)	380.7	292.8	380.7
Relative Displacement (m)	0.212	0.199	0.212

Table 5. 10 Transient Response Results for Simplified Methods Using Three Modes

Response	ABSSUM Method	SRSS Method	NRL Method
Absolute Acceleration (G)	518.9	323.7	447.7
Relative Displacement (m)	0.212	0.199	0.211

5.4 Transient Analysis Results of Antenna Structure Using SDOF Models

SDOF analysis is performed with lumped mass assumption mentioned in Section 4.2.2. SDOF analysis assumes the antenna structure as a spring-mass system with stiffness value calculated by Equation (4.39). Therefore, natural frequency of the antenna structure can be found using Equation (4.40). The remaining part is just to calculate the response of SDOF system using numerical solutions or exact solution. In this study, three different methods are used as proposed in Section 4.2.2. From these methods, exactly the same responses are obtained. After SDOF time history responses are obtained, these results are compared to MDOF analysis results. Since

SDOF is very simple and does not contain any dependency on geometry of the antenna structure and other modal properties, the results are far erroneous for SDOF analysis especially for acceleration response as expected. For relative displacement response, errors are more than simplified methods and results are not close to MDOF model built in this thesis study. SDOF models are used for simplified models mentioned in Sections 4.2.3 and 5.3 and shock profile synthesis in Chapter 3. Moreover, SDOF DRFR method is used as a starting point for MDOF RFR method development.

SDOF transient analysis responses are tabulated in Table 5.11 and plots are presented in Figures 5.17-5.20.

Table 5. 11 SDOF Shock Responses at the Antenna Tip

SDOF Transient Responses	
Absolute Acceleration (G)	69.52
Relative Displacement (m)	0.124

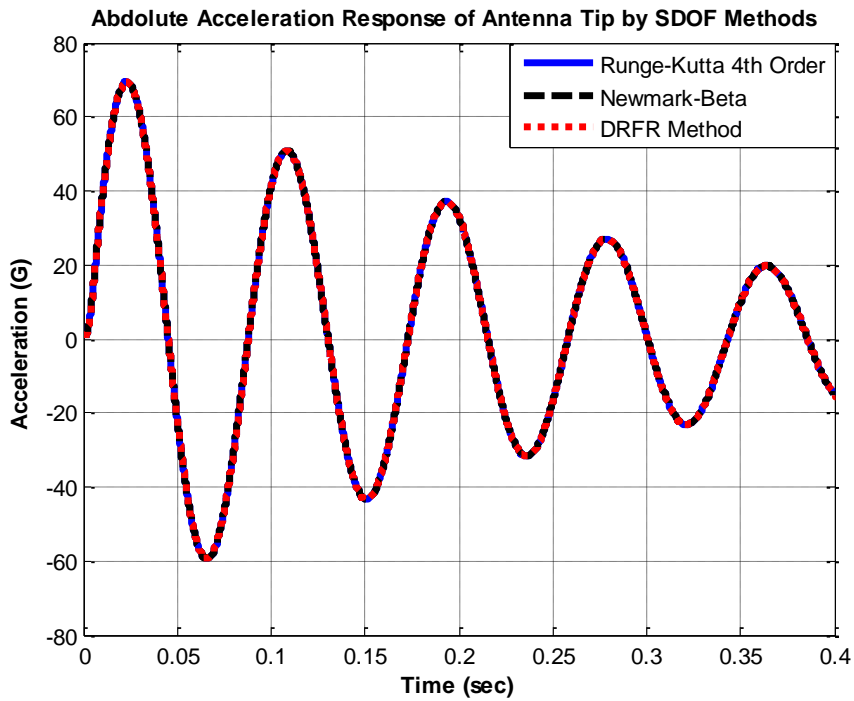


Figure 5. 17 SDOF Absolute Acceleration Response of the Antenna Tip

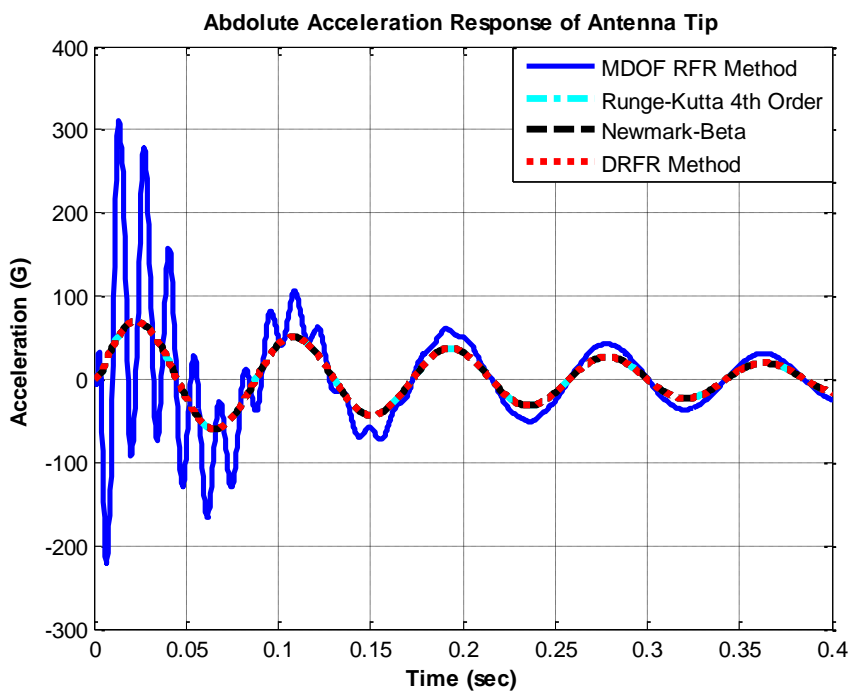


Figure 5. 18 Comparison of Absolute Acceleration Responses of the Antenna Tip

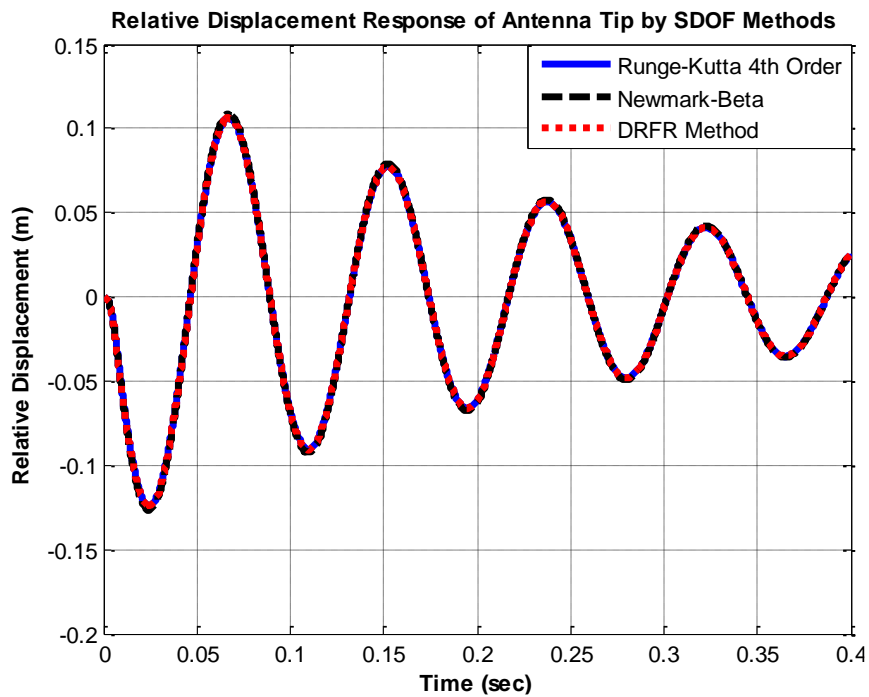


Figure 5. 19 SDOF Relative Displacement Response of the Antenna Tip

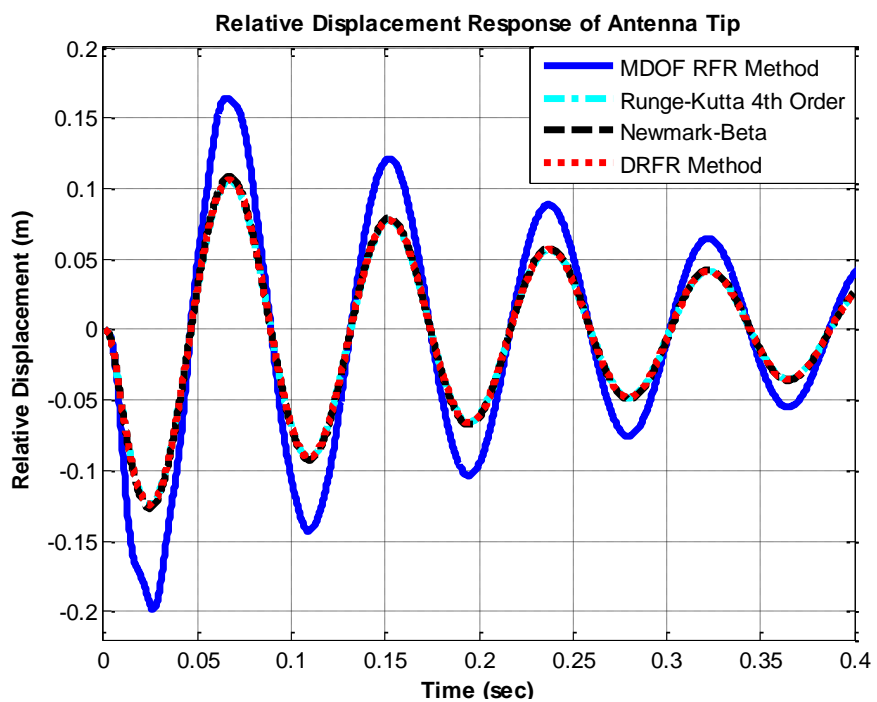


Figure 5. 20 Comparison of Relative Displacement Responses of the Antenna Tip

Phase portrait plot is also another tool to observe the region of SDOF analysis responses in the MDOF transient response analysis. The participation of one mode for transient responses can be clearly monitored in MDOF analysis, hence the importance and contribution of other modes are observed. Thus, the necessity of including at least more than one mode to the transient analysis is concluded.

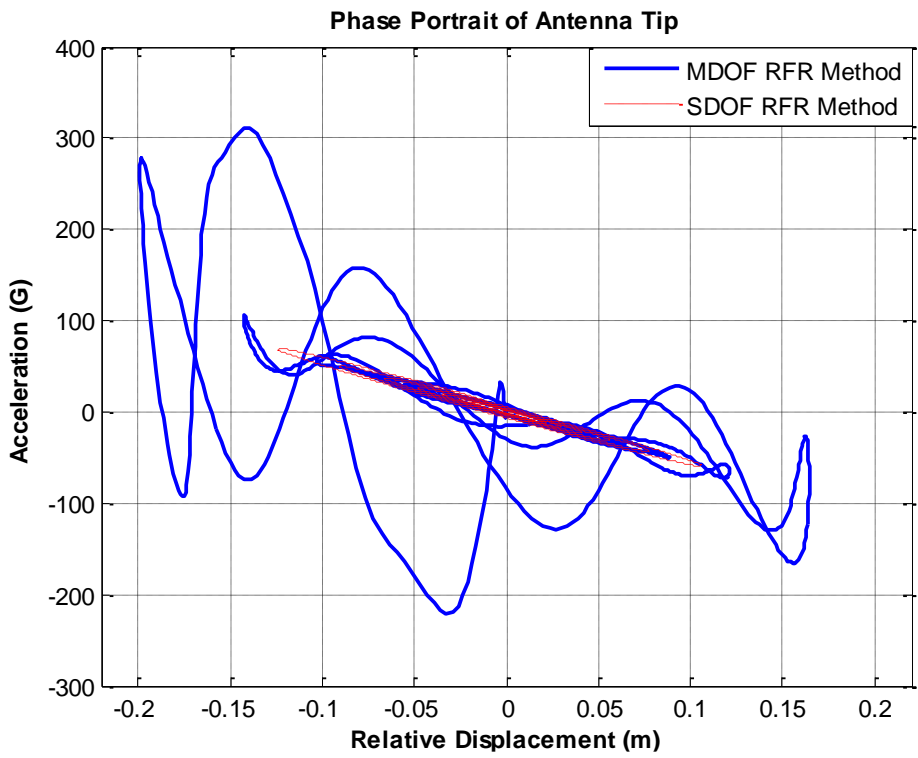


Figure 5. 21 Comparison of Phase Portraits of the Antenna Tip

5.5 Comments of Chapter 5

Results of mathematical modelling are presented in Table 5.12 along with exact solution.

Table 5. 12 Mathematical Model Responses at the Antenna Tip

Maximum Response	Exact Result	MDOF RFR Method/ Error (%)	ABSSUM Method/ Error (%)	SRSS Method/ Error (%)	NRL Method/ Error (%)	SDOF Model/ Error (%)
Absolute Acceleration (G)	310.5	310.6 / 0.03%	380.7/ 22.6%	292.8/ -5.7%	380.7/ 22.6%	69.5/ $\gg 100\%$
Relative Displacement (m)	0.199	0.199 / 0%	0.212/ 6.5%	0.199/ 0%	0.212/ 6.6%	0.124/ -37.7%

Comparing the results, MDOF modeling of antenna structure by RFR Method is very satisfactory so as to present almost exact results. Therefore, validation of MDOF mathematical model is achieved. This is very important to perform further analysis studies for isolation, component fatigue and so on.

Exact solution is obtained from the toolbox by Yang [32] since the excitation is classical pulse, antenna geometry can be modeled as a cantilever beam with initial conditions all kept zero. However, for different types of excitation, for different boundary conditions, it is not possible to find an exact solution. On the other hand, MATLAB® script written for MDOF RFR Analysis is capable to perform analysis with various shock inputs (e.g. square, sine, saw-tooth) and boundary conditions like fixed-fixed or simply supported. Arbitrary shock inputs can even be analyzed by MATLAB® script with some modifications on sampling and discretization.

Simplified methods estimates the transient response of antenna structure with mode-superposition method. Doing this, modal information of antenna structure

and corresponding SRS value of mode interested is used. Therefore, it is better approximation than SDOF analysis. For relative displacement, simplified methods yields very closer results to MDOF analysis while the acceleration response contains certain amount of error. Among these methods, SRSS method gives acceptable results for antenna structure. Therefore, this method can be used as an alternative for further studies like isolation and component fatigue. Other two methods are more successful while differences between natural frequencies are higher. NRL method, for example is the basis of Direct Dynamic Analysis Method (DDAM). For this method, different methodology is followed for modal analysis [55].

Single-degree-of-freedom solution is the most erroneous model among these models because it is independent from geometrical and modal properties of structure considered. In this study, SDOF model is utilized for determination of SRS and building the MDOF model from SDOF basics of RFR Method.

CHAPTER 6

TRANSIENT RESPONSE ANALYSIS OF ANTENNA STRUCTURE BY FINITE ELEMENT ANALYSIS

In this chapter, transient response analysis of antenna structure subjected to underwater shock explosions is performed by means of Finite Element Analysis (FEA). In the scope of this chapter, modal and transient analyses are performed by means of finite element software package ANSYS® R15.0. Antenna geometry created on computer aided drawing software program (NX) is imported to ANSYS® Workbench. Material properties of AA6061-T6 are introduced to the engineering data library. Workbench-Modal and Transient commands are employed for complete analysis along with Enforced Motion Extension. APDL code is also written to introduce boundary conditions, shock inputs, base acceleration input case and shock duration determination and obtain meaningful shock outputs needed like absolute acceleration, relative displacement and relative velocity. Modal analysis is performed to validate the antenna FEA model with MDOF mathematical model results. Then, transient analysis follows with validated model and shock responses are compared to MDOF model results. As an outcome of this study, FEA modeling option is to be proposed as an alternative to mathematical model in order to perform shock analysis from simple to complex antenna structures.

6.1 Modal Analysis of Antenna Structure

ANSYS® Workbench 15.0 is used to perform modal analysis. From workbench selections, “Modal (ANSYS)” is selected and dragged from Workbench to the standalone project created. First, geometry should be created on Design Modeler in ANSYS® Workbench or on any computer aided drawing software and then imported to “Modal”. In the analysis, antenna geometry is imported to ANSYS® as a pre-designed part file created by means of NX® 8.0. Since NX® 8.0 and ANSYS® 15.0 are working interactively, it is the best and easiest way to create and update models to be analyzed on ANSYS® platform. As the antenna material, AA6061-T6 mechanical properties are imported to “Engineering Data Sources” of ANSYS®. Properties are introduced with the values tabulated in Table 5.2. After geometrical and mechanical properties are introduced, modal analysis properties are defined one by one. Boundary conditions are introduced as a fixed support at one end of antenna structure and free otherwise, and all initial conditions are defined as zero. Meshing is defined with normal element sizes since structure is not complex and it does not have irregular surfaces. As an output, total deformations are selected and assigned for first five modes. From these assignments, natural frequencies and mode shapes of corresponding modes can be monitored. After modal analysis is performed, mode shapes and numerical results of natural frequencies for bending modes are obtained. Mode shapes obtained from FEA are presented in Figures 6.1 to 6.4.

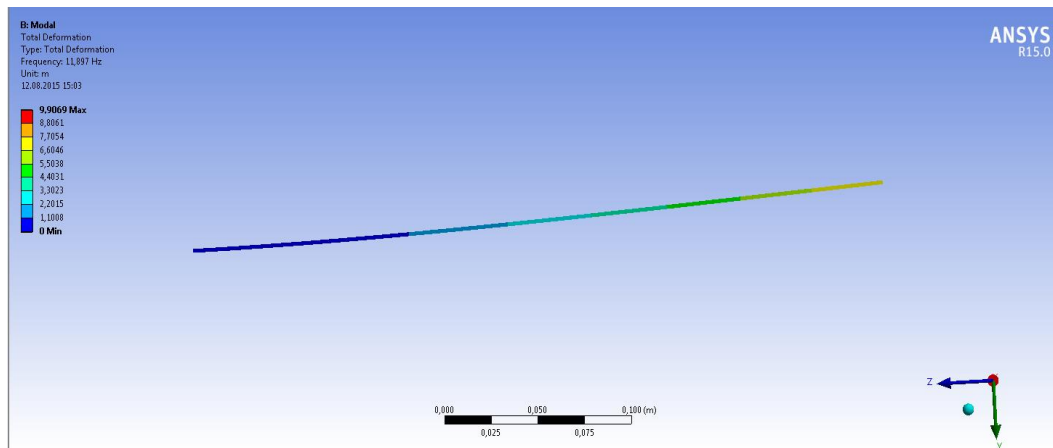


Figure 6. 1 First Mode Shape of the Antenna Structure (FEA Result)

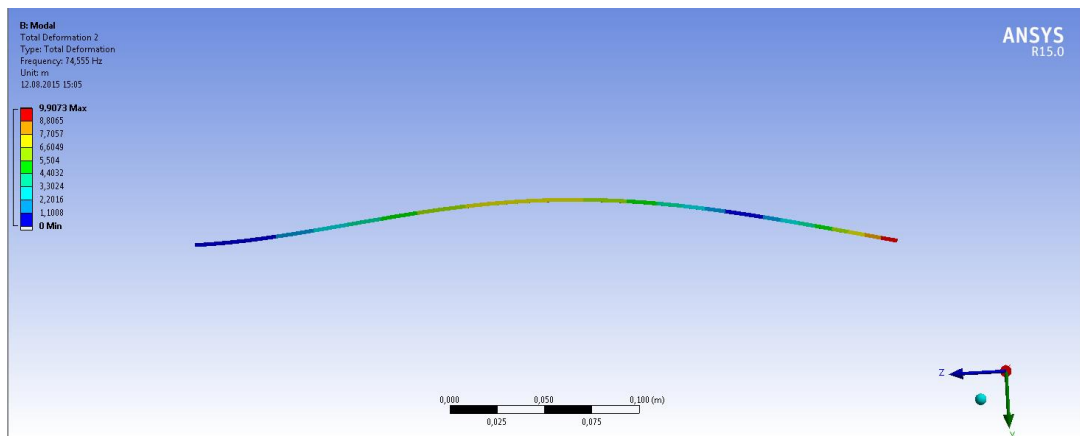


Figure 6. 2 Second Mode Shape of the Antenna Structure (FEA Result)

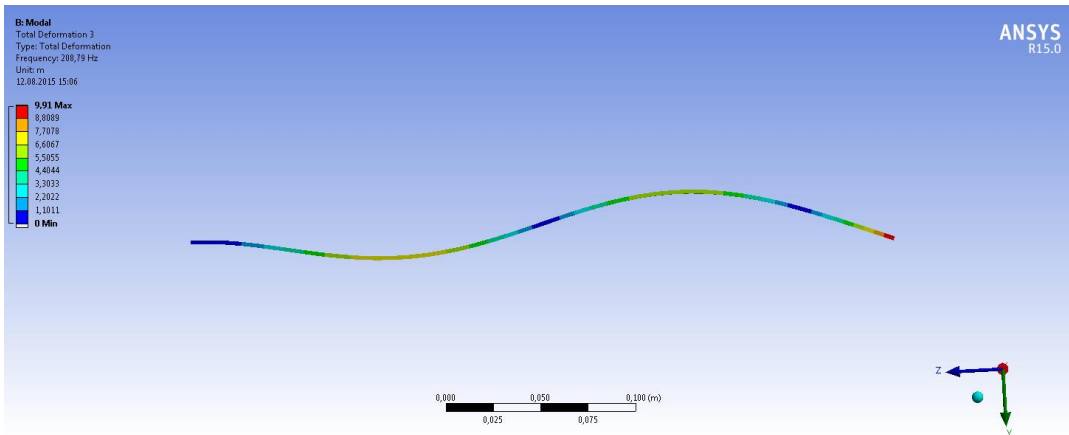


Figure 6. 3 Third Mode Shape of the Antenna Structure (FEA Result)

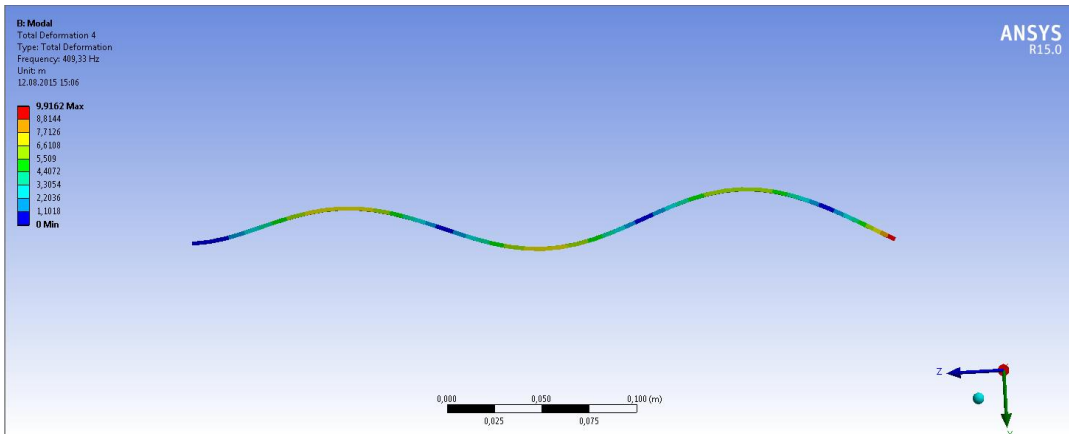


Figure 6. 4 Fourth Mode Shape of the Antenna Structure (FEA Result)

Comparing the mode shapes with mathematical model results presented in Figure 5.2, the mode shapes obtained from FEA model display expected shapes from theoretical background. Natural frequencies are also obtained from FEA modal analysis for the first four bending mode. It should be noted that in the ANSYS® results, the third mode is not a bending mode. So the third mode is skipped and the fourth mode reported by ANSYS® is taken as the third bending mode. Therefore, first, second, fourth and fifth modes predicted by ANSYS® are the first four bending modes of antenna structure. The reason behind this is that ANSYS® analysis formulation used is based on Timoshenko beam theory which includes

shear-deformation effects and this effect is neglected in the Euler-Bernoulli beam theory. First four bending modes presented by ANSYS® is tabulated in Table 6.1 and compared with mathematical model results obtained in Section 5.1.

Table 6. 1 Natural Frequencies of the Antenna Structure

Modes	Mathematical Model Results (Hz)	ANSYS® Results (Hz)	Percentage Difference of FEA Results
1	11.78	11.89	0.93 %
2	73.79	74.75	1.30 %
3	206.62	208.67	0.99 %
4	404.90	409.33	1.09 %

ANSYS® results and theoretical results are not different more than 1.3% for the first four modes. Thus the ANSYS® results match quite well with Euler-Bernoulli beam theory. Transient analysis can be performed since model is validated.

6.2 Transient Response Analysis of Antenna Structure

Transient analysis is performed by means of ANSYS® Workbench. Transient Structural command is selected for the transient analysis. For material properties and antenna geometry, pre-defined data to Modal is exerted to Transient Structural. Therefore, there is no need to define material or antenna geometry again. As a starting point of the transient analysis, the antenna base is defined as a “Named Selection”. Then, this selection is introduced as fixed support. After that, APDL command is added in order to define 200g 8ms half-sine shock input as the base acceleration. Total response time and effective shock duration are also defined within. In order to define input position of the base acceleration, antenna base defined as a “Named Selection” is used. APDL code also defines the outputs in a meaningful manner. Since “Transient Structural” does not present acceleration

output, acceleration output is defined in the code with manipulations of displacement or velocity output. From “Transient Structural”; number of time steps, total duration, and damping values are entered. For damping value, numerical damping entered manually as a Rayleigh damping stiffness and mass coefficients calculated for 0.05 modal damping or $Q=10$ which is compatible with mathematical modeling. Number of time steps (sampling) is selected as 4000 which is nearly the same as the number of time steps defined in the RFR method. As outputs, acceleration, displacement and velocity at antenna tip are selected. For relative displacement and velocity values of antenna tip, relative responses of antenna tip is calculated by subtracting the antenna base responses from absolute counterparts of antenna tip.

For solution methodology, ANSYS® Transient uses Newmark Time Integration Method to solve Equation (6.1) at discrete time points [54]. Briefly, the theory behind the algorithm is presented.

$$KD + C\dot{D} + M\ddot{D} = F \quad (6.1)$$

Newmark’s method solves this differential equation by implicit algorithm in Equations (6.2) and (6.3). The theoretical background of the algorithm is presented in Equations from (6.2) to (6.6).

$$D_{t+\Delta t} = D_t + (\Delta t)\dot{D}_t + (\Delta t)^2 \left[\left(\frac{1}{2} - \beta\right)\ddot{D}_t + \beta\ddot{D}_{t+\Delta t} \right] \quad (6.2)$$

$$\dot{D}_{t+\Delta t} = \dot{D}_t + (\Delta t) \left[(1 - \gamma)\ddot{D}_t + \gamma\ddot{D}_{t+\Delta t} \right] \quad (6.3)$$

In Equations (6.2) and (6.3) β and γ are constants. Responses are obtained from Equation (6.1) by substituting Equations (6.2) and (6.3) in Equation (6.1).

$$K \left\{ D_t + (\Delta t)\dot{D}_t + (\Delta t)^2 \left[\left(\frac{1}{2} - \beta\right)\ddot{D}_t + \beta\ddot{D}_{t+\Delta t} \right] \right\} + \dots \quad (6.4)$$

$$C \left\{ \dot{D}_t + (\Delta t) \left[(1 - \gamma)\ddot{D}_t + \gamma\ddot{D}_{t+\Delta t} \right] \right\} + M\ddot{D}_{t+\Delta t} = F_{t+\Delta t}$$

$$F_{t+\Delta t}^{residual} = F_{t+\Delta t} - K \left\{ D_t + (\Delta t)\dot{D}_t + (\Delta t)^2 \left(\frac{1}{2} - \beta \right) \ddot{D}_t \right\} - \dots \quad (6.5)$$

$$C \left\{ D_t + (\Delta t)(1-\gamma)\dot{D}_t \right\}$$

Accelerations can be obtained as presented in Equation (6.6). Other response information can be obtained from the acceleration response.

$$\ddot{D}_{t+\Delta t} = K^{-1} F_{t+\Delta t}^{residual} \quad (6.6)$$

With the guide of analysis process presented above, transient responses are obtained and compared to MDOF analysis using RFR Method. Shock input is the same as before, that is, 200g 8ms half-sine base acceleration is applied to the structure (Figure 6.5). Absolute acceleration response of the antenna tip is presented in Figure 6.6.

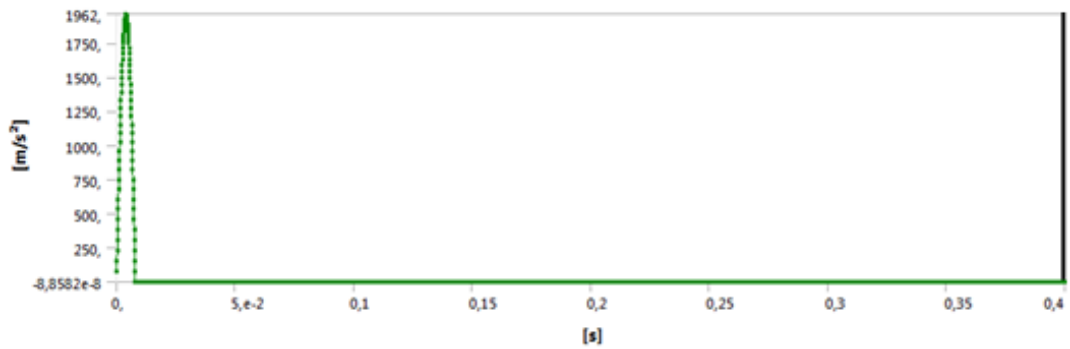


Figure 6. 5 200g 8ms Half-sine Acceleration Input Defined to ANSYS®

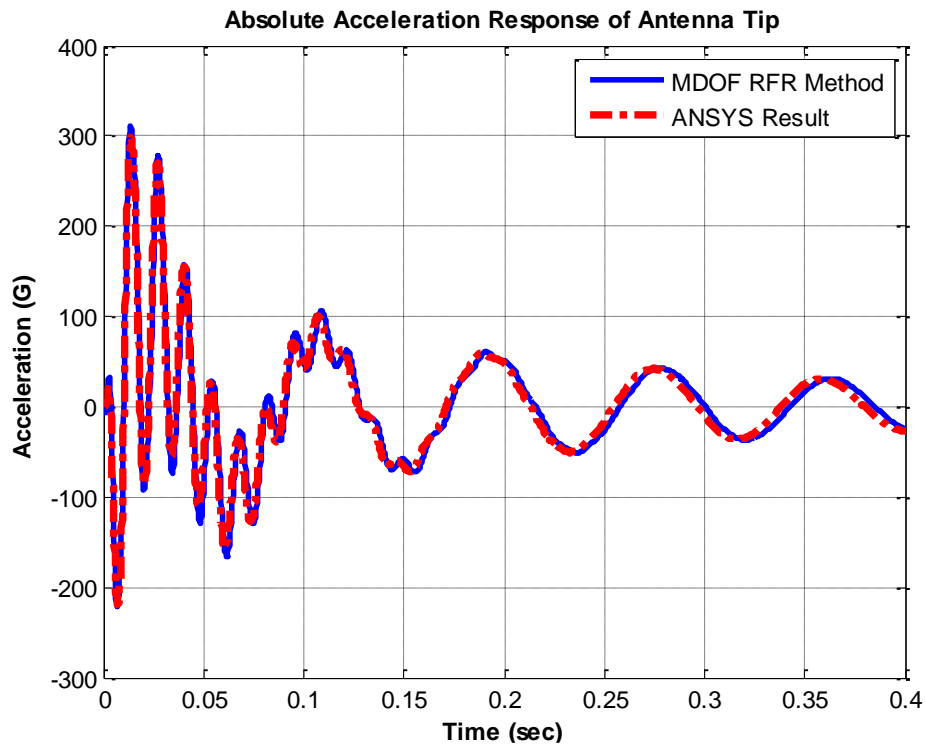


Figure 6. 6 ANSYS® Absolute Acceleration Response of the Antenna Tip

Relative displacement response of the antenna tip using ANSYS® along with MDOF RFR method result is presented in Figure 6.7. Finally in Figure 6.8, relative velocity response of the antenna tip is illustrated.

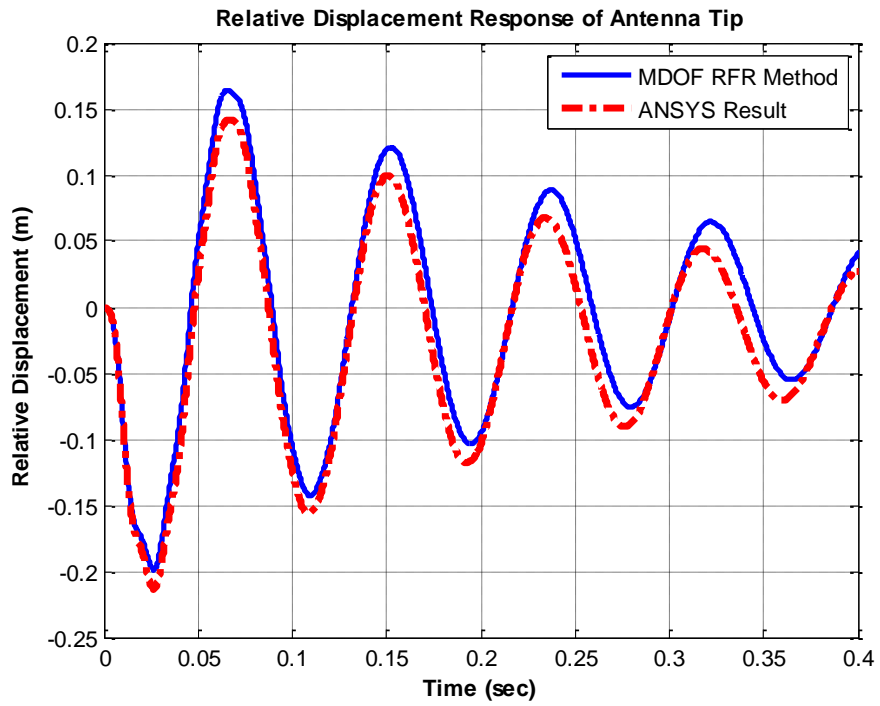


Figure 6. 7 ANSYS® Relative Displacement Response of the Antenna Tip

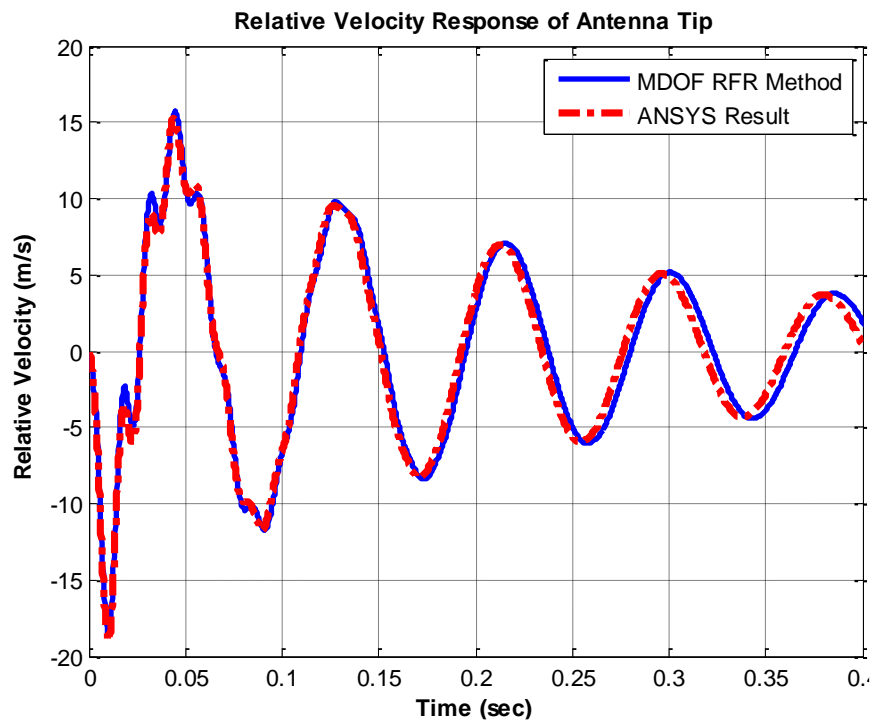


Figure 6. 8 ANSYS® Relative Velocity Response of the Antenna Tip

6.3 Discussion for Chapter 6

Results of finite element analysis are presented in Table 6.2 along with MDOF mathematical model and exact solution.

Table 6. 2 Comparisons of Maximum Transient Responses

Maximum Response	Exact Results	MDOF Mathematical Model Results/ Percentage Error	FEA Results/ Percentage Error
Absolute Acceleration (G)	310.5	310.6 / 0.03%	302.7 / -2.51%
Relative Displacement (m)	0.199	0.199 / 0%	0.208 / 4.50 %
Relative Velocity (m/s)	18.52	18.58 / 0.03	19.00 / 2.59 %

As seen from Figures 6.5 to 6.8 and Table 6.2, finite element analysis results can be termed satisfactory within the 4.5-percent error range compared to exact result. Therefore, for complex geometries and for the cases whose mathematical model is hard to obtain, finite element analysis can be the alternative way of solution. As an important remark, during design process, 5 to 6-percent error margin can be defined in order to be on the safe side by finite element analysis for transient analysis.

Comparing mathematical model and finite element analysis, a slight difference is observed. Although antenna structure is analyzed with full modal-transient method with ANSYS®, there are reasons behind this slight difference. ANSYS® model uses Newmark algorithm for the solution methodology while the mathematical model only uses recursive algorithm to solve convolution integrals. Therefore, the

solution formulation for mathematical model is almost exact. Moreover, in the mathematical model beam element is modeled as 1-D for forcing directions. Thus, only transverse forces are considered in the model. However, finite element analysis software uses “beam” elements on which three-directional forcing is applied. This causes the additional effects that change the dynamic responses of beam element. Because of this reason, finite element modeling may present closer results to real-life cases. Since both methods present very close responses, they can be used interchangeably for different cases regards to the ease of use.

CHAPTER 7

EXPERIMENTAL ANALYSIS OF ANTENNA STRUCTURE

7.1 Introduction

Theoretical models presented in previous chapters are tried to be verified by means of both modal and transient experimental analyses.

Experimental analysis for modal verification is performed by impact hammer tests. The antenna structure is clamped in cantilever beam configuration to the experimental setup base. An impact hammer is triggered to excite antenna modes and monitor the response measured from the antenna tip by means of a micro-accelerometer. The tip response is collected as a frequency response function. Excitation is taken as the forcing by hammer and the response is measured by the accelerometer on antenna tip in the forms of acceleration per unit force. Therefore, natural frequencies and modal damping values are calculated via acquired data. Experimental setup and experimental procedures are explained in detail.

Shock testing is performed after modal verification. Shock testing is executed by means of a drop table. Desired acceleration input values in desired time interval is only possible with high impact shock machines or drop table as a simple shock machines. Shock profile synthesis is performed in order to be able to perform shock testing with drop table test set-up instead of high impact shock machines because of the inadequacy of such experimental infrastructure in Turkey. Therefore, it has become possible to perform drop tests for verification of models or qualification of structures instead of complex test procedures. Shock tests are performed using drop table and data acquisition system. Data is acquired by means of high acceleration (up to 1000g) durable shock accelerometers.

7.2 Modal Verification of Antenna by Impact Hammer Test

Experimental modal analysis of the antenna structure is performed for determination of modal characteristics like natural frequencies and modal damping ratios. Theoretical models are compared to the experimental results. Thus, modal verifications are to be completed.

Experimental modal analysis requires the following experimental set-up. An exciter is to apply a desired input force to the antenna. A transducer is required to convert the mechanical motion of the antenna into an electric signal. Then, amplifier (or signal conditioning amplifier) makes the transducer characteristics compatible with the data acquisition system using calibration values of the transducer. Finally, an analyzer capable to perform required tasks such as signal processing and modal analysis by means of an integrated software is needed.

For modal analysis of antenna structure, special equipment are used in order to perform the analysis with minimum possible error. Dimensions and weight of antenna limits the hammer and accelerometer selection. Therefore, miniature hammer which is PCB PIEZOTRONICS® 086E80 and small accelerometer which is PCB PIEZOTRONICS® 356A01 are used to avoid mass loading. As an amplifier and analyzer, IOTECH® Data Acquisition System with Ethernet Interface, 516/E is used. Hammer input signal and accelerometer output signal are collected by this system and converted to meaningful outputs what user desires to monitor. Technical data-sheets of these equipment are presented in Appendix B.



Figure 7. 1 PCB PIEZOTRONICS® 086E80 Miniature Impact Hammer



Figure 7. 2 IOTECH® Data Acquisition System

eZ-Analyst software is used as the interface. By means of this software, IOTECH® system can be used as measurement and playback modes. For measurement modes, one of the alternatives is modal analysis. Within preparation steps, analyzer settings are adjusted initially. Maximum frequency of interest, number of spectral lines, Nyquist factor, filter options, trigger options and averaging options can all be set. For antenna structure, interested frequency range is set as up to 1000Hz since first

6 mode is within. Spectral lines are set as 3200. Low-pass filter for anti-aliasing and high-pass filter for AC coupling is selected. This selection is adjusted to 0.1 Hz for the accelerometer used in the experiment. Trigger option is set for every hammer input and averaging is set to 10 samples per experiment. After analyzer settings, input settings are adjusted for input channels (hammer and accelerometer). In this step, sensitivity values, coordinate definition and units of devices should be defined properly in order to obtain correct signals. Finally FFT and recording adjustments are followed. For modal analysis, “Block Rejection” option is activated in order to see trigger, double hit or overload warnings on analysis interface to test the “goodness” of acquired data..

The antenna test structure is manufactured from AA6061-T6 material with exact size and weight. Experimental jigs are also manufactured in order to attach antenna structure to the base and clamped the antenna to the base properly. Antenna attachment to the experimental jig is presented in Figure 7.3.

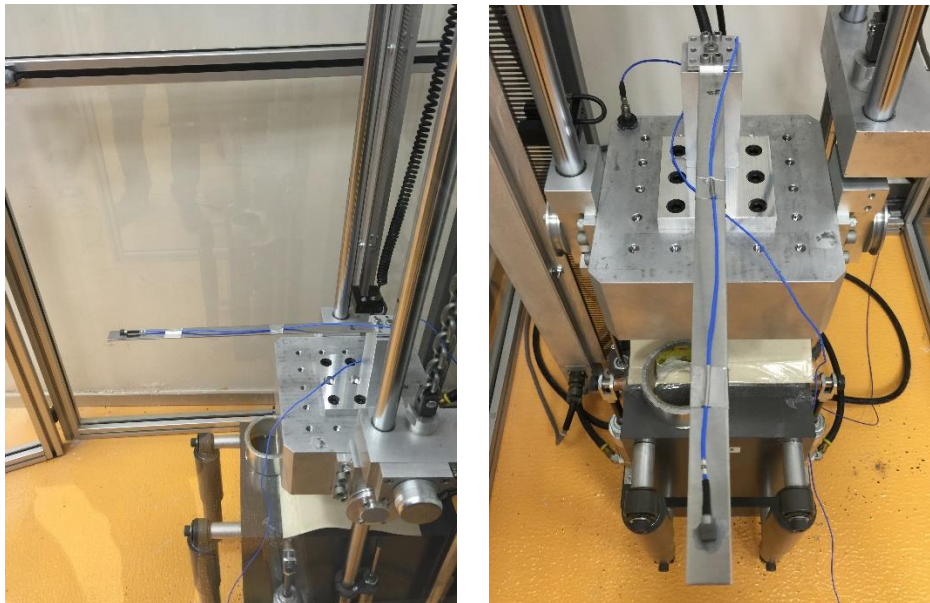


Figure 7. 3 Antenna Attachment to the Experimental Set-up

Starting to modal analysis, accelerometer is attached to the antenna tip, impact hammer and accelerometer cables are connected to IOTECH channels properly. Adjustments on the eZ-Analyst software are made accordingly. Then, 10 consecutive hammer forcing is applied to the antenna structure per experiment and this experiment is repeated five times. Therefore, total collected data is averaged and Frequency Response Function (FRF) of antenna as g/N is observed. By means of eZ-Analyst software, FRF data and coherence information is transferred to MATLAB® in order to compare with theoretical models.

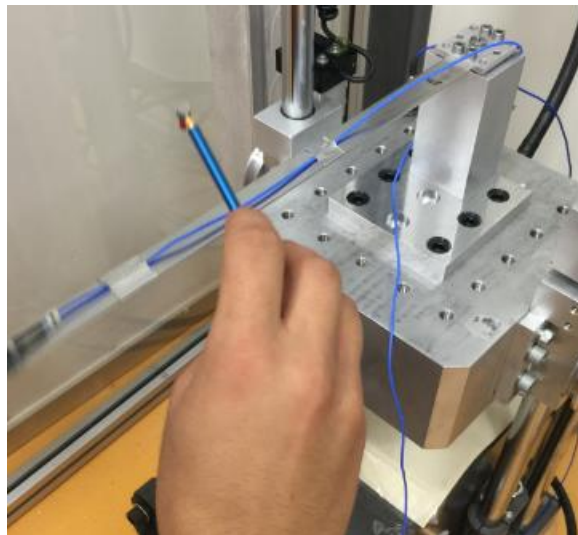


Figure 7. 4 Hammer Test of Antenna Structure

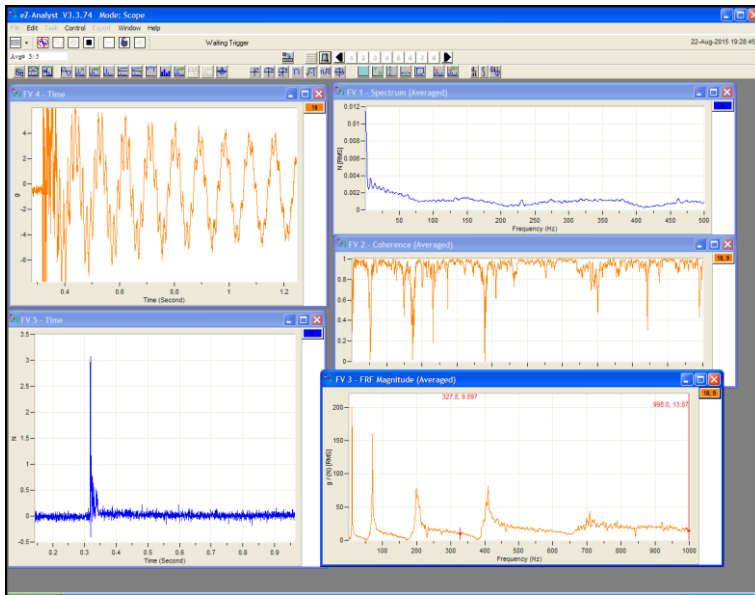


Figure 7. 5 eZ-Analyst Screen During Experiment

From collected data of modal testing, FRF in the form of accelerance is plotted on Figure 7.6.

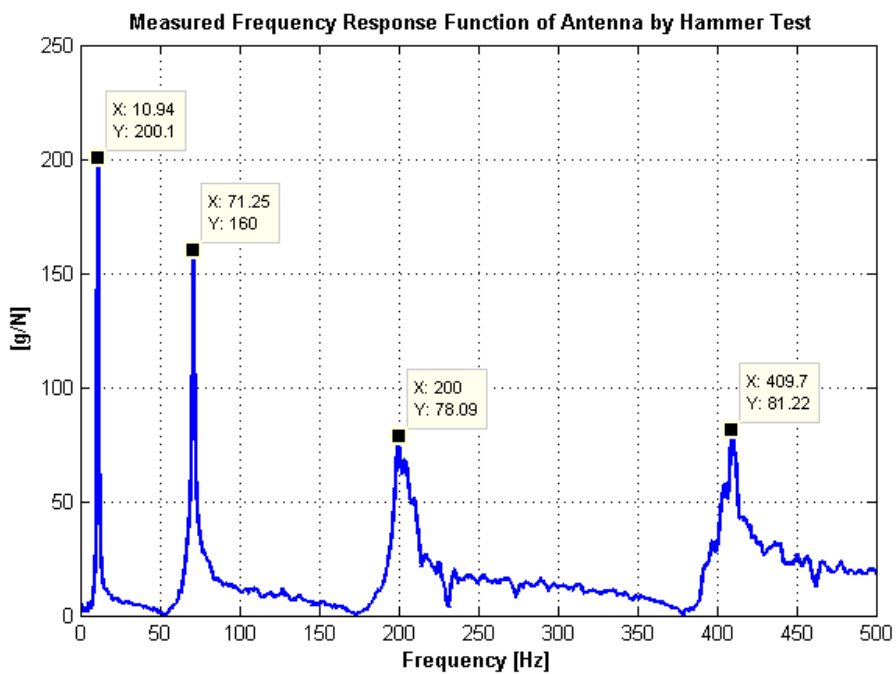


Figure 7. 6 Measured FRF of Antenna Structure

Table 7. 1 Natural Frequencies of Antenna Structure

Modes	Experimental Results (Hz)	Coherence	Mathematical Model Results (Hz) / Error (%)	ANSYS® Results (Hz) / Error (%)
1	10.94	0.937	11.78 / 7.69%	11.89 / 8.68%
2	71.25	0.909	73.79 / 3.55%	74.75 / 4.91%
3	200.00	0.901	206.62 / 3.31%	208.67 / 4.34%
4	409.68	0.910	404.90 / 1.11%	409.33 / 0.09%

As observed from Table 7.1, mathematical model results and ANSYS® results are very close to experimental results in natural frequency point of view. Below 7.5 percent error is a very satisfactory for modeling the antenna structure as Euler-Bernoulli beam with certain assumptions discussed in Chapter 4. Moreover, this error may be misleading; because, accelerometer weight should be added to the antenna tip as a point mass on mathematical and FEA models. With that enhancement on the mathematical the model, for the first mode natural frequency can be calculated in Equation (7.1), where “M” is antenna mass and “m” is accelerometer mass with its cable which is 0.003 kg.

$$f_1 = \frac{1}{2\pi} \sqrt{\frac{3EI}{(0.2235ML + m)L^3}} \quad (7.1)$$

From Equation (7.1), first natural frequency can be approximated as 11.08 Hz. Therefore, the error calculated for first mode is updated as 1.28%.

The finite Element Model is also updated for accelerometer mass and modal analysis is performed again. Comparisons of updated natural frequencies with experimental result are presented in Table 7.2.

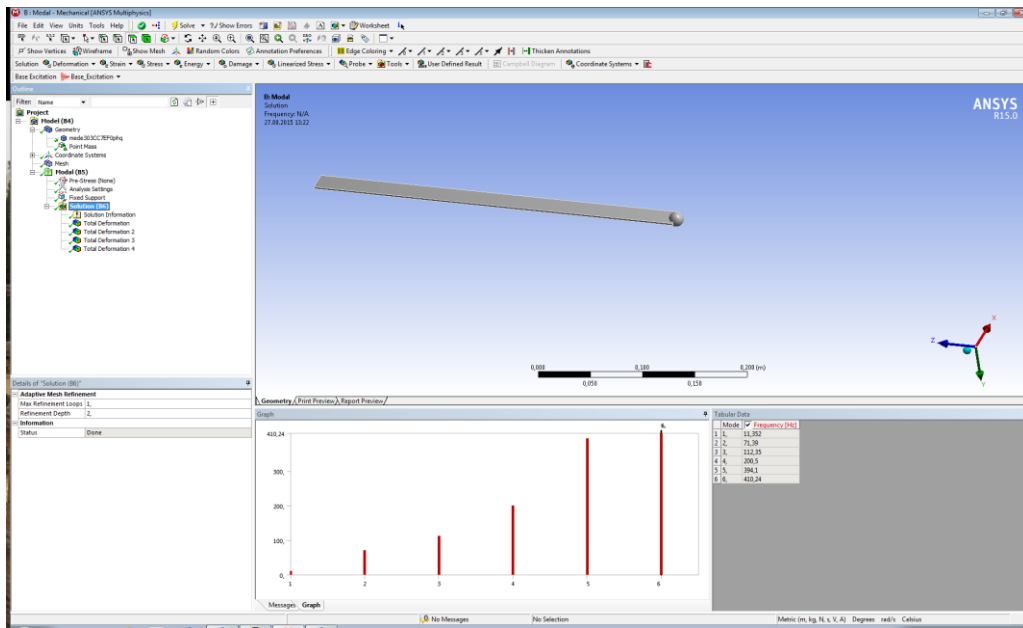


Figure 7. 7 Modal Analysis by ANSYS® with tip mass

Table 7. 2 Natural Frequencies of Antenna Structure with Tip Mass

Modes	Experimental Results (Hz)	ANSYS® Results with Tip Mass (Hz)	Error (%)
1	10.94	11.35	3.74%
2	71.25	71.39	1.96%
3	200.00	200.5	0.25%
4	409.68	410.4	0.18%

As observed from Table 7.2, after the mass addition to antenna tip, FEA results become very close to the experimental results. Therefore, it can be concluded that both mathematical model and FEA model is verified with experimental modal analysis point of view.

Modal damping ratios are found by means of half power point method [44]. The formulation is presented as Equation (7.2).

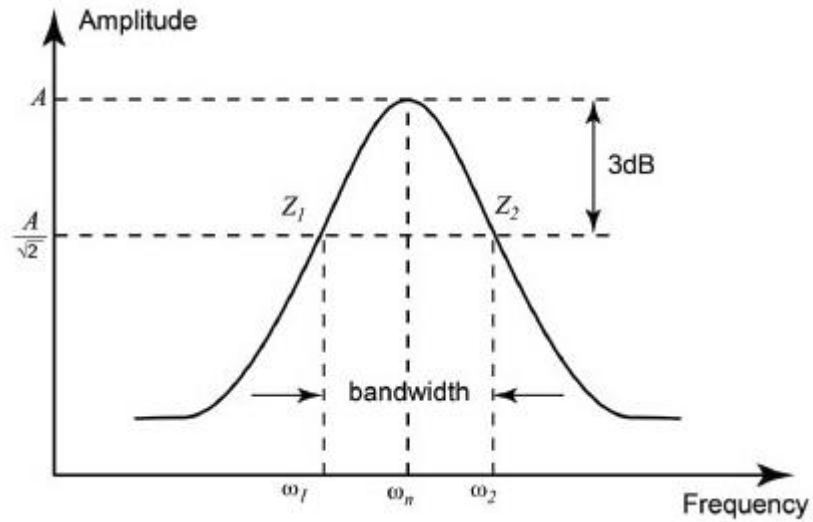


Figure 7. 8 Response Curve Showing Half-Power Points and Bandwidth [44]

$$\Delta\omega = \omega_2 - \omega_1 \approx 2\xi\omega_n \quad (7.2)$$

Equation (7.2) holds if damping is light; therefore, light damping assumption is to be checked after modal damping ratio calculations. From Table 7.3, it is concluded that damping can be considered as light (below 10%). However, for transient analysis verification, 5% modal damping should be updated (for mathematical and FEA models) to the values presented in Table 7.3.

Table 7.3 Modal Damping Ratios of Antenna Structure

Modes	ω_n	ω_1	ω_2	Modal damping ratio (ξ)
1	10.938	10.776	11.239	0.0210
2	71.25	70.559	71.649	0.00765
3	200.00	197.876	206.189	0.0207
4	409.68	407.826	412.403	0.00559

7.3 Drop Experiment of Antenna Structure

Underwater shock explosion profile which antenna structure is exposed to, is synthesized in Chapter 3 as half-sine profile. This introduces a convenience for the experimental procedure. While double half sine pulses are very hard to generate in small-to-medium scale laboratory conditions, half sine can easily be created by drop test experiment. Shaker test can be proposed as another alternative for half-sine input but it is limited up to 50-60 g's from amplitude point of view. Thus, drop test experiment is set to be performed for experimental transient analysis of antenna structure. Drop test experiment is again performed on laboratory located in ASELSAN. For drop test experiment, a drop table and built-in signal processing system is used. Drop table used for experiment is LANSMONT® PDT 80 with built-in controller and signal processing system produced by DataPhysics Corp.®. Data sheets of both products are presented in Appendix B. Additionally, IOTECH® data acquisition system mentioned in Section 7.2 with mini-accelerometer PCB PIEZOTRONICS® 356A01 which is capable of up to 1000g shock acceleration are used. Accelerometer is again placed at the antenna tip to monitor and record shock response time history while another accelerometer is placed onto the drop table to monitor shock input exposed to antenna base. FRFs and time history data can be collected and monitored by means of IOTECH® and eZ-Analyst® software. 200g-8ms shock input is adjusted by changing the drop

table properties. Release height affects the amplitude of shock while pad rebound affects the effective shock duration. Therefore, as the preliminary work, proper pad arrangement and release height is found by dummy drop experiments with and without antenna structure. Dummy drop test without antenna structure is performed in order to determine rebound coefficient of pads. After rebound coefficients are determined approximately, release height is found easily. After one or two trial-and-error, the exact height is determined. Shock duration is adjusted afterwards by changing pad thickness.

For the first trial, formulation given in Equation (7.3) to (7.6) which are taken from ANSI/ASA S2.62-2009 Standard [67] is used. Then, exact release height and pad configuration is found with small adjustments.

$$\Delta v = v_2 - v_1 \quad (7.3)$$

$$A = \frac{\pi \Delta V}{2D} \quad (7.4)$$

$$h = \frac{\Delta v^2}{2g} \quad (7.5)$$

$$h_r = \frac{\left(\frac{\Delta v}{1 + e_{res}} \right)^2}{2g} \quad (7.6)$$

where; “ v_1 ” is velocity before impact, “ v_2 ” is velocity after impact, “ h ” is no rebound drop height, “ g ” is gravitational acceleration, “ D ” is threshold pulse duration, “ A ” is threshold pulse amplitude “ e_{res} ” is coefficient of restitution and “ h_r ” is drop height with rebound.

Exact release height is set to 153 mm with POM/C pad material and 8 unit 1/6” felt above the pad. When everything is set, drop experiment is performed via controller

of the drop table and data is taken from both drop table for input signal profile and from antenna tip in order to measure the antenna response.

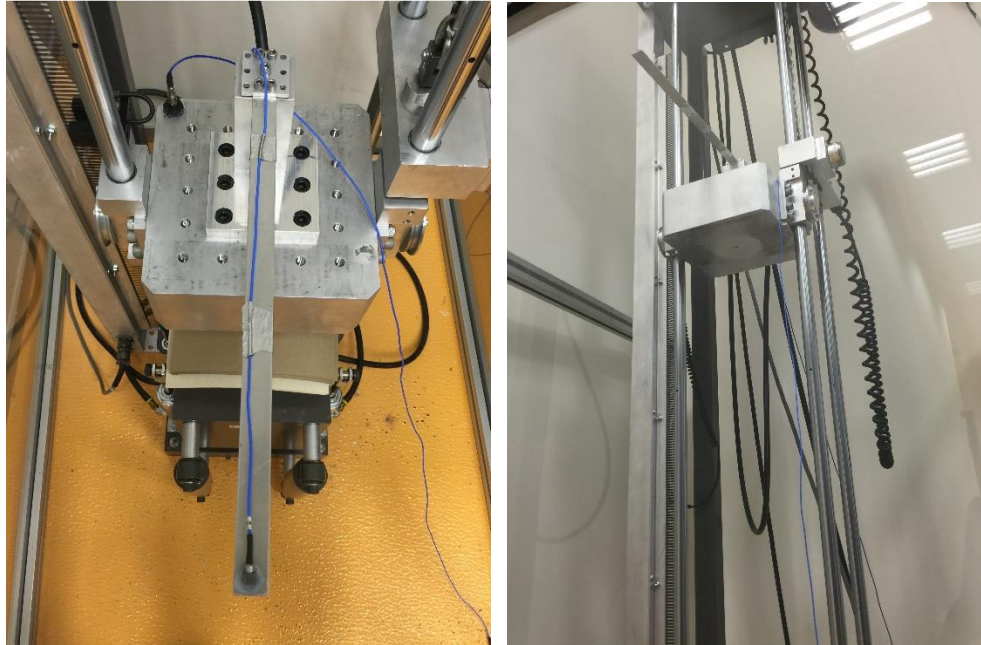


Figure 7.9 Drop Test Experiment

Input acceleration signal is measured from drop table jig base, and the output response is measured from antenna tip as can be seen in Figure 7.9. Responses are taken as the time history data for acceleration response at antenna tip.

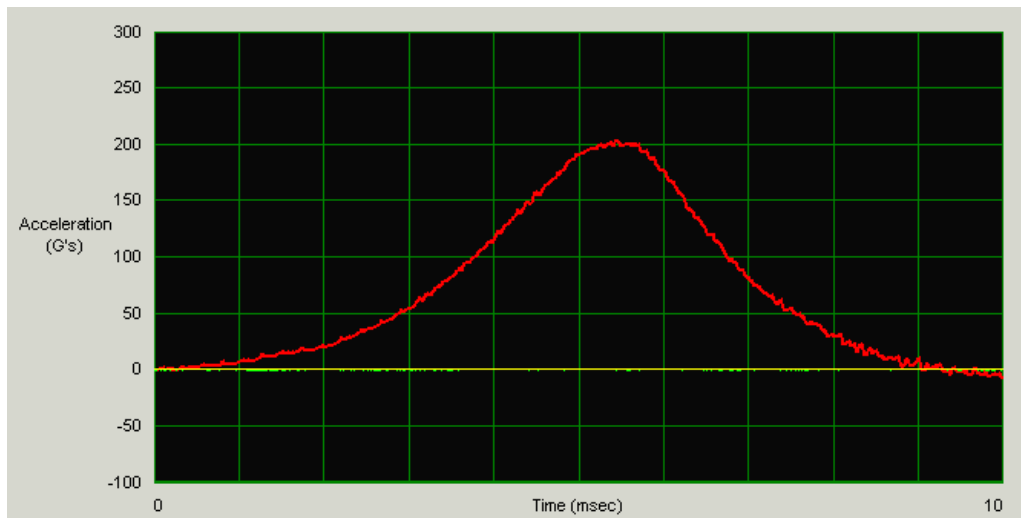


Figure 7. 10 Shock Input Measurement Taken From Drop Table

Acceleration response measured from the antenna tip is compared to theoretical model results in Figures 7.11 and 7.12.

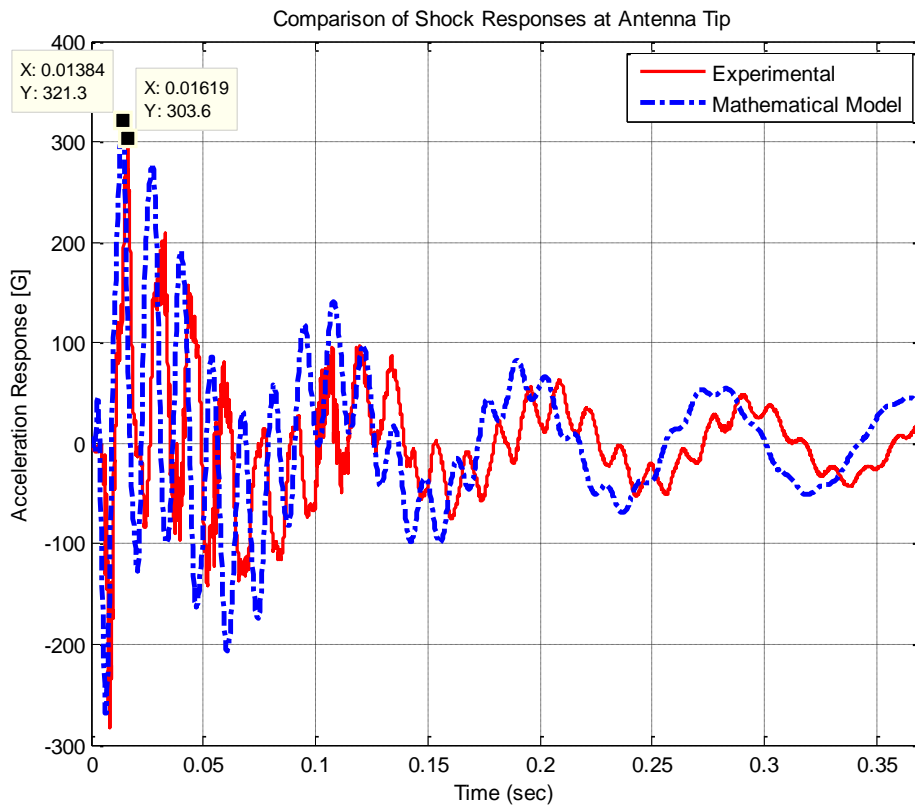


Figure 7. 11 Mathematical Model and Experiment Comparison

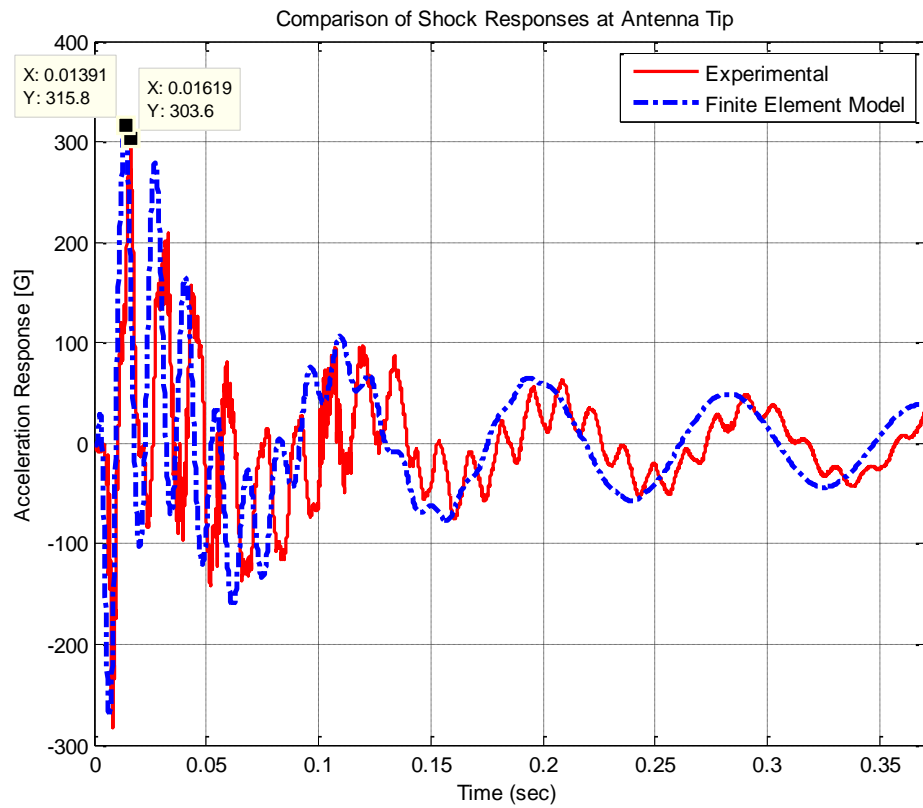


Figure 7. 12 FEA Model and Experiment Comparison

Acceleration response measured from experiment is validated by checking the frequency content of the signal. Frequency content of signal contains natural frequencies of antenna structure, therefore, it is assured that acceleration data contains meaningful data for antenna structure.

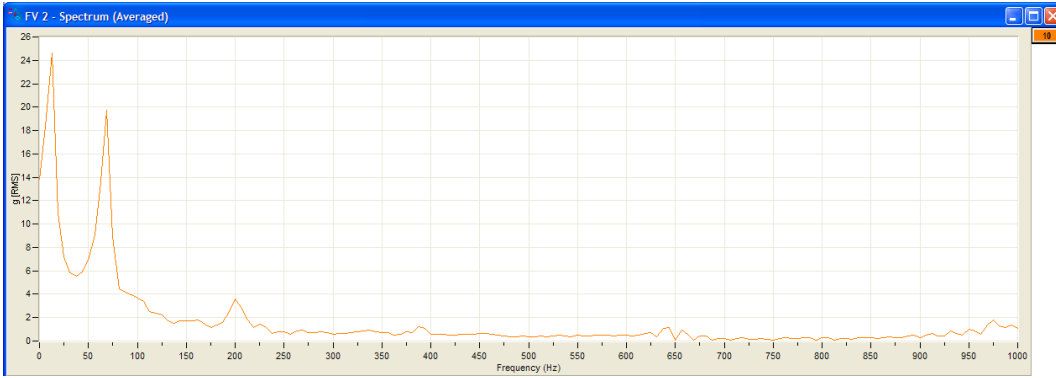


Figure 7. 13 Frequency Content of Measured Data

Results are tabulated in Table 7.4. The experimental result is taken as the reference and modeling results are compared to experimental results.

Table 7. 4 Maximum Absolute Acceleration Results of All Analyses

	Experimental	Mathematical Model	ANSYS®
Absolute Acceleration (G)	303.6	321.3	315.8
Error	-	5.83%	4.02%

7.4 Comments on Verification Results

In this chapter, verification of the theoretical models, namely, the mathematical model and the FEA model is performed. Antenna model as Euler-Bernoulli beam with Classical Approach is verified by means of hammer testing. In the light of test results, natural frequencies are found to be very close to the experiment in 5-percent error interval. After enhancement of antenna model with additional tip mass (accelerometer mass), this error interval is reduced to almost 3-percent.

Therefore, mathematical and FEA models are verified with very fair natural frequency results. Moreover, in order to update mathematical model, modal damping ratios are calculated from FRF curve of experimental results by means of Half Power Point Method. Tip-mass addition and damping ratio correction is immediately performed for updated models. These models are used for transient response comparison to experimental shock responses.

In the second part of this chapter, models are verified with drop test experiments gathering transient response of the antenna. Comparing the acceleration responses of mathematical model and experiments, response characteristics are found to be very close. As frequency spectrum of experimental results contains natural frequency peaks, experimental results are cross-checked. Maximum acceleration response is the most important point to compare the results. As seen on Table 7.4, both models give higher responses than experimental results. However, up to 5% error for modeling shock phenomena is reported to be very satisfactory. Due to the fact that model results are higher than experimental results, designs are to be conservative and safe from failure as to be seen in Chapter 8. Noting that input half sine profile measured for drop experiment is not an exact shape of desired half sine input. However, the difference between the maximum acceleration response to measured and theoretical responses is almost one percent. Thus, this small variation is not taken into considerations for experimental shock analysis.

Upon considering Figure 7.11, general characteristics of responses are very similar. However, shift of time axis for experimental results is observed after the effects of harmonics are dominant. There are also some irregularities on the sinusoidal shape of response curve. Possible reason for these differences is geometrical nonlinear effects or nonlinear effects associated with boundary conditions which are not considered in linear model. These effects are seen less on the FEA model, because FEA model contains certain amount of nonlinear effect inherently. For the FEA model, as seen in Figure 7.12, there is also a slight difference between damping characteristics to experimental results. After updating the modal damping ratios, only first two modal damping ratios can be defined to ANSYS® due to the use of

Rayleigh Damping Modeling. This yields some harmonical differences on last parts of time history. As four modal damping ratio can be defined on mathematical model, this differences are not observed that much.

After the experimental analysis is performed for antenna structure, it can be concluded that mathematical model and FEA models are satisfactory enough for use in design, qualification and isolation stages. In the lights of these verifications, these models are readily employed for shock severity considerations at shock survival stage of electromechanical design.

CHAPTER 8

SHOCK SEVERITY FOR ANTENNA STRUCTURE

Shock input can have so severe effects that antenna performance may decrease in unacceptable levels, electrical components attached on antenna may fail, and antenna structure may face mechanical failure. Therefore, preliminary analysis is performed by mathematical models and precautions are held in order not to face with adverse effects of shock mentioned above. In this chapter, shock effects on the antenna structure are examined, design limitations are drawn and precautions onto the adverse effects of underwater shock are presented and verified with experiments.

8.1 Shock Effects on Antenna Performance

One of the most important operational considerations in design of an antenna is the direction of the radiation and angular location of the maximum radiation of antenna pattern. If an antenna is bent through the axis where the pattern of it is symmetrical with respect to that; this situation may lead to significant angular position shift on the location of the maximum radiation on the antenna pattern. The shift mentioned has directly affected the effective range of the antenna and some other parameters. Moreover, this may lead to high error rates and false (artificial) results in case of some applications such as direction finding (DF) and direction of arrival (DoA). Dipole antenna structure examined in this study is with narrow bandwidth placed through the z-axis. If it is deformed by 8 degrees, the decrease in gain may reach to 1.6 dB approximately at the plane of azimuth. This change in gain of the antenna leads to decrease in effective range approximately 4700 km. The limitation of the

antenna is at most 1.6 dB gain decrease. In order to compensate the decrease in effective range; higher power may be applied to the antenna. However, this is not an effective solution because components of antenna may not withstand to this level of power along with high power consumption. Therefore; the required solution is to keep the bending degree of the antenna in an acceptable range where the gain of the antenna varies on values that are appropriate according to proposed utilization of the antenna. Thus; shock isolation of antenna structure should keep the amount of bending of the antenna in the allowable range which comes from the electrical design and pattern analysis of the antenna, that are, operational constraints. The collinear antenna array of four dipole elements is given with the effect of bending angle of the antenna pattern and gain. As a limitation comes from antenna performance is maximum deflection of antenna structure should be in region of **-18.6 to +18.6 cm**. Therefore, in electromechanical design stage of antenna, from mathematical model or FEA model, maximum displacement is observed and antenna performance decrease can be estimated. For the antenna mentioned in this thesis, for synthesized shock value of 200g 8ms, relative displacement curve is plotted as follows. The analysis is performed for damping values found from the experimental analysis with the tip mass added to the antenna.

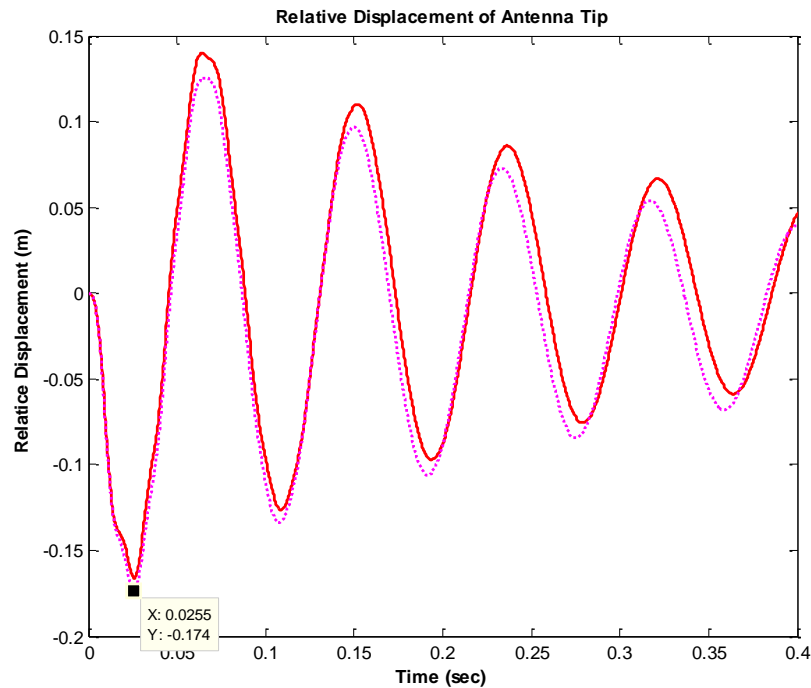


Figure 8. 1 Relative Displacement of the Antenna Tip

From transient analysis, maximum relative displacement of antenna is found as 17.4 cm. The antenna performance decrease for corresponding bending value is found as 1.57 dB on radiation patterns. Therefore, it is within the allowable limits for proper functioning of the antenna. Furthermore, the mathematical model is proved to be conservative comparing the experimental analysis. The antenna performance is then expected to be higher than the predicted one and the antenna performance can be regarded as “safe”.

In designer point of view, as a general design approach, shock effects on antenna performance can be added to design process by applying the iterative design procedure for the antenna structure. Shock analysis and electromagnetic analysis can be performed together and optimum antenna design structure can be achieved by changing antenna geometry, electromagnetic design or implementing isolation concerns. Electromagnetic analysis results are given in Figure 8.2 and 8.3.

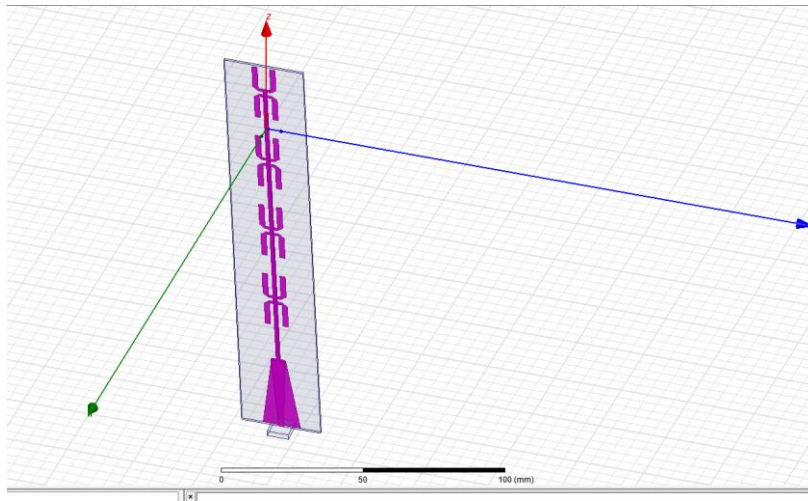


Figure 8. 2 Electromagnetic Analysis of Dipole Antenna by HFSS®

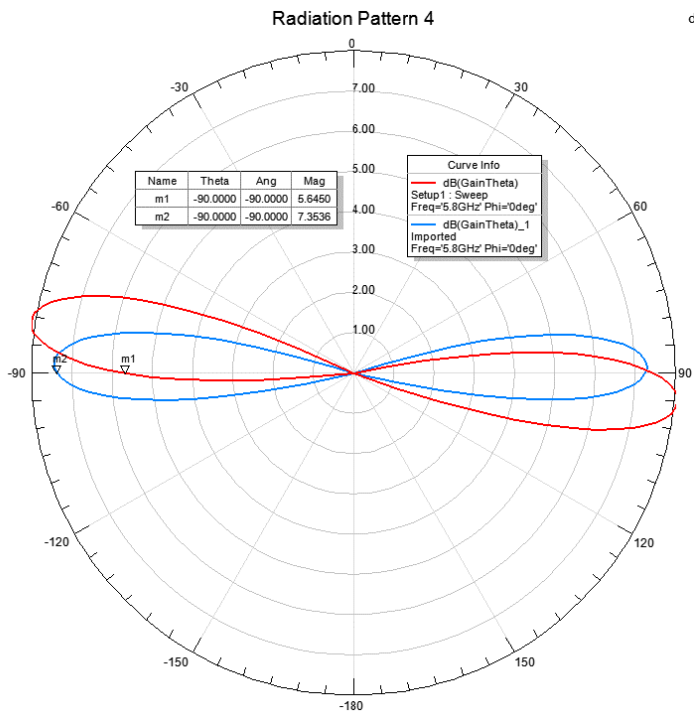


Figure 8. 3 Radiation Pattern HFSS® Analysis of Antenna with Maximum Allowable Deformed Position

8.2 Shock Severity Limits for Electrical Components on Antenna Structure

Antenna structure given in Figure 4.2 contains electrical components at vicinity of antenna tip where the most vulnerable part to the shock effect is. Shock environment produce dynamic stresses which may cause possible failure on electrical components. The possible failure modes may include fatigue, ultimate stress limit or yielding [55]. Hunt [56] presents the relationship between stress and velocity on his seminal paper. Gaberson [57-59] enhanced the research on this topic and presented the papers, presentations and some test results. Shock severity limit is defined for military equipment with the study performed based on pseudo velocity by Hunt, Gaberson, Morse, et al. These limits are used to determine whether component qualification testing is necessary or not. In some cases further action should be taken in order to maintain component survival.

Shock severity limit for electrical components are defined in military standards in a very coarse form. In MIL-STD-810E standard, the empirical rule is proposed for shock severity on components. Rule states that, shock should be considered as severe only if defined threshold value is exceeded. Threshold value is defined in Equation (8.1).

$$Threshold = [0.8(G / Hz) \times NaturalFrequency(Hz)] \quad (7.7)$$

MIL-STD-810E also states that, it is observed from military-quality equipment tests, shock failures are not observed below a shock response spectrum velocity of 2.54 m/s [60]. However, both values are very conservative and far from reality; because these effects are mostly considered for vibration case. For shock case, shock severity should be considered thoroughly. The following theories are presented for shock severity cases which are closer to the real-life applications.

From the experiments and studies followed on shock severity for components by Gaberson and Morse [61-62], two different shock limit criteria are proposed. From these studies, damage thresholds are proposed for different materials with 6 dB

tolerance interval. In Appendix C, for different materials velocity limits are presented. As an example, velocity limits of shock severity for mild steel are presented in Figure 8.1. From these tables, limitation for antenna structure as AA6061-T6 beam is **10.51 m/sec** with 6dB tolerance. Antenna response from the mathematical model is given in Figure 8.4. Since maximum relative velocity value is 16.1 m/s and it is bounded barely between 6-dB tolerance band; it is considered as critical.

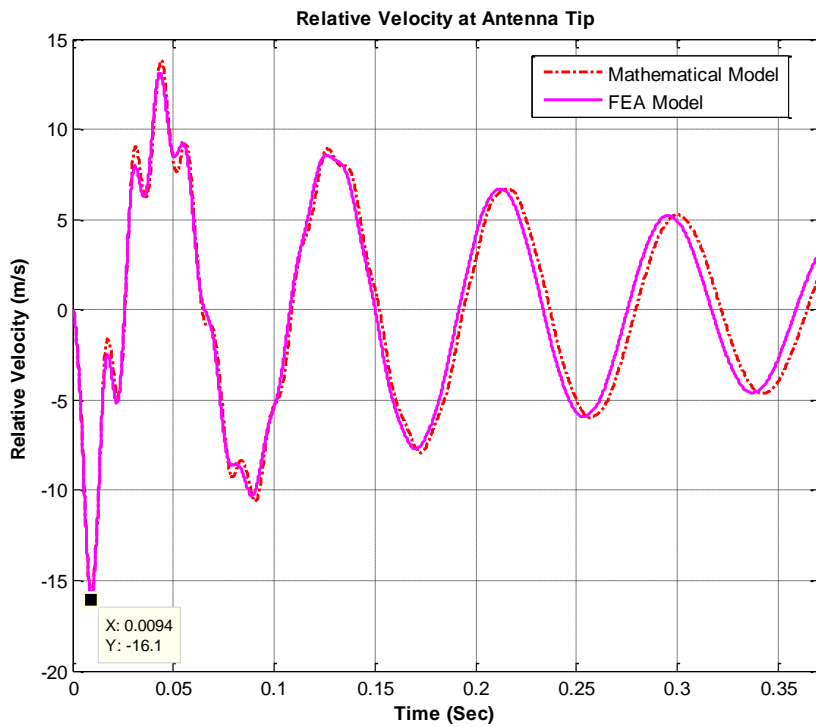


Figure 8. 4 Relative Velocity Response of the Antenna from Updated Models

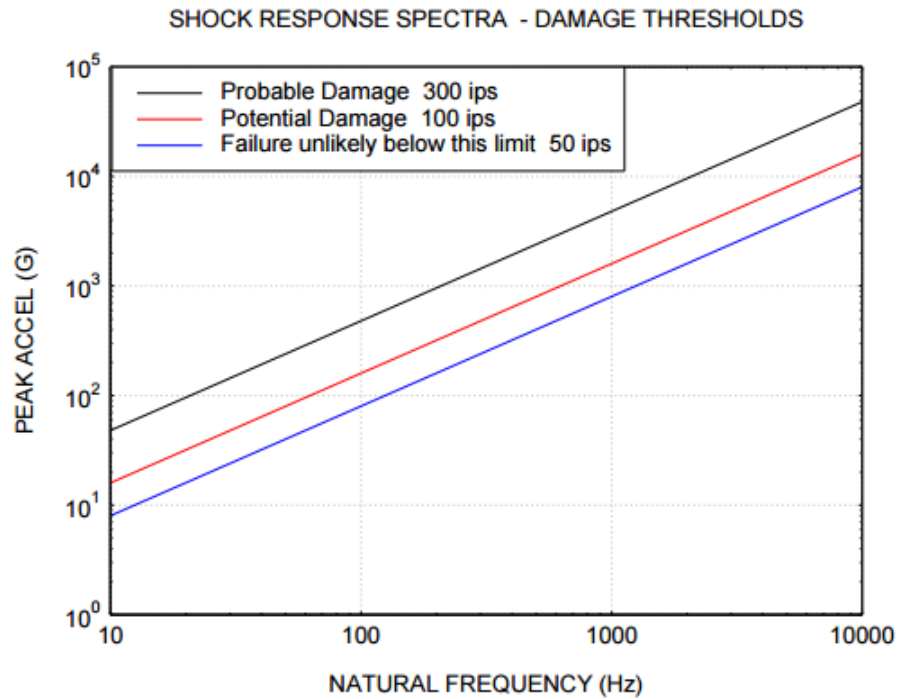


Figure 8. 5 Morse Chart for Mild Steel Beams [62]

Another shock severity limit is Steinberg’s Relative displacement limit. Steinberg [63] defined “Z” as a “single-amplitude displacement at the center of the electronic board” which gives a fatigue life of about 20 million stress reversals in random vibration environment. This definition is based on 3σ circuit board relative displacement.

Steinberg’s empirical formula is presented in Equation (8.2) in inches. Geometrical parameters can be seen on Figure 8.2.

$$Z_{3\sigma \text{ limit}} = \frac{0.0000426B}{Chr\sqrt{L}} \quad (7.8)$$

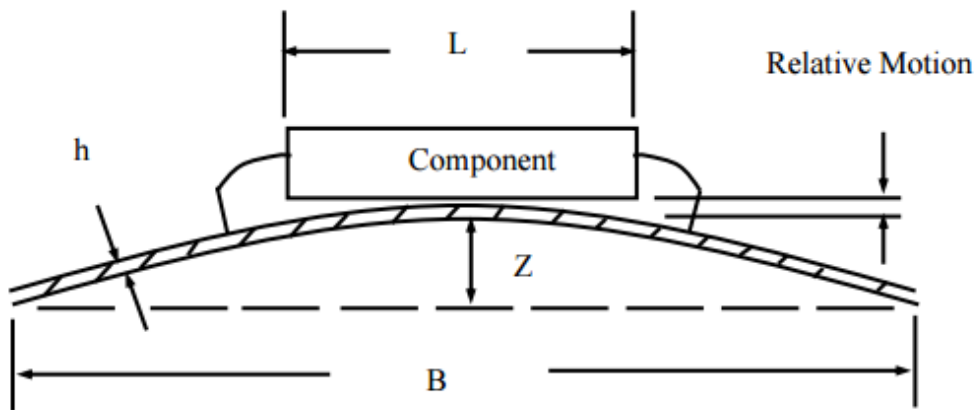


Figure 8. 6 Component Bending on the Antenna Structure [63]

In Equation (8.2), B is the length of the antenna edge parallel to the component, L is the length of electronic component, h is the antenna thickness, r is the relative position factor for the component mounted presented in Table 8.1 and C is the constant for different types of electronic components presented in Appendix D.

Table 8. 1 Relative Position Factors for Component on Circuit Board

r Value	Component Location
0.5	When component is at quarter point X and quarter point Y
0.707	When component is at half point X and quarter point Y
1	When component is at center of PCB

Finally, Steinberg’s relative displacement limit for shock input is calculated as six times the 3-sigma-limit value. This shock limit is only valid for up to 200 cycles created by strain hardening effect [63]. Thus, Steinberg’s empirical formula for shock peak relative displacement limit in inches is presented in Equation (8.3).

$$Z_{peak} = 6 \times Z_{3\sigma limit} \quad (7.9)$$

Corresponding pseudo-velocity limit for shock severity is calculated as in Equation (8.4).

$$PV_{peak} = 2\pi f_n Z_{peak} \quad (7.10)$$

The limitations of Steinberg's method are presented below.

- Component's fatigue life may be below or over 20 million cycles.
- 3-sigma relative displacement may not be seen due to the non-stationary or non-Gaussian distribution of random vibration.
- Circuit board likely behaves as a MDOF system, therefore higher modes should not be neglected. Thus, reversal cycle rate can be counted as greater than that of the fundamental frequency alone.

Because of these limitations, it is not expected that results are exact but they show the correct order-of-magnitude for antenna design and qualification stages. Therefore, safe designs can be achieved with safety factor with this approach.

For antenna structure, mentioned in this thesis study, there are two resistors and one capacitor placed on antenna span longitudinally. From Equations (8.2) and (8.3) with Table 8.1 and Appendix D, antenna displacement should be below **22.29 cm**. Comparing the maximum displacement of antenna tip given in Figure 8.1, antenna structure considered to be safe.

Furthermore, for electrical resistor used for the antenna structure, it is advised that component should be used below 250g mechanical shock loading (Appendix E). Therefore, the antenna structure response should be below 250g. Since maximum acceleration response is found as 321.3 G in Figure 7.11, this limitation is considered as very critical.

8.3 Shock Stress Severity on Antenna Structure

For the antenna structure modeled in Figure 4.3 with the base acceleration shock loading illustrated on Figure 4.4, shock stress and velocity relation is presented in this section with different methods [64].

8.3.1 Shock Stress from Single Mode Modal Transient Analysis

In this method modal transient analysis is performed for fundamental natural frequency of antenna structure. Transient relative velocity response is considered among modal transient responses. The maximum bending stress formulation is given in Equation (8.5).

$$\sigma_{\max} = \hat{c} \sqrt{\frac{Em}{IL}} v_{n,\max} \quad (7.11)$$

In Equation (8.5), \hat{c} is distance to neutral axis, E is elastic modulus, m is antenna mass, “I” is area moment of inertia, “L” is antenna length and “ $v_{n,\max}$ ” is modal maximum relative velocity response. Maximum bending stress at fixed boundary is, thus, calculated from the maximum relative velocity at the free end by means of transient analysis using only fundamental frequency of the antenna. Results can be compared to bending stress calculated from the second derivative of mode shape of the antenna structure.

8.3.2 Shock Stress from Single Mode Direct SRS

In this method, acceleration SRS curve is taken into consideration for fundamental velocity. From acceleration output at fundamental frequency, pseudo-velocity can be calculated as presented in Equation (8.6) where V is a pseudo-velocity.

$$V = \frac{\ddot{z}}{\omega_n} \quad (7.12)$$

As a next step, the approximate relative velocity can be calculated for single mode model as presented in 8.7.

$$\dot{z}_{\max} = \Gamma_1 \hat{q}_{1,\max} V \quad (7.13)$$

In Equation (8.7), Γ_1 is participation factor for the first mode, $\hat{q}_{1,\max}$ is maximum mass-normalized eigenfunction for the first mode and V is pseudo-velocity found in Equation (8.6). Maximum relative velocity value may be used for maximum bending stress calculation presented in Equation 8.5.

8.3.3 Shock Stress from Four Mode Transient Analysis

In this method just the same formulation is followed as the method presented in Section 8.3.1. As a difference, in four fundamental modes are used for transient analysis. It is proved in Section 5.1 that four-mode configuration is enough for 90 percent modal mass participation. The most accurate result is expected to be obtained by this method among others.

8.3.4 Allowable Stress for Naval Applications

Allowable stress for naval applications is defined as NRL sum of the stresses in the form of total membrane stress, total membrane plus bending stress, total buckling stress and total bearing stress. Antenna structure is subjected to bending stresses at fixed end and stress concentration is observed around bended region. Therefore, total membrane plus bending stress is applied on antenna structure. The factors defined are due to experimental results in the safe margin. Since the shock energy is applied on structure within very small interval, the actual effect is less than expected. Components which are attached to naval platform is categorized as Grade A and Grade B type components according to their importance. “Grade A items are systems or equipment which are essential to the safety and continued mission capability of the ship. Grade B items, which are not essential to safety or the combat mission, are those items that could become a hazard to personnel or to Grade A items. [6]” Antenna structure is, hence, classified as Grade A component. For Grade A and Grade B components, allowable stress limits are tabulated in Table 8.2.

Table 8. 2 Grade A Allowable Stress Criteria and Applicable Design Levels [6]

ALLOWABLE STRESS	SHOCK INPUT	TYPE OF STRESS	ALLOWABLE STRESS	
			GENERAL	LOCAL
Case 1: Alignment sensitive, no permanent deformation allowed	Elastic	σ_{membrane}	$1.0 \sigma_{\text{yield}}$	$1.0 \sigma_{\text{yield}}$
		$\sigma_{\text{membrane}} + \sigma_{\text{bending}}$	$1.0 \sigma_{\text{yield}}$	$1.0 \sigma_{\text{yield}}$
		σ_{column}	Buckling	Buckling
		σ_{bearing}	$1.6 \sigma_{\text{yield}}$	$1.6 \sigma_{\text{yield}}$
Case 2: Alignment sensitive, slight permanent deformation allowed	Elastic	σ_{membrane}	$1.0 \sigma_{\text{yield}}$	$1.5 \sigma_{\text{yield}}$
		$\sigma_{\text{membrane}} + \sigma_{\text{bending}}$	$1.0 \sigma_{\text{eff}}$	$2.0 \sigma_{\text{eff}}$
		σ_{column}	Buckling	Buckling
		σ_{bearing}	$1.6 \sigma_{\text{yield}}$	$1.6 \sigma_{\text{yield}}$
Non-alignment sensitive equipment and foundation, slight perm deform allowed	Elastic-Plastic	σ_{membrane}	$1.0 \sigma_{\text{yield}}$	$1.0 \sigma_{\text{yield}}$
		$\sigma_{\text{membrane}} + \sigma_{\text{bending}}$	$1.0 \sigma_{\text{yield}}$	$1.0 \sigma_{\text{yield}}$
		σ_{column}	No Limit	No Limit
		σ_{bearing}	No Limit	No Limit
No perm deformation allowed; bolts	Elastic	σ_{membrane}	$1.0 \sigma_{\text{yield}}$	$1.0 \sigma_{\text{yield}}$
Non-alignment sensitive equipment and foundations, considerable deform allowed	Elastic-Plastic	σ_{membrane}	$1.0 \sigma_{\text{yield}}$	$1.0 \sigma_{\text{yield}}$
		$\sigma_{\text{membrane}} + \sigma_{\text{bending}}$	$2.0 \sigma_{\text{yield}}$	$2.0 \sigma_{\text{yield}}$
		σ_{column}	No Limit	No Limit
		σ_{bearing}	No Limit	No Limit

Using Equation (8.5) with 4-mode updated (tip mass and modal damping) transient response analysis of antenna structure performed in Chapter 7, the maximum stress is found as **386.4 MPa**. From Table 8.2, for Grade A components, allowable stress is two-times of yield stress of structure. Yield stress for AA6061-T6 is 276 MPa. Therefore, the maximum allowable stress is 552 MPa for the antenna structure, which is above the maximum stress and antenna structure can be considered as “safe”. Stress analysis is further performed by ANSYS® Transient analysis and the maximum stress is observed at antenna head as around 413 MPa. However, this value is kind of artificial due to the fact that stress waves are moving from free end to the cantilever base and cancelling each other while coming back to the antenna tip due to the direction change.

Further study is performed about stress consideration while shock testing. In experimental analysis, shock input level of antenna structure is increased gradually and reached up to 2658 g – 6ms half-sine input. After tests are performed, there is any failure or deformation observed on antenna structure. Therefore, it is stated that, for shock phenomenon, since effective shock duration is limited real effects of shock as stress on antenna structure is less than expected. Therefore, NRL limitation of allowable stress on structures subjected to underwater explosions is very conservative and structures below these limits can be considered as “safe” enough.

8.4 Antenna Limitations Caused by Shock Severity

Antenna limitations have been explained in previous sections. For these limitations, antenna structure should be re-designed or isolation precautions should be taken. Since electromagnetic design limits any change of antenna dimensions and of material change. For example, in order to increase maximum velocity limit, the material can be changed to AA6061-T6 to Titanium Alloy. However, this brings additional tangent loss to the antenna performance and additional mass to the total system. Therefore, it is not possible to apply geometrical or material change in antenna structure. Instead of design change, shock isolation is performed to achieve the safe design for certain limitations. In Table 8.3, shock severity limitations are presented.

Table 8. 3 Shock Severity Limitations

Criteria	Response Limitation	Limit	Maximum Value from Mathematical Model	Severity
Antenna Performance	Relative Displacement (cm)	18.6	17.4	Safe
Electrical Component Analysis (Morse)	Relative Velocity (m/s)	10.51	16.1	Critical
Electrical Component Analysis (Steinberg)	Relative Displacement (cm)	22.29	17.4	Safe
Resistor Mechanical Shock Limit	Absolute Acceleration (G)	250	321.1	Very Critical
Maximum Allowable Stress	Stress (MPa)	552	386.4	Safe

8.5 Shock Isolation of Antenna Structure

In recent years, shock problems of antenna structures mounted on naval platforms have arisen, and they are expected to continue. In order to sustain the performance of antenna structure and to take precautions to the possible concerns mentioned on Sections 8.1 to 8.3, shock isolation should be performed. Because of these reasons, the study on selection of shock isolation materials and shock isolation theory is presented.

8.5.1 General View on Shock Isolation

Sensitive components like antenna structures are required to be treated with shock isolation where precautions cannot be taken in modal design or structural modification stages. Therefore, shock amplitude is tried to be reduced by means of force or energy transfer to the isolator material. Especially, materials with low stiffness have decreasing effects on shock forces acting on the structure to be isolated. Isolators cannot damp shock effects if frequency is very low and may amplify the shock effects if frequency of interest is close to the natural frequency.

System is successful in isolation standpoint, if the natural frequency of isolator together with the antenna structure is considerably low. However, isolator material should not be so soft due to the endurance and stabilization problems. Therefore, the optimum isolator material is to be selected. Attachment of isolator to the antenna structure should be designed so that loading is distributed to each while the same amount of deformation is observed.

For systems subjected to shock excitation used for naval applications, antenna structure and other components survived by means of shock isolators. Shock isolators absorb the energy of shock motion by means of squeezing in a short time interval, then release this energy by means of elongation in relatively long time interval. In other words, isolators convert high amplitude-short duration shock signal to relatively low amplitude-long duration response (Figure 8.7).

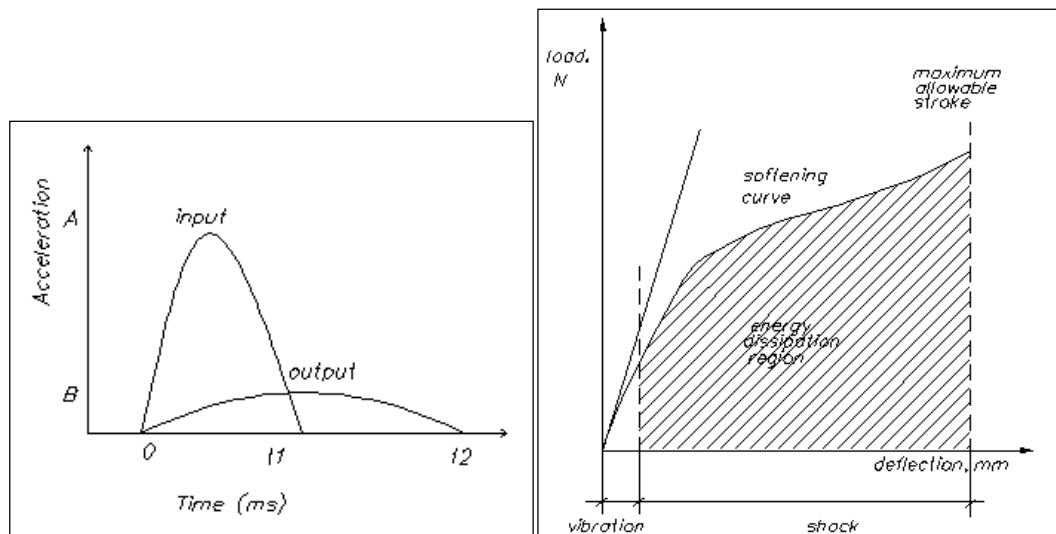


Figure 8. 7 Shock Damping by means of Isolators on, a) Acceleration-time plot, b) Force-displacement plot [63]

Important remarks on proper use of shock isolator are following: Isolator selected should meet the dynamic displacement required. Otherwise, isolator may amplify the shock effects which may be observed with qualification tests or on operations. Since large displacements occur in shock isolation, stiffness of isolator should not be linear. Success of isolation is monitored by the displacement of isolator required. For many operations, linear isolators cannot supply large displacements, therefore nonlinear isolators should be opted instead of linear ones. For example, wire rope type isolators are very suitable for shock applications. Because, they are capable of high energy storage and their form can change easily. Therefore, they may show linear and non-linear characteristics together. If metal isolators cannot be used for applications like antenna isolation, gel type isolators can be used. These types of isolators can also show both linear and non-linear characteristics like wire rope. However, shock isolation level of gel type isolators are not that high as wire rope.

8.5.2 Shock Isolator Selection

It is essential to select appropriate shock isolator in order not to face with adverse effects of shock on warfare structures such as antennas. In this part, shock isolator selection steps are presented. For the calculation step, Equations (8.8) and (8.9) along with Figure (8.8) are taken from isolator selection catalogue [65].

Generally, the first step of isolator selection starts with taking integrals of shock input profile in order to find velocity values. Velocity value V_{shock} is the initial velocity of the system reached by means of the response to the shock input. V_{shock} values along with different forms of shock inputs are presented in Figure 8.8. After that step, considering the shock output g_{out} as a magnitude of desired acceleration response, natural frequency of the system is calculated by Equation (8.8), noting that g is “gravitational acceleration”.

$$f_{n,system} = \frac{g_{out} g}{V_{shock} 2\pi} \quad (7.14)$$

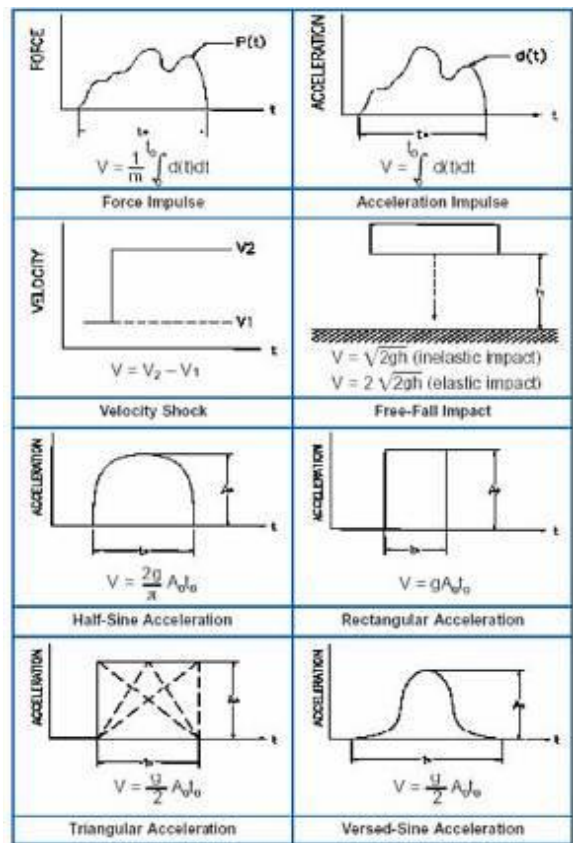


Figure 8. 8 Shock Velocity Formulation for Different Types of Shock [65]

Then, the displacement value that isolator should reach is found with Equation 8.9.

$$\Delta D = \frac{V_{shock}}{2\pi f_{n,system}} \tag{7.15}$$

Finally, isolator should be selected considering the following rules.

- Natural frequency of isolator should be lower than the natural frequency of the system calculated in Equation (8.9).
- Minimum displacement value of shock isolator should be higher than the displacement value calculated in Equation (8.9).
- Isolator material should not be of metal due to the electromagnetic reflection with antenna structure.

For antenna structure considered in study, limitation is set to 240 G output acceleration because the shock severity limitation is found as 250 G in Section 8.4. For this acceleration value, relative velocity criteria is checked and verified as to be safe. Thus, it is guaranteed that all limitations are covered with this value. Moreover, mathematical model results are higher than experimental results. This also brings more safety for conservative isolator selection.

Therefore, for limitation of 240 G, V_{shock} is found as 10.01 m/s, $f_{n,system}$ is found as 37.5 Hz and ΔD is found as 0.042 m.

Next step of isolator selection is to select possible isolator type. For isolator type selection, dimension and material limitation are very important. Since antenna structure have width of 0.02 m at base interface, miniature isolator that meet the requirements should be selected.

In electromagnetic point-of-view platform analysis with isolator material is performed. In this analysis, the higher loss tangent value of the isolator material, the lower unexpected reflection losses will be. Therefore, wire materials cannot be selected as isolator materials. For the detailed research of insulation materials used for shock isolators, material loss tangents are measured by experimental setup for Original GEL, Beta-GEL, Theta-GEL, Urethane, Rubber, Natural Rubber and APDM rubber samples. GEL type isolators are selected due to the minimum effect on antenna performance. From data sheets of Taica® GEL isolator, MN Type Theta-GEL isolator with approximately 17 Hz natural frequency and up to 10 cm displacement capability is selected. Data Sheet of the product is given in Appendix F.

8.6 Isolator Verification by Drop Experiment

Drop experiment is repeated in order to observe isolator performance and check the achievement of shock severity requirements.

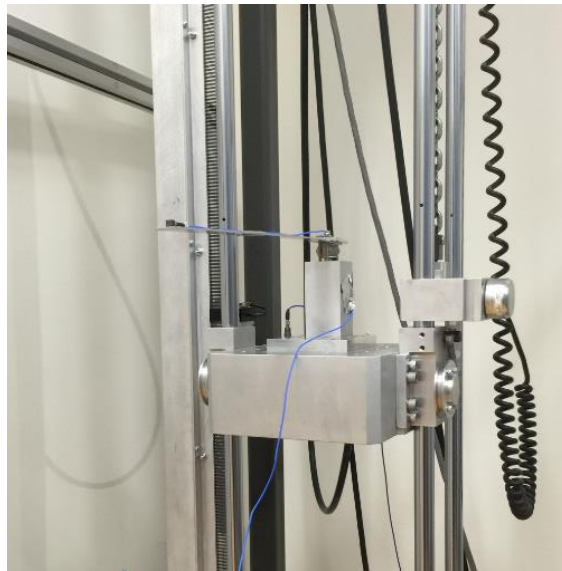


Figure 8. 9 Drop Experiment of Antenna with Isolator

Measured acceleration response at antenna tip is presented in Figure 8.10 with acceleration response measured without isolator.

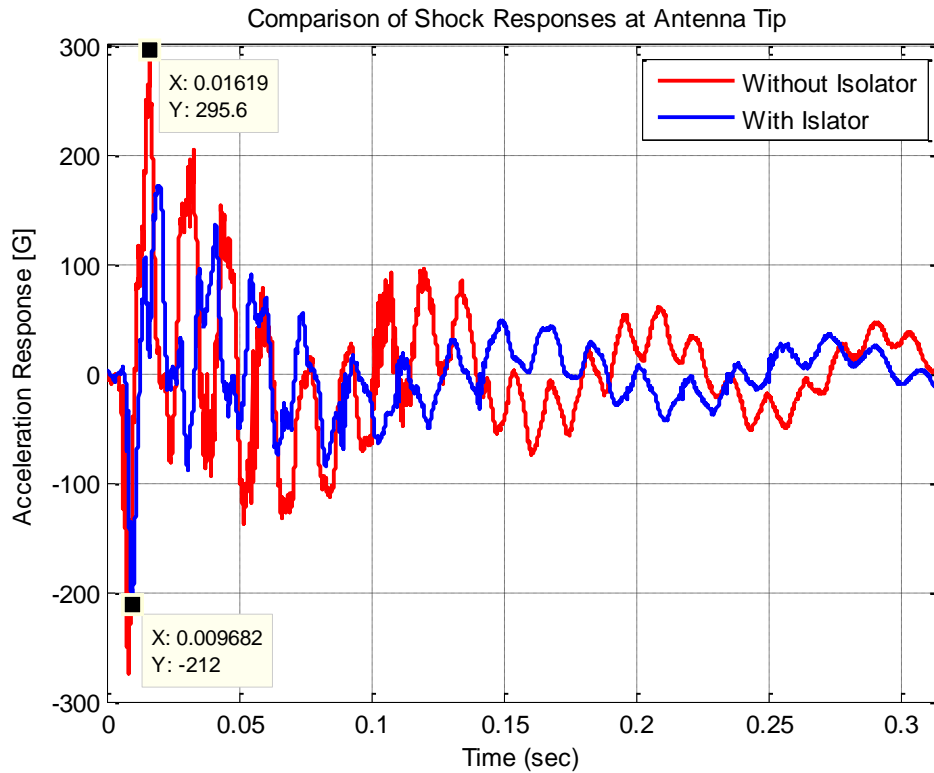


Figure 8. 10 Acceleration Response for the Antenna with Isolator

As observed from the response plot with isolator, 28.3% reduction of maximum acceleration is measured and desired output acceleration limit (240G) is achieved with some safety margin. Therefore, the isolator verification holds. In order to observe relative velocity response, acceleration response is integrated in frequency domain data obtained by Fast Fourier Transform, then Inverse Fast Fourier Transform yields the time domain relative velocity data with certain amount of error. MATLAB® script written for this calculation is presented in Appendix G. As seen on Figure 8.11, maximum relative velocity value of the antenna structure is decreased to under allowable limits. For that maximum relative velocity, corresponding stress is calculated as 212.6 MPa which is seventy seven percent of yield strength of aluminum. Therefore, stress value is reduced to below yield strength with considerable safety margin.

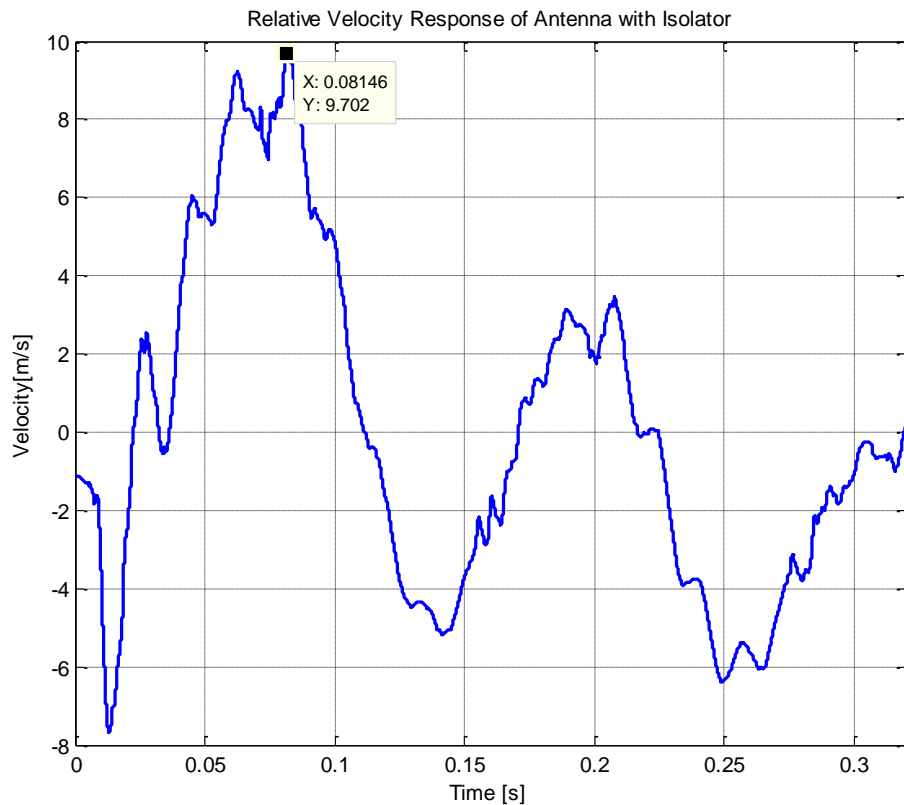


Figure 8. 11 Relative Velocity Response of the Antenna with Isolator

8.7 Discussion

Antenna performance is determined and evaluated from both electromagnetic design and mechanical properties standpoints. Therefore, mechanical shock may have severe effects on both antenna performance and mechanical survival. In order to eliminate these severe effects, some precautions should be taken at mechanical design stage like geometrical or material changes in design and shock isolation. In this chapter, severe effects of shock on antenna structure are presented and design limitations are determined. As there is no chance on design changes of antenna structure, shock isolation is introduced and isolation procedure is explained in detail. Then, the isolator selection of antenna is performed step-by-step considering

the design limitations. Throughout these stages from shock severity limitations to isolator selection, mathematical models are used. After design improvements are performed with isolator addition on system, experimental verification is performed. Experimental results of the system with isolator are compared to those of the system without isolator. Almost 30% reduction in maximum acceleration is obtained with acceptable maximum relative velocity value. As relative displacement values of non-isolated system is safe enough, no further development is performed. Antenna with isolator response behavior is different than antenna without isolator because of the nonlinear effects of isolator material. These different behaviors are observed as natural frequency shift, double peaks at maximum points, fast damping and more harmonics on secondary responses. As antenna structure is approximated by a cantilever beam, strain energy is only obtained from antenna fixed end. Limited location selection for the antenna structure makes isolation performance lower than other applications. GEL type isolators propose the maximum possible performance among others.

This chapter is presented as design guide for shock severity. Mathematical model built throughout this thesis is used to foresee severe effects on shock without performing any qualification tests. Interactive design is also possible for both mechanical and electromagnetic point-of-view, as iterative design can be accomplished by means of proposed design methodology.

CHAPTER 9

SUMMARY AND CONCLUSIONS

9.1 Summary

This study aims to perform complete shock analysis of dipole antenna structure used for ESM/COMINT applications subjected to underwater explosions. The purpose is to protect antenna structure from shock effects and maintain its function in warfare. In mechanical point-of-view, shock considerations for design is very important and not fully solved problems. In order to eliminate adverse effects of shock loading on antenna performance, shock response of an antenna structure is investigated in detailed way. Experimentally verified linear model of antenna structure is used to perform transient response analysis to foresee the shock characteristics. These inputs can be used a starting points to initiate electromechanical design procedure of antenna structures. They can be used in replacement of qualification tests which are hard to perform or they can be used as design updates for the antennas which fail or tend to fail. The mathematical models are capable to perform these analysis for various beam geometries with different boundary conditions. Model is also capable to perform transient response analysis for different shock inputs even if it is wavelet input. Shock severity considerations are another important issue for shock analysis. As an electromechanical device, antenna structure consists of some electronic parts attached to its mechanical base. Therefore, shock severity considerations consist design limitations for electronic devices as do for mechanical structure. To eliminate these effects and to maintain antenna functioning, shock isolation procedure is introduced with shock isolation theory and verified application on the antenna structure.

In the scope of this study, dipole antenna which is attached to submarine periscope with fixed-free boundary conditions is considered. In order to generate shock input classified with standards, shock profile synthesis is performed thus; easily producible shock input is obtained. Antenna structure is modeled as a cantilever beam with Classical Theory and its modal properties are determined. Then, transient shock analysis is performed with MDOF Recursive Filtering Relationship Method which gives the closest results to the exact solution among SDOF methods and other approximate methods. FEA analysis is also performed for antenna structure with full model transient response analysis. Because FEA model and mathematical model yields closer results and they are both verified by experimental studies. They can be interchangeably used according to the ease of use. Experimental verification of these models is performed by hammer tests for modal verification and drop experiment for transient response verification. Finally, shock severity limitations are explained both for electronic and mechanical elements of antenna. Shock isolation is performed in order to overcome these limitations.

Complete shock analysis can be enhanced for different antennas with different application areas. Therefore, apart from underwater shock inputs; gunfire, ballistic, field vehicle shock inputs can be synthesized or used as they are. Mathematical model is capable to perform such different analyses with simple selections in MATLAB® script.

Shock isolation and design guide for shock severity is also verified in Chapter 8 for antenna structure that is to be qualified or designed. Therefore, this design guide is a very useful tool to perform shock analysis for designers and it is very practical to use for whom are not familiar to shock and vibration topics.

9.2 Conclusions

By means of the proposed methodology throughout the study, multi-degree-of-freedom transient response analysis of the antenna structure is accurately performed using four modes (90% of the effective modal mass) of the structure. Transient response analysis of the similar (beam type) antenna structures with different dimensions and different field of applications can be readily applied.

Performing the shock profile synthesis, it is observed that different type of shock inputs can be synthesized for reproducibility. Synthesized profiles are more conservative than original ones due to the fact that shock response spectrum coverage is higher than original pulses for low frequencies as seen in Figure 3.12.

Euler-Bernoulli Beam assumption is made for antenna structure as a slender beam. Assumptions of Euler-Bernoulli beam theory do not under estimate the responses of antenna structures. Modal analysis verifications with very small errors shows that for antenna structures with similar geometry, these assumptions can be done for brevity. For further investigation such as shear effects, Timoshenko Beam Theory can be applied. For such kind of applications, mathematical model can be updated or FE model proposed in this study can be used directly.

For transient analysis of the antenna structure, RFR method is used for solution algorithm. This method is very easy to apply on shock response analysis formulation and it is very fast. Elapsed time for response obtained from this method is almost a second for both modal and transient analysis. For ANSYS® solution it is almost ten seconds for complete solution. Therefore, method developed for transient solution can be considered as very fast and accurate. Different boundary condition selection, material selection, included number of mode selection, modal damping selection, desired response location, different shock input type selection are possible with this model.

SDOF Models and approximate models are easier to build and apply than MDOF analysis. However, if these methods are used, user should be aware of the error possibility from 10% to 100%. Therefore, this may mislead the designer for shock severity considerations.

It is important to acquire reliable responses from experimental analysis if transient analysis is concerned. High coherence values at natural frequencies, spectrum content of transient response and modal updating according to experimental feedbacks assures the reliability of mathematical model and FE solution. Results obtained from analyses and experiments are used for crosscheck in corresponding chapters in this manner.

Theoretical maximum allowable stress values for structures under transient loading are so safe enough not to face with failure of antenna material. In experimental analysis stages, maximum allowable shock loading limits are exceeded and no failure and deformation is observed. Stress values are calculated higher than yield stress of the material due to the forcing duration is very small and forcing behaviors are different than static loading cases.

It is observed that shock isolation material is very effective on antenna performance. Using inappropriate isolator type like wire rope or natural rubber may result in severe decrease on antenna performance. Therefore, material type should be added to isolator criteria steps.

9.3 Future Work

This study can be improved by implementing further capabilities:

- Geometric nonlinearities can be added to model.
- Boundary condition nonlinearities can be added to model.
- Solution methodologies can be combined in order to obtain faster and more accurate responses. These methodologies can be implemented to ANSYS®

to perform interactive response analysis. Therefore, simplicity of analysis and fast solver results with very high accuracy can be obtained.

- Experimental stress analysis can be performed for the antenna structure under shock loading. Stress distribution of antenna structure can be analyzed for three loading conditions (vertical, transverse and longitudinal) and failure conditions of antenna should be defined clearly. Antenna structure may also be investigated for vertical loading in case of stress variations caused by buckling motion. As the vertical shock loading specifications for naval applications are very high, buckling motion is to be examined for continuous and failure-free operations for antenna structure.
- Isolator material can be selected different than GEL type with lower loss tangent value.
- Isolation can be added to mathematical model and they can be investigated together.
- Experimental analysis can be performed with laser vibrometer to measure displacement response.
- Optimization may be studied in order to obtain maximum performance from isolation process.

REFERENCES

- [1] Tembarai Krishnamachari, R. "Dawn of the E-bomb: High-power microwave technology and military implications for India", South Asia Analysis Group, Paper 1089, May 2004.
- [2] "Joint Publication 3-13.1 Electronic Warfare". Chairman of the Joint Chiefs of Staff (CJCS) - Armed Forces of the United States of America. 25 January 2007. pp. i, v – x. Retrieved 2011-05-01.
- [3] IEEE Std. 145TM-2013, IEEE Antennas and Propagation Society, "IEEE Standard for Definitions of Terms for Antennas", New York, USA, December 2013.
- [4] Walter, P.L., "Selecting Accelerometers for Mechanical Shock Measurements", PCB Piezotronics, Depew, New York, TN-24, December 2007.
- [5] MIL-STD-810G, "Environmental Engineering Considerations and Laboratory Tests", Department of Defense Test Method Standard, USA, 2008.
- [6] Scavuzzo R.J., Pusey, H., "Naval Shock Analysis and Design", HI-Test Laboratories Inc., 6th Printing, Virginia, 2013.
- [7] Mercimek, Ümit. "Shock Failure Analysis Of Military Equipments By Using Strain Energy Density", MSc Thesis, Mechanical Engineering, Middle East Technical University, December 2010.
- [8] Harris, C.M., Piersol, A.G., Hill, M., Shock and Vibration Handbook, Fifth Edition, 2002.

[9] Mair, Hans U., “Simulated Ship Shock Tests/Trials?”, Institute for Defense Analyses, Virginia, USA.

[10] Galileo, Galilei, “Discorsi e dimonstrazioni matematiche intorno a due nuove scienze attinenti la meccanica e i movimenti locali”, publication Cierre, Simeoni Arti Grafiche, Verona, 2011.

[11] Biot, M.A., “Theory of Elastic Systems Vibrating Under Transient Impulse”, Proc. Natl. Acad. Sci. U.S., Vol.19, pp.262, 1933.

[12] Biot, M.A., “A Mechanical Analyze for the Prediction of Earthquake Stresses”, Bull. Seismological Soc. Am., Vol.31, No.2, pp.151, 1941.

[13] Biot, M.A., “Analytical and Experimental Methods in Engineering Seismology”, Trans. ASCE, No.108, pp.365, 1943.

[14] Biot, M.A., “Transient Oscillations in Elastic Systems”, Ph.D. Thesis No.259, Aeronautics Department, California Institute of Technology, 1932.

[15] Mindlin, R.A., “Conversation with the author”, 1942.

[16] Housner, G.W., “Behavior of Structures during Earthquakes,” J. of Eng. Mech. Div., ASCE, Vol. 85, No. EM4, pp. 109-129, 1959.

[17] Newmark, N.M., Rosenblueth, “Fundamentals of Earthquake Engineering”, Prentice-Hall, 1971.

[18] Newmark, N.M., “A Method of Computation for Structural Dynamics”, ASCE Journal of the Engineering Mechanics Division, Vol. 85 No. EM3, 1959.

[19] Alexander, J.E., “Shock Response Spectrum – A Primer”, BAE Systems, US Combat Systems Minneapolis, Minneapolis, Minnesota, Sound and Vibration, pp. 6-14, June 2009.

[20] Tuma, J., Koci, P., “Calculation of Shock Response Spectrum”, Colloquium Dynamics of Machines 2009, Prague, February 2009.

[21] Smallwood, D. O., “An Improved Recursive Formula for Calculating Shock Response Spectra”, 51st Shock and Vibration Bulletin, Sandia National Laboratories, Albuquerque, New Mexico, 1980.

[22] Kelly, R.D., Richman, G., “Principles and Techniques of Shock Data Analysis”, The Shock and Vibration Information Center, Washington, D.C., 1969.

[23] Irvine, T., “An Introduction to the Shock Response Spectrum”, Vibration Data, July 2010.

[24] Dorf, R., “Modern Control Systems”, Addison-Wiley, Reading, Massachusetts, 1980.

[25] Irvine, T., “Shock Response of Multi-Degree-of-Freedom Systems”, Revision F, Vibration Data, July 2010.

[26] Parlak, M., “Bir Hava Savunma Sisteminin Deneysel Sok Analizi”, 11. Ulusal Makina Teorisi Sempozyumu, Gazi Üniversitesi, Mühendislik-Mimarlık Fakültesi, Ankara, Eylül 2003.

[27] Burgess, A. , “Transient Response of Mechanical Structures using Modal Analysis Techniques” , Department of Mechanical Engineering, Imperial College, London SW7, January 1988.

[28] Bhat, P., Chandrasekhar, J., “Shock Response Spectrum Analysis Approach for Optimal Design of Electronic Devices”, Axiom Consulting Pvt. Ltd., Bangalore, India.

[29] Wang, G., Xiong Y., Tang, W., “A Novel Heavy-weight Shock Test Machine for Simulating Underwater Explosive Shock Environment: Mathematical Modeling and Mechanism Analysis”, School of Logistics Engineering, Wuhan University of Technology, China, July 2013.

[30] Campos, D.J.G., “A Study of Shock Analysis Using The Finite Element Method Verified with Euler-Bernoulli Beam Theory; Mechanical Effects Due to Pulse Width Variation of Shock Inputs; and Evaluation of Shock Response of a Mixed Flow Fan”, Faculty of California Polytechnic State University, July 2014.

[31] Haukaas, T., “Euler-Bernoulli Beams.” University of British Columbia, November 2012.

[32] Yang, Bingen. “Stress, Strain, and Structural Dynamics: An Interactive Handbook of Formulas, Solutions, and MATLAB® Toolboxes”, Elsevier Inc., San Diego, 2005.

[33] Remala, S.N.R., “Nonlinear Transient Finite Element Simulations of Beam Parametric Response Including Quadratic Damping”, University of Kentucky, 2005.

[34] DeBruin, J., “Shock Isolation for Mobile Pointed Satcom Systems”, General Dynamics SATCOM Technologies, Texas.

[35] Parlak, M., “Vibration Isolation of a Platform with a Shock Disturbance”, Middle East Technical University, Ankara, Turkey, December 2002.

[36] Klembczyk, A.R., “Introduction to Shock and Vibration Isolation and Damping Systems”, Taylor Devices, Inc., New York, 2010.

[37] Tustin,W., Hieber,G.M., “Understanding and Measuring the Shock Response Spectrum”, The Applications Engineering Staff Spectral Dynamics Corporation of San Diego, USA.

[38] “Shock Response Spectrum”, SRSView. Available: <http://www.signalysis.com/> , Retrieved on March 10, 2014.

[39] Building Specification for Ships of the Federal Armed Forces, 043, Shock Resistance Experimental and Mathematical Proof, March 1985.

[40] Majkut, L. “Free and Forced Vibrations of Timoshenko Beams Described by Single Difference Equations.” Journal of Theoretical and Applied Mechanics 47.1 (2009): 193-210.

[41] Tonguei B. H. “Principles of Vibration”, New York. Oxford University Press Inc. 1996.

[42] Whitney, S. “Vibrations of Cantilever Beams: Deflection, Frequency and Research Uses”, University of Nebraska-Lincoln. April 1999.

[43] Sadd, M.H. “Wave Motion and Vibration in Continuous Media”, Kingston: University of Rhode Island, 2009.

[44] Rao, S.S. “Mechanical Vibrations”, Fifth Edition in SI Units, Pearson Inc., Singapore, 2011.

[45] Irvine, T., “Modal Transient Vibration Response of a Cantilever Beam Subjected to Base Excitation”, Vibration Data, January 2013.

[46] Thomson, W. "Theory of Vibration with Applications", Second Edition, Prentice Hall, New Jersey, 1981.

[47] Irvine, T., "Modal Transient Analysis of a System Subjected to an Applied Force via a Ramp Invariant Digital Recursive Filtering Relationship", Revision K, Vibration Data, 2012.

[48] Brandt A., Ahlin, K. "A Digital Filter Method for Forced Response Computation", Society for Experimental Mechanics (SEM) Proceedings, IMAC-XXI.

[49] Irvine, T., "The Generalized Coordinate Method for Discrete Systems", Revision F, Vibration Data, 2012.

[50] Dukkupati, R.V., "Vehicle Dynamics" CRC Press, Narosa Publishing House, New York, 2000.

[51] Bathe, K., "Finite Element Procedures in Engineering Analysis", Prantice-Hall, Englewood Cliffs, New Jersey, 1982.

[52] "Implicit Versus Explicit Methods", Flow science Inc, <http://www.flow3d.com/> .Retrieved on June 24, 2015.

[53] Irvine, T., "Shock Response for Multi-Degree-Of-Freedom Systems", Vibration Data, May 2010.

[54] Wilson E., "Dynamic Analysis by Numerical Integration", Static and Dynamic Analysis, Technical Paper, 1998. Retrieved on July 18, 2015.

[55] Irvine, T., "Shock and Vibration Stress As a Function of Velocity", Vibration Data, April 2013.

[56] Hunt, F.V., “Stress and Strain Limits on the Attainable Velocity in Mechanical Systems”, JASA, 32(9) 1123-1128, 1960.

[57] Gaberson and Chalmers, “Modal Velocity as a Criterion of Shock Severity”, Shock and Vibration Bulletin, Naval Research Lab., December 1969.

[58] Gaberson, H., “Using the Velocity Spectrum for Damage Potential”, SAVIAC, 74th Symposium, San Diego, CA, 2003.

[59] Gaberson, H., “An Overview of the Use of the Pseudo Velocity Shock Spectrum”, Space Craft and Launch Vehicle, Dynamic Environments Workshop, The Aerospace Corporation, El Segundo, CA, 2007.

[60] MIL-STD-810E, “Environmental Engineering Considerations and Laboratory Tests”, Department of Defense Test Method Standard, USA, 1989.

[61] Gaberson, H., “Shock Severity Estimation”, Sound and Vibration, January, 2012.

[62] Morse, R., “Presentation of Spacecraft & Launch Vehicle Dynamics Environments Workshop Program”, Aerospace Corp, El Sagundo, CA, June, 2000.

[63] Steinberg, D.S., “Vibration Analysis for Electronic Equipment”, Second Edition, Wiley-Interscience, New York, 1988.

[64] Irvine, T., “Shock and Vibration Stress-Velocity Examples for Beam Bending”, Vibration Data, April 2013.

[65] Barry Controls Shock and Vibration Isolators Guide, England, 2002.

[66] Irvine, T., “Shock Severity Limits for Electrical Components”, Revision D, Vibration Data, June 2014.

[67] ANSI/ASA S2.62-2009, “Shock Test Requirements for Equipment in a Rugged Shock Environment”, <http://asastore.aip.org>. Retrieved on April 16, 2015.

[68] Sloan, J. L, “Design and Packaging Electronic Equipment”, Van Nost.Reinhold, February 1985.

[69] Roark, R. J. "Formulas for Stress and Strain," 4th ed., McGraw-Hill, 1965.

[70] "MIL-S-901D (Navy), Military Specification: Shock Tests. H.I. (High-Impact) Shipboard Machinery, Equipment, and Systems, Requirements For" . United States, Department of Defense. March 17, 1989.

[71] Iotech Inc. “High Speed Portable Data Acquisition Systems User’s Manual”, Rev. 5.0.

[72] PCB Piezotronics, “Technical Data Sheets”, www.pcb.com/accelerometers. Retrieved on August 18, 2015.

[73] Lansmont Corp., “PDT 80 Product Specifications”, www.lansmont.com/products/shock. Retrieved on August 17, 2015.

[74] American Technical Ceramics, “ATC High Power Flange Mount Resistors Technical Data Sheet”, www.atceramics.com/atc_products. Retrieved on August 18, 2015.

[75] Taica Co., “Taica Alpha Gel MN Series Isolator Technical Details”, www.taica.co.jp/gel-english/products/insulator.htm. Retrieved on May 28, 2015.

APPENDIX A

CALCULATIONS OF SRS VALUES FROM BV043 STANDARD

From Equations (3.10) to (3.14) and the tabulated values given in Table 3.1, acceleration-time signal for the equipment installed on submarine of class >2000t can be calculated.

For Z-direction,

$$V_1 = \frac{2V_0}{3} \quad (\text{A.1})$$

$$V_1 = 6.667 \frac{m}{s}$$

$$a_2 = 0.5A_0 \quad (\text{A.2})$$

$$a_2 = 2 \times 10^3 \frac{m}{s^2}$$

$$a_{2g} = \frac{a_2}{g} \quad (\text{A.3})$$

$$a_{2g} = 204.943$$

$$t_1 = \frac{\pi V_1}{2a_2} \quad (\text{A.4})$$

$$t_1 = 5.236 \times 10^{-3} s$$

$$t_2 = \left(\frac{2d_0}{V_1} \right) - t_1 \quad (\text{A.5})$$

$$t_2 = 6.764 \times 10^{-3} \text{ s}$$

$$a_4 = \frac{-\pi V_1}{2t_2} \quad (\text{A.6})$$

$$a_4 = -1.548 \times 10^3 \frac{\text{m}}{\text{s}^2}$$

$$a_{4g} = \frac{a_4}{g} \quad (\text{A.7})$$

$$a_{4g} = -157.871$$

For Y-direction,

$$a_2 = 1.75 \times 10^3 \frac{\text{m}}{\text{s}^2}$$

$$a_{2g} = 178.45$$

$$t_1 = 5.086 \times 10^{-3} \text{ s}$$

$$t_2 = 9.031 \times 10^{-3} \text{ s}$$

$$a_4 = -985.597 \frac{\text{m}}{\text{s}^2}$$

$$a_{4g} = -100.503$$

For X-direction,

$$V_1 = 2.833 \frac{m}{s}$$

$$a_2 = 875 \frac{m}{s^2}$$

$$a_{2g} = 89.825$$

$$t_1 = 5.086 \times 10^{-3} s$$

$$t_2 = 9.031 \times 10^{-3} s$$

$$a_4 = -492.798 \frac{m}{s^2}$$

$$a_{4g} = -50.251$$

APPENDIX B

EQUIPMENT USED THROUGHOUT TESTS

General Specifications

Warm-up: 30 minutes to rated specifications

Environment

Operating: 0 to 50 °C, 0 to 95% RH, non-condensing
Storage: -20 to 70 °C

Power Consumption: 1.8A max @ 15 VDC

Input Power Range: 10 to 30 VDC

Vibration: MIL STD 810E

PC Communication: 10/100BaseT Ethernet (300 ft. max)

Channel Capacity: 8 built-in voltage channels, expandable to 72 channels with WBK options. Also can accommodate up to 3 additional WBK40 Series options (any combination). Maximum WBK41 capacity is 854 TC input channels, 4 analog output channels, 272 digital I/O channels, and 6 counter/timer channels (see WBK40 on for details).

Dimensions: 285 mm W x 220 mm D x 70 mm H (11" x 8.5" x 2.70")

Weight: 1.9 kg (4.2 lbs)

Handle: One carrying handle is included with each WaveBook

Analog Inputs (18 to 28 °C)*

Channels: 8 differential, expandable up to 72 differential

Connector: BNC

Resolution: 16 bit

Ranges: Unipolar/bipolar operation is software selectable via sequencer

Unipolar*: 0 to +10V, 0 to +4V, 0 to +2V

Bipolar: ±10, ±5V, ±2V, ±1V

Maximum Overvoltage: ±35 VDC

Input Bandwidth: DC to 500 kHz

Input Impedance

Single-Ended: 5M Ohm in parallel with 30 pF

Differential: 10M Ohm in parallel with 30 pF

Accuracy

±2 to ±10V: ±0.012% of reading; 0.006% of range

±1V: ±0.018% of reading; 0.008% of range

Input Noise: <2 LSB (RMS)

Total Harmonic Distortion: -84 dB typ

Signal to Noise and Distortion: +74 dB typ

CMRR: 80 dB typ; 70 dB min; DC to 20 kHz

Anti-Alias Filter**

Type: 5-pole Butterworth; 20 kHz, low-pass software enabled

Triggering

Channel 1 Analog & Pulse Trigger

Input Signal Range: -10 to +10V

Bandwidth: 1 MHz

Latency: 300 ns

Multi-Channel Analog Trigger (up to 72 channels)

Range: Selectable per channel to input range

Latency: 2 µs/channel, plus 4 µs max

TTL Trigger

Input Signal Range: 0 to 5V

Input Characteristics: TTL-compatible with 10k Ohm pull-up resistor

Latency: 300 ns

Software Trigger

Latency: 100 µs typical

Pulse Trigger Input

Input Signal Range: ±5V

Input Characteristics: 75 Ohm

Input Protection: ±10V max

Minimum Pulse Width: 100 ns

Maximum Pulse Width: 0.8 sec

Latency: 300 ns

External Clock

Connector: Available on DB25 digital input

Input Signal Range: 5V TTL compatible

Input Characteristics: 50k Ohms pull up (to +5V) in parallel with 50 pF

Input Protection: Zener clamped -0.7 to +5V

Delay: 200 ns

Signal Slew Rate Requirement: 20V/µs min

Rate: Up to 1 MHz

Divisor Ratio: Divide by 1 through 255, selectable

Clock Counter Accuracy: <0.02% error

Clock Counter Range: 0.01 Hz to 100 kHz

Sequencer

Operation: Programmable for channel, gain, and for unipolar/bipolar range in random order

Depth: 128 location

Channel-to-Channel Rate: 1 µs to 1.1 µs/channel, all channels equal

Maximum Repeat Rate: 1 MHz

Minimum Repeat Rate: 100 seconds per scan

Expansion Channel Sample Rate: Same as on-board channels, 1 to 1.1 µs, fixed

High-Speed Digital Inputs/General-Purpose Outputs

Connector: DB25 Female

Configuration: 16 TTL-compatible pins, selectable for input or output

Input Characteristics: TTL-compatible

Output Characteristics: ALS TTL output in series with 33 Ohms

Output Updates: Outputs may be changed via program control

Input/Output Protection: Diode clamped to ground and +5V

* The following applies when outside 18 to 28 °C and is additive to the above specification:

Range	±Gain Error	±Offset Error
±10V	24 ppm/°C	60 µV/°C
±5V or 0 to 10V	24 ppm/°C	30 µV/°C
±2V or 0 to 4V	24 ppm/°C	12 µV/°C
±1V or 0 to 2V	36 ppm/°C	8 µV/°C

Figure B. 1 General Specifications of IOTECH® WaveBook Data Acquisition System [71]

Performance	ENGLISH	SI
Sensitivity(± 20 %)	5 mV/g	0.51 mV/(m/s ²)
Measurement Range	± 1000 g pk	± 9810 m/s ² pk
Frequency Range(± 5 %)(y or z axis)	2 to 8000 Hz	2 to 8000 Hz
Frequency Range(± 5 %)(x axis)	2 to 5000 Hz	2 to 5000 Hz
Frequency Range(+1 dB)(x axis)	≥ 8 kHz	≥ 8 kHz
Resonant Frequency	≥ 50 kHz	≥ 50 kHz
Broadband Resolution(1 to 10,000 Hz)	0.003 g rms	0.03 m/s ² rms
Non-Linearity	≤ 1 %	≤ 1 %
Transverse Sensitivity	≤ 5 %	≤ 5 %
Environmental		
Overload Limit(Shock)	± 10,000 g pk	± 98,100 m/s ² pk
Temperature Range(Operating)	-65 to +250 °F	-54 to +121 °C
Temperature Response	See Graph	See Graph
Electrical		
Excitation Voltage	18 to 30 VDC	18 to 30 VDC
Constant Current Excitation	2 to 20 mA	2 to 20 mA
Output Impedance	≤ 200 Ohm	≤ 200 Ohm
Output Bias Voltage	7 to 12 VDC	7 to 12 VDC
Discharge Time Constant	0.24 to 1.0 sec	0.24 to 1.0 sec
Settling Time(within 10% of bias)	<3 sec	<3 sec
Spectral Noise(1 Hz)	1200 µg/√Hz	11,772 (µm/sec ²)/√Hz
Spectral Noise(10 Hz)	300 µg/√Hz	2943 (µm/sec ²)/√Hz
Spectral Noise(100 Hz)	100 µg/√Hz	981 (µm/sec ²)/√Hz
Spectral Noise(1 kHz)	30 µg/√Hz	294 (µm/sec ²)/√Hz
Physical		
Sensing Element	Ceramic	Ceramic
Sensing Geometry	Shear	Shear
Housing Material	Titanium	Titanium
Sealing	Hermetic	Hermetic
Size (Height x Length x Width)	0.25 in x 0.25 in x 0.25 in	6.35 mm x 6.35 mm x 6.35 mm
Weight(without cable)	0.04 oz	1.0 gm
Electrical Connector	Integral Cable	Integral Cable
Electrical Connection Position	Side	Side
Cable Length	5 ft	1.5 m
Cable Type	034 4-cond Shielded	034 4-cond Shielded
Mounting	Adhesive	Adhesive

Typical Sensitivity Deviation vs Temperature

Temperature (°F)	Sensitivity Deviation (%)
-50	10
0	5
100	-5
200	-10
300	-12
350	-15

Figure B. 2 General Specifications of PIEZOTRONICS® 356A01 Accelerometer [72]

	ENGLISH	SI	
Performance			
Sensitivity(± 20 %)	100 mV/lbf	22.5 mV/N	[2]
Measurement Range	50 lbf pk	222 N pk	
Resonant Frequency	≥ 100 kHz	≥ 100 kHz	
Non-Linearity	≤ 1 %	≤ 1 %	[1]
Electrical			
Excitation Voltage	20 to 30 VDC	20 to 30 VDC	
Constant Current Excitation	2 to 20 mA	2 to 20 mA	
Output Impedance	<100 Ohm	<100 Ohm	
Output Bias Voltage	8 to 14 VDC	8 to 14 VDC	
Discharge Time Constant	≥ 100 sec	≥ 100 sec	[1]
Physical			
Sensing Element	Quartz	Quartz	
Sealing	Epoxy	Epoxy	
Hammer Mass	0.17 oz	4.8 gm	[3]
Head Diameter	0.25 in	6.3 mm	
Tip Diameter	0.10 in	2.5 mm	
Hammer Length	4.2 in	107 mm	[3]
Electrical Connection Position	Side	Side	
Extender Mass Weight	0.044 oz	1.25 gm	
Electrical Connector	5-44 Coaxial	5-44 Coaxial	[4]

Figure B. 3 General Specifications of PIEZOTRONICS® 086E80 Impact Hammer [72]

☛ Product Features Highlights

- High-velocity pneumatic cylinder, precision cam design and unique brake system allow extremely accurate, flat drop testing that exceeds industry standards, such as ASTM D5276.
 - Handheld control, allowing for positioning of the drop assembly, triggering of the drop sequence, and resetting of the drop platen.
 - Electric hoist for positioning drop assembly and lifting heavy packages.
 - Footswitch, providing an alternative method of operation for triggering and resetting of the platen.
 - Precision cam and bearing design for producing flat drops.
-

☛ Product Specification Highlights

Max Payload:

177 lbs. (80 kg) – Standard Platen
150 lbs. (68 kg) – Extended Platen

Max Item Size (Front/Back):

24 in. (61.0 cm) – Standard Platen
36 in. (91.5 cm) – Extended Platen

☛ Product Options Highlights

- Edge & corner fixture.
- Extended platen.
- Slotted and over-sized bases.
- Test Partner data acquisition.

Figure B. 4 General Specifications of LANSMONT® PDT 80 Drop Table [73]

APPENDIX C

VELOCITY LIMITS OF MATERIALS

Table C. 1 Severe Velocities, Fundamental Limits to Modal Velocities in Structures [59]

Material	E (psi)	σ (psi)	ρ (lbm/in ³)	Rod V_{max} (ips)	Beam V_{max} (ips)	Plate V_{max} (ips)
Douglas Fir	1.92e+06	6450	0.021	633	366	316
Aluminum 6061-T6	10.0e+06	35,000	0.098	695	402	347
Magnesium AZ80A-T5	6.5e+06	38,000	0.065	1015	586	507
Structural Steel, High Strength	29e+06	33,000	0.283	226	130	113
		100,000		685	394	342

Table C. 2 Values from Roark, 1965, p 416 [69]

Material	E (1e+06 psi)	μ	ρ (lbm/in ³)	σ_{ult} (ksi)	σ_{yield} (ksi)	V_{rod} (ips)	V_{beam} (ips)
Aluminum Cast Pure	9	0.36	0.0976	11	11	230.6	133.3
Al Cast 220-T4	9.5	0.33	0.093	42	22	459.9	265.8
Al 2014-T6	10.6	0.33	0.101	68	60	1139.4	658.6
Beryllium Cu	19	0.3	0.297	150	140	1158.0	669.4
Cast Iron, Gray	14	0.25	0.251	20	37	357.8	224.2
Mg AZ80A-T5	6.5	0.305	0.065	55	38	1148.7	663.0
Titanium Alloy	17	0.33	0.161	115	110	1306.5	755.2
Steel Shapes	29	0.27	0.283	70	33	226.3	130.8
Concrete	3.5	0.15	0.0868	0.35	0.515	18.4	10.6
Granite	7	0.28	0.0972	-	2.5	59.6	34.4

Table C. 3 Severe Velocity Values from Sloan, 1985 [68]

Material	E (1e+06 psi)	μ	ρ (lbm/in ³)	σ_{ult} (ksi)	σ_{yield} (ksi)	V_{rod} (ips)	V_{beam} (ips)
Aluminum 5052	9.954	0.334	0.098	34	24	477.4	275.9
Aluminum 6061-T6	9.954	0.34	0.098	42	36	716.2	413.9
Aluminum 7075-T6	9.954	0.334	0.1	77	66	1299.8	751.3
Be	42	0.1	0.066	86	58	684.5	395.7
Be-Cu	18.5	0.27	0.297	160	120	1005.9	581.5
Cadmium	9.9	0.3	0.312	11.9	11.9	133.0	76.9
Copper	17.2	0.326	0.322	40	30	250.5	144.8
Gold	11.1	0.41	0.698	29.8	29.8	210.4	121.6
Kovar	19.5	-	0.32	34.4	59.5	468.0	270.5
Magnesium	6.5	0.35	0.065	39.8	28	846.4	489.3
Nickel	29.8	0.3	0.32	71.1	50	318.1	183.9
Silver	10.6	0.37	0.38	41.2	41.2	403.4	233.2
Solder 63/37	2.5	0.4	0.30008	7	7	158.8	91.8
Steel 1010	30	0.292	0.29	70	36	239.8	138.6
Stainless	28.4	0.305	0.29	80	40	273.9	158.3
Alumina al203	54	-	0.13	25	20	148.3	85.7
Beryllia Beo	46	-	0.105	20	20	178.8	103.4
Mira	10	-	0.105	-	5.5	105.5	60.0
Quartz	10.4	0.17	0.094	27.9	27.9	554.5	320.5
Magnesia Mgo	10	-	0.101	12	12	234.6	135.6
EPO GLS G10 X/Y	2.36	0.12	0.071	25	35	1680.1	971.1
EPO GLS G10 Z	2.36	0.12	0.071	25	35	1680.1	971.1
Lexan	0.379	-	0.047	9.7	9.7	1428.1	825.5
Nylon	0.217	-	0.041	11.8	11.5	2395.6	1384.8
Teflon	0.15	-	0.077	-	4	731.3	422.7
Mylar	0.55	-	0.05	25	25	2962.2	1712.3

APPENDIX D

“C” CONSTANTS FOR DIFFERENT TYPES OF ELECTRICAL COMPONENTS

Table D. 1 Constant for Different Types of Electronic Components [66]


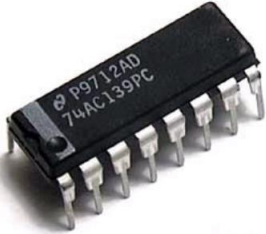
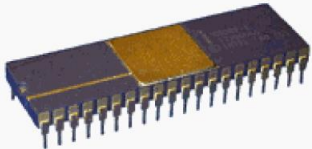
C	Component	Image
0.75	Axial leaded through hole or surface mounted components, resistors, capacitors, diodes	 A photograph of an axial leaded resistor. It has a cylindrical brown body with two metal leads extending from opposite ends. A central band is marked with four color-coded rings: yellow, purple, orange, and red.
1.0	Standard dual inline package (DIP)	 A photograph of a standard dual in-line package (DIP) component. It is a black rectangular integrated circuit with two rows of pins. The top surface is labeled with the part number '74AC1397C' and a manufacturer's logo.
1.26	DIP with side-brazed lead wires	 A photograph of a dual in-line package (DIP) component with side-brazed lead wires. The component is a dark blue rectangular chip with a gold-colored top surface. It has two rows of pins, and the leads are connected to the component via side-brazing.

Table D. 1 Constant for Different Types of Electronic Components (continued)
[66]

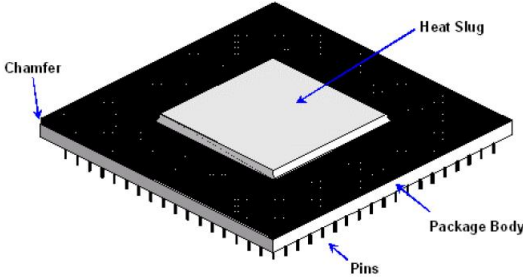



C	Component	Image
1.0	Through-hole Pin grid array (PGA) with many wires extending from the bottom surface of the PGA	
2.25	<p>Surface-mounted leadless ceramic chip carrier (LCCC).</p> <p>A hermetically sealed ceramic package. Instead of metal prongs, LCCCs have metallic semicircles (called castellations) on their edges that solder to the pads.</p>	
1.26	Surface-mounted leaded ceramic chip carriers with thermal compression bonded J wires or gull wing wires.	

Table D. 1 Constant for Different Types of Electronic Components (continued)
[66]

C	Component	Image
1.75	<p>Surface-mounted ball grid array (BGA).</p> <p>BGA is a surface mount chip carrier that connects to a printed circuit board through a bottom side array of solder balls.</p>	
0.75	<p>Fine-pitch surface mounted axial leads around perimeter of component with four corners bonded to the circuit board to prevent bouncing</p>	<p>—</p>
1.26	<p>Any component with two parallel rows of wires extending from the bottom surface, hybrid, PGA, very large scale integrated (VLSI), application specific integrated circuit (ASIC), very high scale integrated circuit (VHSIC), and multichip module (MCM).</p>	<p>—</p>

APPENDIX E

ATC® HIGH POWER FLANGE MOUNT RESISTOR

High Power, Flange Mount Resistor

P/N: FR19560NxxxxJ

General Specifications

- Resistance: 100Ω standart (other Ω values are available)
- Resistive Tolerance ±5% standard (±2% available)
- Power: 75 Watts
- Capacitance: 4.15 pF
- Operating Temperature Range: -55°C to +150°C
- Temperature Coefficient: <150 ppm/°C
- Shock Durability <250g
- Tabs: Silver
- Lead Free, RoHS Compliant
- Non-Magnetic available



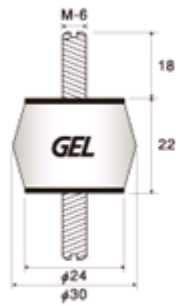
AMERICAN TECHNICAL CERAMICS

Figure E. 1 General Specifications of ATC® High Power Flange Mount Resistor [74]

APPENDIX F

TAICA ALPHA-GEL® MN SERIES ISOLATOR

Optimum load is adjusted by changing hardness, in same shape.



Part No.	Optimum Load (kg/4 legs)	Resonance Point(Hz)	Resonance Magnification (dB)
MN-3	8~14	12~10	12
MN-5	14~22	11~10	14~13
MN-7	22~34	11~10	16~15
MN-10	34~50	11~10	20~18

Figure F. 1 General Specifications of Taica ALPHA-GEL® MN Series Isolator

[75]

APPENDIX G

MATLAB® SCRIPT FOR FREQUENCY DOMAIN DIFFERENTIATION

```
clear all;close all;clc
data=fopen('deney_MATLAB@_iso.txt');
acccdata=textscan(data,'%s %s',16384);
t=str2double(acccdata{1});
L=length(t); %points
S=L/t(L); % sampling Frequency
acceler(:,1)=acccdata{2};
acceleration=zeros(L,1);
for i=1:L
acceleration(i)=str2double(acceler(i,1));
end

NFFT=2^nextpow2(L);
Freqaccel=fft(acceleration,NFFT)/L;
f=S/2*linspace(0,1,NFFT/2);
f=f';

i=sqrt(-1);

%%%VELOCITY%%%
velfreq=Freqaccel(1:8192)./(i*2*pi*f);
A=velfreq(2:end);
B= flipud(real(velfreq(2:end))-i*imag(velfreq(2:end)));
velfreq=[0;A;0;B];
velocity=L*ifft(velfreq); %Inverse FFT in order to obtain time
domain data of velocity.

figure
plot (t,velocity);
title('Relative Velocity Response of Antenna')
xlabel('Time [s]')
ylabel('Velocity Amplitude [m/s]')
grid on
```